Universitat Autònoma de Barcelona

Applications of Dissipative Particle Dynamics on Nanostructures: Understanding the Behaviour of Multifunctional Gold Nanoparticles

Aslı Raman Martín Dombrowski

Universitat Autònoma de Barcelona

Applications of Dissipative Particle Dynamics on Nanostructures: Understanding the Behaviour of Multifunctional Gold Nanoparticles

Aslı Raman Martín Dombrowski

Doctoral Thesis

Doctoral Studies in Chemistry

Supervisor: Carlos Jaime Cardiel

Departament de Química

Facultat de Ciències

2017

Thesis submitted to aspire for the Doctor Degree

Aslı Raman Martín Dombrowski

Director's Approval:

Dr. Carlos Jaime Cardiel Professor of Organic Chemistry

Bellaterra (Cerdanyola del Vallès), 12 June 2017

Funding Acknowledgments

Universitat Autònoma de Barcelona is gratefully acknowledged for the fellowship Personal Investigador en Formació (PIF). This work was carried out under the financial aid from the Ministerio de Economía y Competitividad (Grant no. MAT2015-70725R).

This work was performed, in part, using the computer facilities from Consorci de Serveis Universitaris de Catalunya (CSUC).

Acknowledgments

This dissertation would not have been possible without the help of others. Therefore, a few brief words of gratitude are in order.

Öncelikle bana her zaman destek olan aileme çok teşekkür ederim. Sevgili annem,babam ve kardeşim bu uzun süreç boyunca hep yanımda oldular.

I would like to thank my family for their love and for always believing in me. I cannot thank my dear husband enough for all his love, encouragement and great support.

I have been very fortunate to have a supervisor like Prof. Carlos Jaime Cardiel. I owe my gratitude to him for his guidance in this journey. I would like to thank him for his support, encouragement and for allowing me to pursue research on topics for which I am truly passionate. I would also like to thank his family for always making me feel like I am a part of the family.

Prof. Víctor F. Puntes is acknowledged for his collaboration in most of the studies presented herein. I would like to thank him for his contribution.

Prof. Raphaël Lévy deserves a special mention for his great hospitality in my research stay at the University of Liverpool. I would like to thank him and his group for their welcoming. I was lucky to be a part of his group and I would like to thank him for his mentorship and our philosophical talks.

I would like to thank Prof. Albert Virgili Moya for his help in my first year. Special thanks to Miriam for being a great friend and advisor when needed. I would also like to thank my students Rosa and Ana for their support and for giving me the chance to help them in their final projects.

The friends I made from my previous research group NanoSFun were always there with me when I needed. Thank you to all.

I would also like to thank to my friends in the Turkish lunch group at the university. Special thanks to Onur for everything.

I would like to thank Delfina for the friendship we developed during our PhDs. We shared a lot of great moments and supported each other.

I would like to truly thank every single person who has contributed along the way.

Abstract

A gold nanoparticle (AuNP) conjugate formed with 11-mercaptoundecanoic acid (MUA) and thiolated polyethylene glycol (SH-PEG) is simulated using Dissipative Particle Dynamics (DPD) and coarse-grained methods, obtaining a good agreement with previous experimental observations.

The simulations cover the isolated components, as well as pairs of components and finally the three components at the same time. The AuNPs are formed by independent units (beads) and keep an almost spherical shape along the simulation. MUA forms micelles of 4-6 MUA units in water while SH-PEG stays well solvated. Both molecules show a tendency to form patches on the AuNP surface. SH-PEG displays two conformations depending on its concentration and presence of other molecules at the nanoparticle surface. When combined at subsaturation concentrations, MUA arrives faster to the AuNP surface than SH-PEG and forms patches once landed while SH-PEG occupies the remaining free surface. The order of addition of the different components alters these results: if SH-PEG is added over an already formed MUA/AuNP partial layer, it adopts a radial conformation over the formed MUA patches; if MUA is added over an already formed SH-PEG/AuNP partial layer, less SH-PEGs adopt radial conformation and MUA patches are significantly smaller. Besides, conformation changes depend on the SH-PEG/MUA ratio.

Bovine serum albumin (BSA) is simulated using DPD methods and added to the simulations to complete the investigation of conformational changes on AuNPs. Limitations were encountered due to the large scale of these simulations. The colloidal stability of AuNPs in the presence of increasing number of MUAs is studied. An alternative AuNP design is proposed to overcome the deformation caused by the oversaturation of the ligands.

Resumen

Una combinación (*conjugate*) compuesta por una nanopartícula de oro (AuNP), ácido 11-mercaptoundecanoico (MUA) y polietilentioglicol (SH-PEG) fue estudiada por métodos teóricos utilizando simulaciones computacionales con métodos de Dinámica de Partículas Disipativas (DPD), que a su vez usan técnicas de grano grueso (*coarse-grained*) para reducir las variables del sistema. Los resultados obtenidos reproducen razonablemente bien las observaciones experimentales previas.

Las simulaciones se realizaron sobre los componentes aislados, así como sobre pares de componentes y finalmente con los tres componentes al mismo tiempo. Las AuNPs están formadas por perlas independientes y mantienen una forma casi esférica a lo largo de la simulación. En solución acuosa, MUA forma micelas de 4-6 unidades, mientras que SH-PEG se mantiene bien solvatado. Ambas moléculas muestran una tendencia a agregarse en zonas (parches) en la superficie de la AuNP. SH-PEG muestra dos conformaciones distintas, dependiendo de su concentración y de la presencia de otras moléculas en la superficie de las nanopartículas. Cuando se combina a concentraciones de subsaturación, el MUA llega más rápido que el SH-PEG a la superficie de la AuNP y forma parches una vez depositada sobre ella, mientras que el SH-PEG ocupa la superficie libre restante. También se estudió el efecto que ejerce el orden de adición de los diferentes componentes, que altera estos resultados: si se añade SH-PEG sobre una capa parcial de MUA/AuNP ya formada, aquel adopta una conformación radial sobre los parches de MUA formados. Si se añade MUA sobre una capa parcial de SH-PEG/AuNP ya formada, menos SH-PEGs adoptan la conformación radial y los parches de MUA son significativamente más pequeños. Además, los cambios de conformación dependen de la relación SH-PEG/MUA.

Para finalizar, se simuló el efecto de la albúmina sérica bovina (BSA) sobre la combinación de AuNP, MUA y SH-PEG, también mediante métodos de DPD, para completar la investigación sobre los cambios conformacionales en las AuNPs. Aparecieron diversas limitaciones, en parte debido a la gran escala de estas simulaciones.

Asimismo, se estudió la estabilidad coloidal de las AuNPs en presencia de un número creciente de MUAs que mostró una deformación importante de la AuNP para concentraciones elevadas de MUA, por lo que se desarrolló un modelo de AuNP alternativo y rígido con el objetivo de evitar la deformación causada por la sobresaturación de la superficie de la AuNP provocada por los ligandos.

TABLE OF CONTENTS

TABLE OF CONTENTS

LIST OF ABBREVIATIONS

AFM	Atomic Force Microscope
AuNP	Gold Nanoparticle
BCE	Before the Common Era
BSA	Bovine Serum Albumin
DFT	Density Functional Theory
DLS	Dynamic Light Scattering
DPD	Dissipative Particle Dynamics
DPD-MC	Dissipative Particle Dynamics-Monte Carlo
ESA	Equine Serum Albumin
GROMACS	GROningen Machine for Chemical Simulations
HSA	Human Serum Albumin
LSA	Leporine Serum Albumin
MUA	11-mercaptoundecanoic acid
MUS	11-mercapto-1-undecanesulfonate
NAMD	Nanoscale Molecular Dynamics
OT	1-octanethiol
PEG	Polyethylene glycol
PDB	Protein Data Bank
Rdf	Radial Distribution Function
SAMs	Self-assembled monolayers
SH-PEG	Thiolated polyethylene glycol
STM	Scanning Tunneling Microscope
UV–vis	Ultraviolet–Visible Spectroscopy

Chapter 1

INTRODUCTION

Chapter 1

INTRODUCTION

Nanotechnology is a field that has attracted tremendous interest over the past decades. What is nanotechnology? The word *nano*, derived from the Greek *nanos*, meaning dwarf, is used to describe any material or property which occurs with dimensions on the nanometre scale, which is about 1 to 100 nanometers. The foundations of nanotechnology begin with the Nobel prized physicist Richard Feynman when he made his famous speech "*There's Plenty of Room at the Bottom"* at an American Physical Society meeting at the California Institute of Technology (CalTech) on December 29, 1959, long before the term nanotechnology was used.[1] He is usually referred as the father of nanotechnology. Over a decade later, the term "nano-technology" was first used by the Japanese scientist called Norio Taniguchi in a conference at 1974.[2] His definition was to be changed several times up to today. The definition of The U.S. National Nanotechnology Initiatve (NNI) is as follows:

"The understanding and control of matter at dimensions between approximately 1 and 100 nanometers, where unique phenomena enable novel nanotechnology applications. Encompassing nanoscale science, engineering, and technology, nanotechnology involves imaging, measuring, modeling, and manipulating matter at this length scale."[3]

We can briefly say that nanotechnology is science, engineering, and technology conducted at the nanoscale. The modern nanotechnology began later at 1981 with the invention of the Scanning Tunneling Microscope (STM), which is an instrument that provides visualization at atomic level.[4] The inventors Gerd Binnig and Heinrich Rohrer at

IBM's Zurich won the Nobel Prize in Physics in 1986. Binnig, Quate and Gerber also invented the Atomic Force Microscope (AFM).[5]

1.1 Nanomaterials

Although nanotechnology is a relatively recent field, nanomaterials have existed in nature for a longer period of time and it is possible to see their use going back to ancient times. Perhaps the most famous example is the Lycurgus Cup, that was made by Romans in the 4th century, which is exhibited at the British Museum in London (Figure 1.1). This one of a kind glass cup is an example of dichroic glass; colloidal gold and silver in the glass allow it to look opaque green when lit from outside but translucent red when light shines through the inside. The dichroic effect is due to the presence of tiny proportions of nanoparticles of gold and silver dispersed in colloidal form throughout the glass material.[6,7] Nanoparticles were used by artisans as far back as the ninth century in Mesopotamia for creating a glittering effect on the surface of pots. These glowing, glittering luster ceramic glaze decorations contained silver and copper nanoparticles, origin of the incredible optical properties of the decorated objects.[8] Stained glass windows in European cathedrals owed their rich colours to nanoparticles. The silver nanoparticles in the glass matrix of these windows are responsible for the bright colour that can be varied from yellow to red.[9]

Modern nanomaterials are prepared over a wide range of length scale where they present morphological features between 1 to 100 nanometers. The physical and chemical properties of materials can change as their size is scaled down to small clusters of atoms which leads to different properties on the nanoscale than in bulk thanks to their tunability. Approaches for the preparation of nanomaterials can be carried out in a wide variety of methods, these methods are divided in two main categories; *top-down* and *bottom-up*.[10]

Figure 1.1 The Lycurgus Cup at the British Museum in London, lit from the outside (left) and from the inside (right).

A major feature that discriminates various types of nanomaterials is the concept of dimensionality (Figure 1.2). The dimensionality plays a major role in the characteristic of the nanomaterials such as physical, chemical and biological characteristics. Considering the importance of the dimensionalities of nanomaterials, all examples of innovative nanomaterials are classified as 0-D nanomaterials, where all dimensions are at the nanoscale (nanoparticles, quantum dots); 1-D nanomaterials, where two dimensions are at the nanoscale and one dimension is at the macroscale (nanowires, nanotubes); 2-D nanomaterials, where one dimension is at the nanoscale and two dimensions are at the macroscale (nanosheets, graphene) and 3-D nanomaterials, where all dimensions are at the macroscale (bulk sized materials).[11]

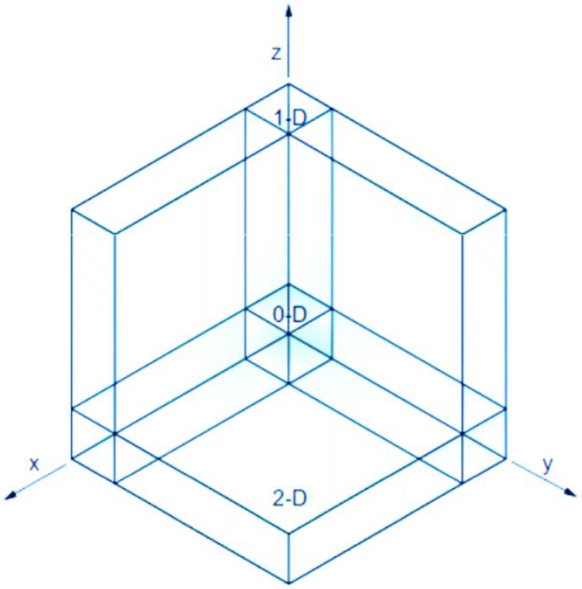

Figure 1.2 Representation of the dimensionality concept of nanomaterials: 0-D, 1-D, 2-D and 3-D as the bulk material.

Here we are going to focus on 0-D nanomaterials, specifically talking gold nanoparticles (AuNPs). Noble metal nanoparticles like AuNPs are excellent candidates for nanomaterials because of their strongly size dependent electronic,[12] optical[13,14] and catalytic[15] properties.

1.2 Gold Nanoparticles

Gold always played an important role in human history since the old ages. The history of gold goes way back to 9000-7000 BCE (Before the Common Era). For example, in Iran and in Anatolia, humans began using gold to create tools and possibly jewellery.[16] Gold artefacts in the Balkans appear from the 4000 BCE near Varna on the Black Sea coast, which is located in modern day Bulgaria.[17] The largest discovery of gold was found in the tomb of Tutankhamun in Egypt (1333-1324 BCE) which contained a collection of gold and jewellery, including a gold coffin.[16] It is probable that colloidal gold was first used in applications like ceramics around the 5th or 4th century BCE in Egypt and China.[18,19]

The first scientific report describing the synthesis of AuNPs was in 1857 when Michael Faraday investigated the optical properties of AuNPs.[20] However, the history of AuNPs as tools for biological research and medical diagnostics starts in 1912 when Carl Friedrich August Lange introduced AuNPs to detect diseases.[21] For several decades, the Lange test on AuNP colour change was used in clinics and its existence motivated better synthesis of AuNPs.[22,23]

One of the most popular approaches for the synthesis of AuNPs was developed by Turkevich in 1951 using citrate reduction of Au^{III} to Au^{0} in water where citric acid acts as both reducing and stabilizing agent and provides AuNPs with diameters of 20 nm.[24] Figure 1.3 illustrates the creation of AuNPs capped with citrate. Although the work of Turkevich and his co-workers is certainly a landmark for the synthesis of AuNP, the naming of the synthesis is historically not quite correct considering Turkevich *et al.* referred to the textbook Experiments in Colloid Chemistry by Ernst A. Hauser and J. Edward Lynn, already published in 1940.[25] Later in the 1970s, the so called Turkevich method was refined by Frens.[26,27] In the Turkevich-Frens method, the actual AuNP stabilizer is dicarboxy acetone resulting from the oxidation of citrate, rather than citrate itself. Recent modifications of the Turkevich method have allowed better size distribution and size control within the 9-120 nm range.[28] The popularity of this method relies on the resulting versatile citrate layer on the nanoparticle surface which allows an easy (multi)functionalization.[29]

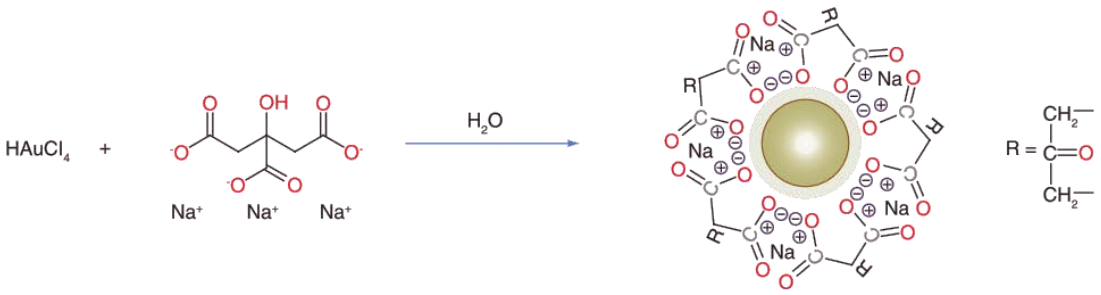

Figure 1.3 AuNP synthesis using the Turkevich method. Adapted from reference 30.

Although AuNPs can be stabilized by a large variety of stabilizers, the most robust AuNPs were disclosed by Giersig and Mulvaney to be stabilized by thiolates using the strong thiol-gold bond between the soft acid gold and the soft thiolate base.[31] Later on, a significant breakthrough in the field of AuNP synthesis was achieved by Brust and Schiffrin in 1994 when they reported a two-phase synthetic strategy utilizing strong thiol-gold interactions to protect AuNPs with thiol ligands.[32] These thiol-protected AuNPs feature superior stability because of the strong thiol-gold interaction and they can be easily handled, characterized, and functionalized. Different characteristics of AuNPs are observed according to the method used (Table 1.1).

Table 1.1 Summary of Brust-Schiffrin method and Turkevich method.

Reduction method	Reaction media	Reductant	Surface protecting agent	Particle size range (nm)	Reaction temperature (℃)	Ref.
Brust-Schiffrin method	organic	$NaBH_4$	organothiol	2-10	room temperature	32, 33
Turkevich method	aqueous	citrate	citrate	10-20	100	24

In thiol-stabilized AuNPs place exchange reactions, substitution of thiol ligands, can be carried out in order to modify the nanoparticle surface, which was reported by Murray.[34,35,36] In this method, the initially anchored thiol ligands are exchanged in by the free thiol ligands. Secondary modification is also possible when the surface functionality on AuNPs has activated groups such as carboxylates and hydroxyls (Figure 1.4). The secondary reaction on the surface is achieved using chemical coupling,[37] polymerization,[38] electrostatic interaction,[39] and selective interaction between biological molecules.[40]

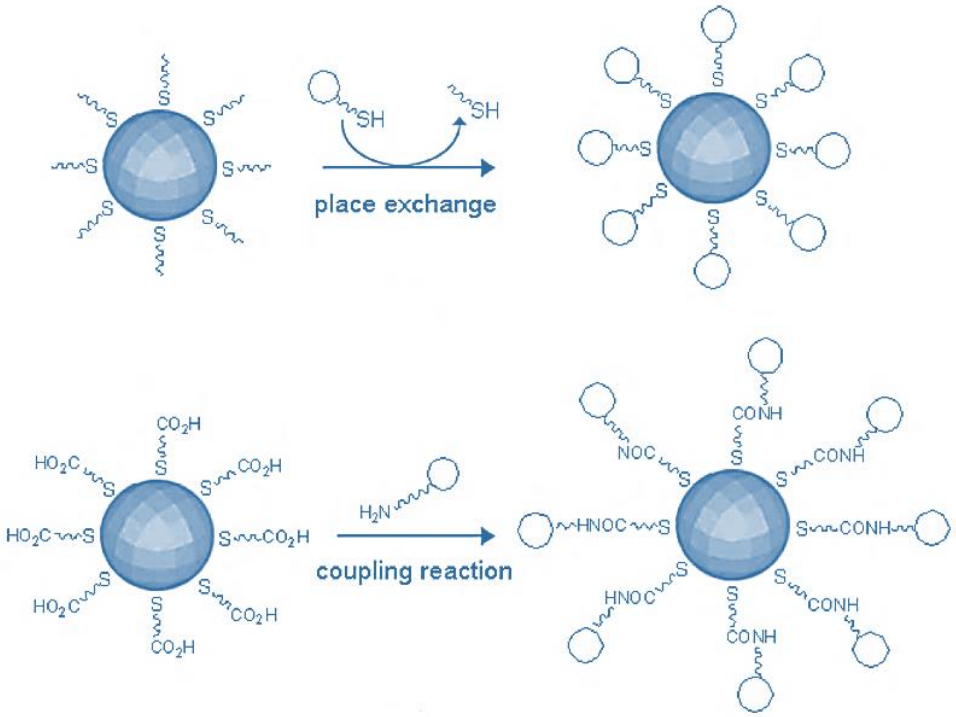

Figure 1.4 Schematic representation of surface modification method through place exchange in organothiol system and secondary modification of ligand end groups. Adapted from reference 41.

1.2.1 Properties of Gold Nanoparticles

Noble metal nanoparticles, in particular gold, possess distinct physical and chemical attributes that make them excellent scaffolds for the fabrication of novel chemical and biological applications.[42,43] Gold is inert and chemically very uninteresting in bulk form but it has rich ligand chemistry in nanometre-scale molecular complexes.[44]

Perhaps one of the most important aspect at the nanoscale is the increase in the surface-to-volume ratio of materials. AuNPs provide high surface-to-volume ratio with excellent biocompatibility using appropriate ligands.[18] Figure 1.5 shows the increase in surface area possible merely by reducing the diameter of spherical nanoparticles of gold.

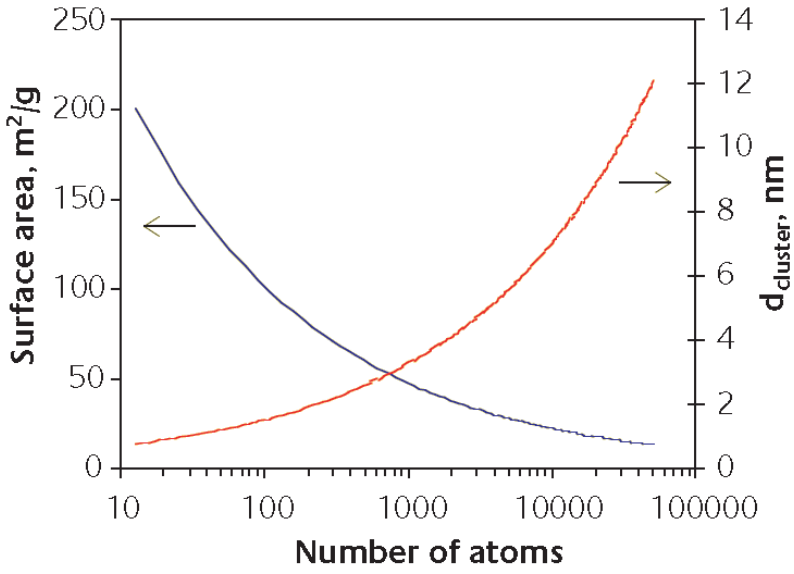

Figure 1.5 Graph showing approximate size and specific surface area of spherical nanoparticles of gold. Adapted from reference 45.

What makes gold at nanoscale a good candidate for biological applications is that AuNPs have low cytotoxicity.[46] The combination of their low inherent toxicity, high surface area and tunable surface chemistry contributes to their growing applications. Gold is a promising material at the nanoscale due to its chemical stability and biocompatibility,[47] along with its unique size and shape-dependent optical properties.[48]

1.2.2 Surface Functionality of Gold Nanoparticles

Surface functionality plays a very important role in many aspects of AuNPs. The composition of the coating layer, and more importantly, its structure, defines the final identity of the nanoparticle. This in turn, affects not only the properties of the nanoparticle, such as its final size, surface charge, surface hydrophilicity and surface chemistry, but also its stability, interactions with other biological entities, particularly proteins (what is known as protein corona[49]), and biodistribution.[50] All this factors are ultimately responsible in eliciting the desired effect on cellular and molecular responses.[51] Furthermore, this precise control of the surface chemistry[52] of the AuNPs is

of especial importance when addressing their interactions with the immune system, responsible for dealing with external invasion.

After synthesis of the particles the stabilizer molecules can be replaced by other stabilizer molecules in a ligand exchange reaction. A well-known example is AuNPs synthesized by citrate reduction where the citrate layer can be easily replaced by other ligands. The ligand layers have higher affinity for the particle surface, such as thiol- and amine- containing ligand molecules, allowing simple and easy functionalization. As thiol moieties bind with high affinity to gold surfaces, most frequently thiol-modified ligands are used in binding to the surface of the Au particles by formation of gold–thiolate bonds.[53] Thus, AuNPs have been selectively delivered to target regions, providing enhanced opportunities for controlled drug delivery,[54] cancer treatment,[55] biomedical imaging[56] and diagnosis.[57]

For applications in aqueous solution generally thiol-based surfactants with carboxylic groups are used as ligands. These molecules provide colloidal stability due to their negative charges; in addition they can also be used as anchor points for the further attachment of biological molecules.[58] Thiolated polyethylene glycol (SH-PEG) is the most commonly employed surface ligand used with AuNPs where PEGylation refers to the surface modification with polyethylene glycol as a particle stabilizer.[59] Pun *et al.* have recently reported how different physicochemical properties, such as size, PEGylation, regulate non-specific versus target-specific uptake.[60] Targeting ligands can also be tethered to the surface of AuNPs through a SH-PEG linker (Figure 1.6). Paciotti *et al.* carried out in vivo study to investigate the therapeutic effect of PEGylated gold colloids with adsorbed protein.[61] PEGylation is also used to avoid opsonisation (where molecules of the immune system bind to a target to induce its phagocytosis) to avoid interaction with immune cell transmembrane receptors (Patron Recognition Receptors), and to provide colloidal stability to the nanoparticle via steric repulsion.[62,63,64] Remarkably, it can be adsorbed on the nanoparticle surface in a flat or radial configuration and only the radial conformation stabilizes nanoparticles against aggregation and/or opsonization.[65]

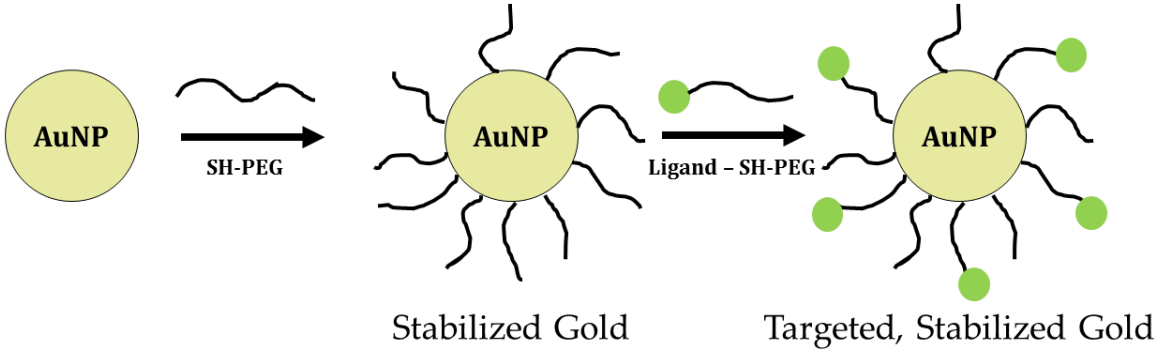

Figure 1.6 Schematic illustration of the surface functionalization of AuNPs. Self-assembly of SH-PEG monolayers on AuNPs confers colloidal stability under physiological conditions.

Self-assembled monolayers (SAMs) are molecular assemblies formed spontaneously on surfaces by adsorption and are organized into ordered domains.[66] SAMs of thiols on gold surfaces have been studied for decades. The literature is abounding with examples of functionalized AuNPs for several applications usually illustrated with inspiring schemes. Nevertheless, the actual structure and organization of the SAMs at the AuNP surface are challenging to assess and remain often poorly characterized. Additionally, the investigation of the relationship between structure and function needs to be described explicitly to define physicochemical and structural properties.[67]

1.3 Stripy Nanoparticles

A different model of ligand organisation was presented in a series of studies starting in 2004 by Stellachi and co-workers,[68] which reported the existence of "stripy" domains of alternating hydrophobic and hydrophilic ligands on the surface of small nanoparticles. However, the systematic evaluation of these aspects is greatly limited by the experimental techniques and resources available to study the distribution and conformation of two different molecules attached to a nanoparticle surface in the liquid phase. Thus, the interpretation of these results and the existence of stripy nanoparticles is controversial.

After the first work on AuNPs presenting a stripe-like arrangement of ligands was published, a series of articles followed it.[69] Throughout this series the authors base their research on the existence of "stripy" domains on the surface of AuNPs, where two different thiolated organic ligands self-organise into alternating stripes across the nanoparticle surface. The authors claimed that STM images demonstrated the presence of ordered domains such domains were described as parallel stripe-like patterns circling around the gold cores with shape and size tunable by selecting the composition of the ligand mixture and the AuNP size, and with quite alluring properties arising from their small dimensions, such as avoiding the nonspecific adsorption of proteins. However, this proposed stripy structure has been a subject of controversy, the published results are re-examined by Cesbron *et al.*[70] and Stirling *et al.*[71] and have been suggested to be the result of instrumental artefacts (Figure 1.7). Artefacts in atomic/molecular resolution images arising from, e.g., double or multiple tips,[72] and/or tip asymmetry,[73] are noted in the literature before. Lévy and his co-workers commented on the possibility on these artefacts in their article "Stripy Nanoparticles Revisited".[70] They consider this as a simple geometrical problem. They have commented as follows: "*An STM topography image of a spherical particle is, in first approximation, a 2D projection of the top hemisphere. If a spherical particle is covered with regularly spaced stripes, what should be the apparent width of the stripes? For a 5.8 nm-diameter sphere with 18 regularly spaced 1 nm-wide stripes (9 per hemisphere), the width of the projected stripes on a 2D image decreases rapidly as the STM tip goes from the top of the sphere to its edge, perpendicularly to the stripe direction (Figure 1.7.a top). A model theoretical STM image of the 5.8 nm stripy nanoparticle is constructed (Figure 1.7.a bottom) and a theoretical line profile of it is shown (Figure 1.7.b).*"[70]

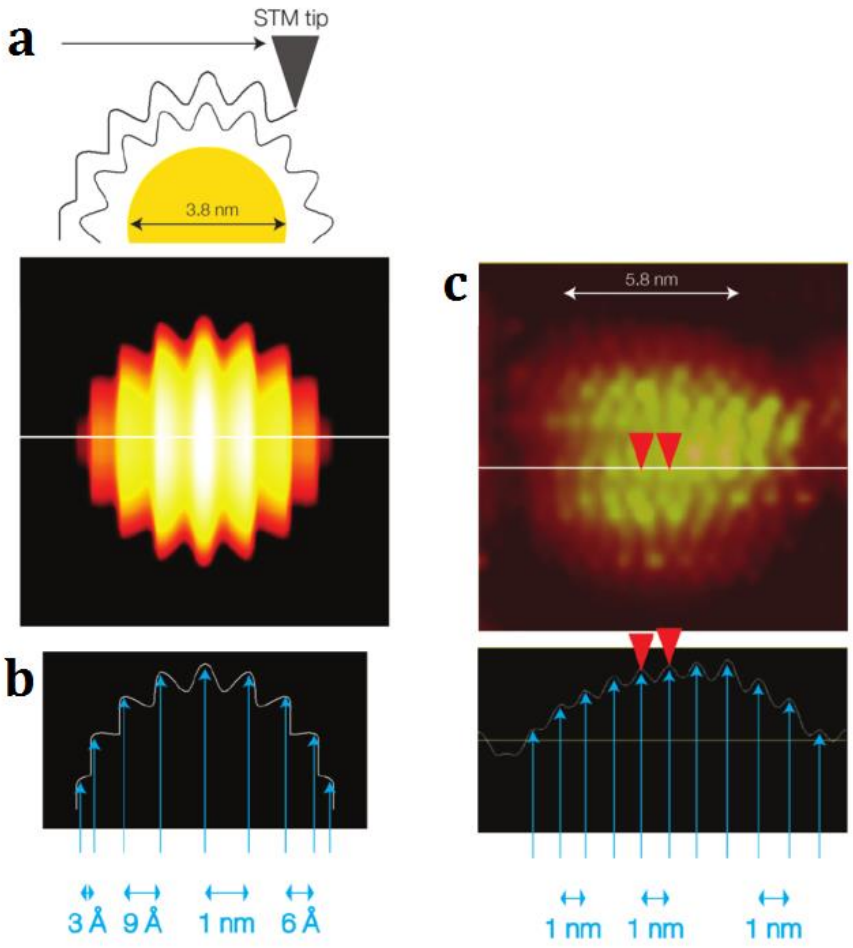

Figure 1.7 Comparison of the predicted and report stripe widths on a 5.8 nm diameter AuNP. **a**. (top) STM tip scanning a stripy nanoparticle orientated perpendicularly to the scanning direction, and (bottom) resulting STM image with colour coding depicting sample heights. **b.** Height profile corresponding to the white lines drawn. **c.** Experimental STM image (adapted from figure 1b of Jackson *et al*. 68). Adapted from reference 70.

Both analyses received a response from the authors of the original publication that addressed the arguments of invalidation of the results obtained.[74,75] Besides their response on the image quality on their work, the authors also referred modelling and theoretical work on these systems.[69d,76,77,78] On the other side of the discussion, computer simulations on these domains received a different comment saying that "*if the experimental evidence for the structure is called into question it is tautological to use a simplistic simulation designed to understand this structure as evidence that the structure itself does exist.*".[71] The response from the authors on this matter continued as follows *"…*

nothing in the simulations was done to bias the result. It remains unquestionable that many different simulation codes (from coarse grained, to self-consistent field, to full atomistic) have all found stripes. The excellent matching between experiment and simulations cannot be denied.".[75] Nevertheless, computer simulations play an important role in the understanding of the interactions between a AuNP surface and the surrounding biological environment. This field is still in a discovery phase with the help of the advances on the biological imaging techniques.[79] Due to the high interest, knowledge of gold (and other) nanoparticles in their biological environment are improving gradually. The critical question is how can we claim that a simulation is good enough while there are several controversies and limitations about the subject itself? What justifies the simulations and what makes them accurate?[80] The following section will focus on the computational studies on AuNPs to search for answers to these questions and to give us another perspective.

1.4 Computer Modelling Studies

Theoretical and computational approaches to complement experiments are essential in investigating the necessary molecular insight into the structural and dynamic behaviour of the gold surface and the biological interface. Despite the significant recent advancements in experimental techniques,[81] a comprehensive multiscale understanding of the structure and dynamics at the AuNP surface is still lacking. Computational studies can help us understand what is happening on the surface of nanoparticles and can be used to guide the experimental design of new classes of AuNPs for biological applications.

The fundamental physicochemical description of the nanoparticle such as size, shape, composition, surface decoration, and surface charges should be designed very carefully in computer simulations. The gold–bio interface should in principle involve multiple time and length scale regimes corresponding with the physicochemical phenomena occurring at this interface.[82] Examples of theoretical and computational approaches to complement experiments at multiple time and length scales are shown in Figure 1.8. It is crucial to choose the right simulation method for the corresponding problems.

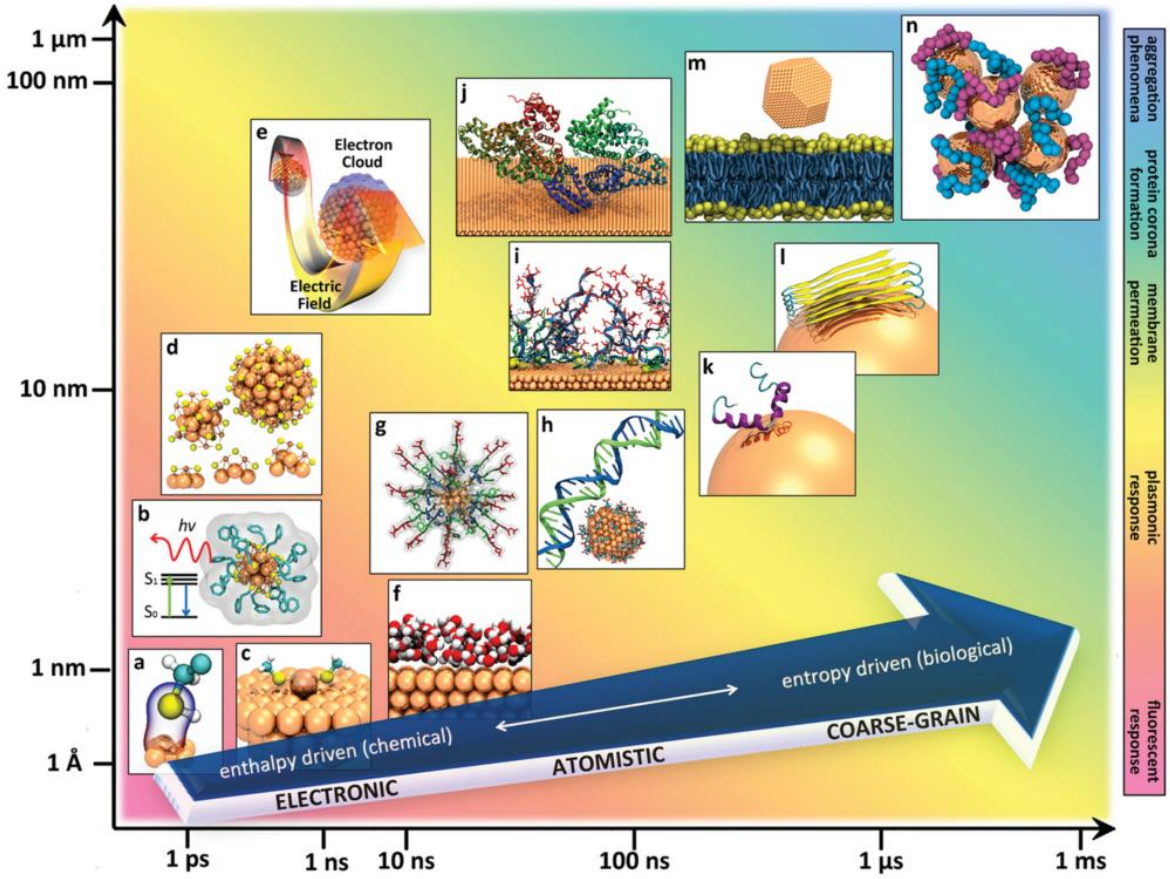

Figure 1.8 Schematic illustrating molecular models (a–n) and simulation approaches (blue arrow) aiming to capture physicochemical interactions at the interface between AuNPs and biological matter at chemically and biologically relevant time and length scales: **a.** Gold surface functionalization reactions, **b.** Gold nanocluster electronic excitation and fluorescence, **c.** AuNP growth and surface reconstruction, **d.** AuNP structure/morphology, **e.** AuNP surface plasmon resonance, **f.** Gold-solvent interactions and polarization, (g–l) biomolecular interactions and adsorption on Au surfaces and nanoparticle, including (in order of appearance) grafted functional chains/peptides, DNA, self-assembled monolayers, protein complexes, individual proteins, fibrillar protein aggregates, **m.** AuNP-lipid membrane interactions and internalization mechanisms, and **n.** AuNP aggregation. The relevance of the models and simulation methods to biomedical applications of gold is indicated by the spectrum of background color. The temporal and spatial resolution shown on the axes reflect the scale of the AuNP properties (a–n) and the blue arrow is (currently) indicative of the modelling approaches capable to treat the respective phenomena, however the latter can be expected to change (i.e., each method will move up the time and length scales) with further increase of high-performance computing capabilities. Adapted from reference 82.

Quantum Mechanics calculations are primarily used for AuNP structure determination, analysis of electronic and optical properties, chemical functionalization and force field parameterization for Molecular Mechanics and Molecular Dynamics simulations.[82] Quantum Mechanics methods are used to investigate the dynamics of AuNP formation, including aspects such as self-assembly/aggregation,[83,84] doping,[85,86] metal oxidation,[87] ligand exchange,[88,89,90] and the binding of small molecules to gold surfaces.[91,92,93] As the number of atoms and time scale of the physicochemical phenomena of interest increase, so does the computational demand. Therefore, atomistic models can be complemented with lower-resolution coarse-grained methods. In these models a small group of atoms is treated as a single interaction unit, where the interaction is governed by a simplistic forcefield, and then Molecular Dynamics is applied as in all-atom methods.[94,95] Small groups of gold atoms can be mapped into single beads using coarse-graining.[96,97] Many examples exist in simulating AuNPs using coarse-grained methods such as translocation of AuNPs through cellular membranes.[98,99] Nanoparticles used in coarse-grained studies can either be bare[100] or coated with various ligands, for instance alkanethiols,[101] polymer brushes,[96] peptides[102] or a mixture of hydrophobic and hydrophilic ligands.[103] Other examples include the interaction of proteins with citrate-capped AuNPs[104,105] and the aggregation of alkanethiol–AuNPs.[97,106] In 2013, The Nobel Prize in Chemistry was awarded "for the development of multiscale models for complex chemical systems," recognizing the early achievements of Michael Levitt, Ariel Warshel, and Martin Karplus that included the coarse-grained modelling of proteins[107,108] as an important step in the investigation of larger biomolecular systems.[109]

Density Functional Theory[110] (DFT) provides very precise information at the atomistic level. Häkkinen's group have been working on ligand-stabilized metal nanoparticles for a long time using DFT calculations and they are specifically interested in nanoparticles termed as clusters which have a countable number of atoms (less than 150 atoms).[111] Gold clusters correspond to particles smaller than 2 nm and they exhibit a rich array of interesting electronic, optical, chemical and catalytic properties.[112] This regime is distinct from the larger nanoparticles that are discussed in most of the other chapters in here. Häkkinen states gold clusters having a diameter less than 1.7 nm are expected to turn from "metallic'' to "semiconducting''.[113] Their work on the pseudo covalent bond between gold and sulfur on thiolate protected gold surfaces explains how

the covalent interaction between gold and sulfur forms, indicating that the gold-thiolate bond has strength close to the gold-gold bond.[114] This signifies that the gold-thiolate bond can significantly modify the gold–gold bonding at the gold–sulfur interface. A schematic representation of possible gold-sulfur interface is shown in Figure 1.9.

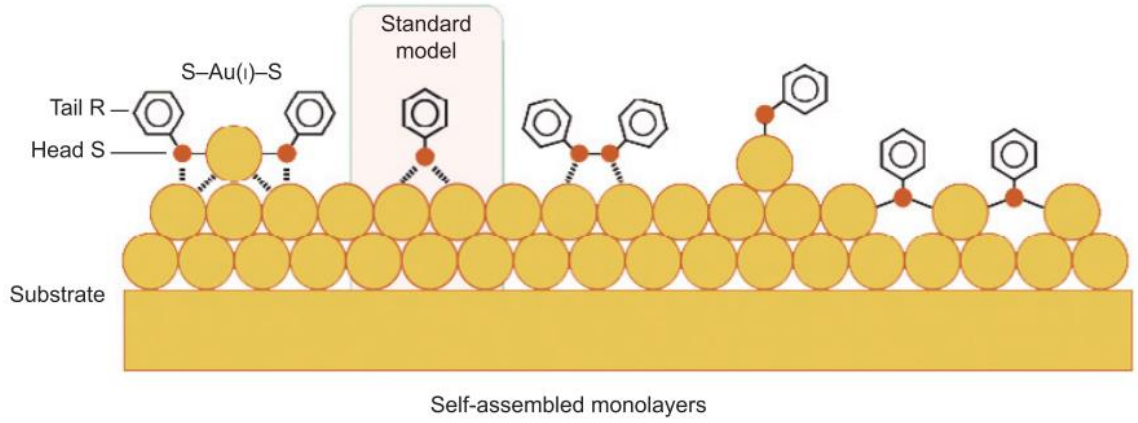

Figure 1.9 Over the past 20 years, several atomic structures for the gold–sulfur interface of the close-packed thiolate-SAM on Au(111) have been suggested. The 'standard model' describing a monothiolate binding at atop, bridge or hollow site on an unreconstructed Au(111) surface has been challenged by (from middle to right): disulfide bonding, a complex involving an Au adatom and a thiolate, and a polymeric chain structure where monothiolates are bridging Au adatoms. New experimental and theoretical evidence shows that a key structural unit in the low- and medium-coverage SAM layer may be the complex RS–Au(I)–SR where the bridging gold atom is in a formal oxidation state of +1 (left). Adapted from reference 114.

The gold-thiolate bond depends on the residual, since the six electrons of the S atom can lead to different hybrid orbitals manifest in the different ''oxidation states'' of S.[115] A recent review by Reimers *et al.* investigates gold–sulfur surfaces in nanoparticles and discusses about the computational methods to understand these interactions deeply.[116] An alternative arrangement occurs when the Au-d orbitals are involved in bonding with sulfur rather than the Au-s orbital (Figure 1.10). The presence of Au(0) thiyls actually stabilizes gold surfaces and nanoparticles.[117]

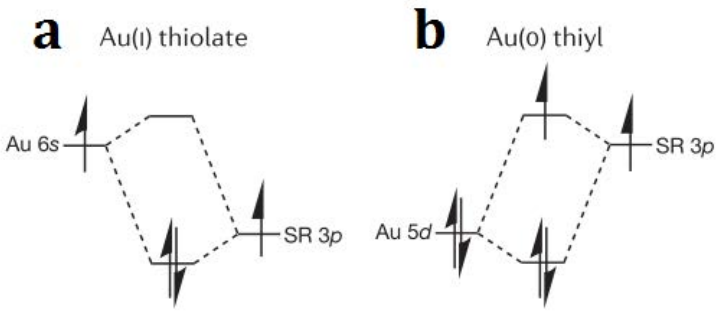

Figure 1.10 Gold-sulfur bonding: **a.** When gold uses its 6s orbitals to bond to SR, the system takes on Au(I)-thiolate character. **b.** If gold instead uses its 5d electrons when bonding to SR, a Au(0) thiyl forms. Adapted from reference 116.

Possible structures for gold surfaces and nanoparticles covered by organosulfur ligands indicated by Reimers and his colleagues are shown in Figure 1.11. RS-Au-SR motifs on the cluster surface are termed as the "staple" motif. Thiolated gold cluster assemblies that exhibit symmetric gold cores which are surrounded by adatom gold are referred as "staples".[82] Many computational examples on the formation of the "staples", both for gold clusters[118,119] and surfaces[120] exist up to date. This view of gold clusters is quite contrasting to previous models that proposed thiolates simply formed a protective layer on the cluster surfaces.[114] Further discussion on "staples" can be found in a review by De-en Jiang.[121]

The nature of the thiol bond has attracted significant literature debate, with some studies suggesting that gold atoms are formally oxidized by the addition of thiols,[118] while Reimers and others have suggested that the gold-sulfur bond is predominantly covalent.[114,122,123]

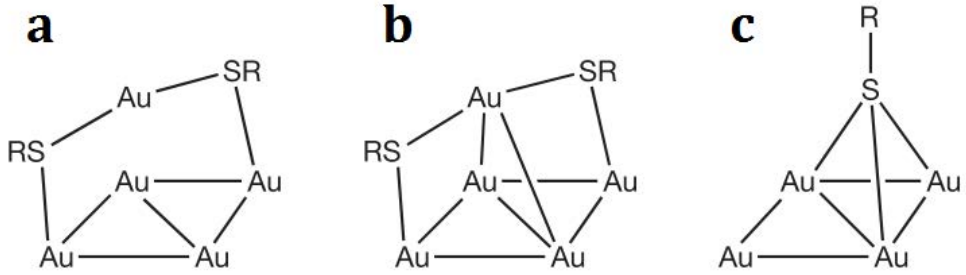

Figure 1.11 Diverse bonding motifs shown when gold surfaces bind organosulfur ligands. **a.** A typical representation of the "staple'' motif involving a Au adatom bonding to RS-decorated Au(111). **b.** The "staple'' motif needs to be replaced by depicting additional aurophilic interactions that serve to stabilize adatom binding. **c.** RS bound to three Au atoms in the face-centred cubic plane features four-coordinate S. Adapted from reference 116.

Velachi *et al.* performed atomistic Molecular Dynamics simulations to investigate the relationship between the arrangement of alkanethiols and the hydration properties of mixed SAMs constituted of equimolar alkanethiols of different lengths with either a hydrophilic or hydrophobic terminal functional group on AuNPs of different sizes.[124] Van Lehn and co-workers showed that particles with mixed, striped, and random morphologies exhibit similar behaviours (Figure 1.12) and atomistic Molecular Dynamics simulations indicate that long hydrophobic ligands always deform to allow shorter hydrophilic ligands to access water, leading to a significant distortion of the interface if the hydrophobic ligands are much longer than the hydrophilic ones. [125]

The gold parameters for coarse-grained methods should ensure the essential features necessary to adequately describe the chemistry and physics of the processes of interest.[18] As these methods are a simplified version because of the reduction in the system's degrees of freedom, care must be taken.

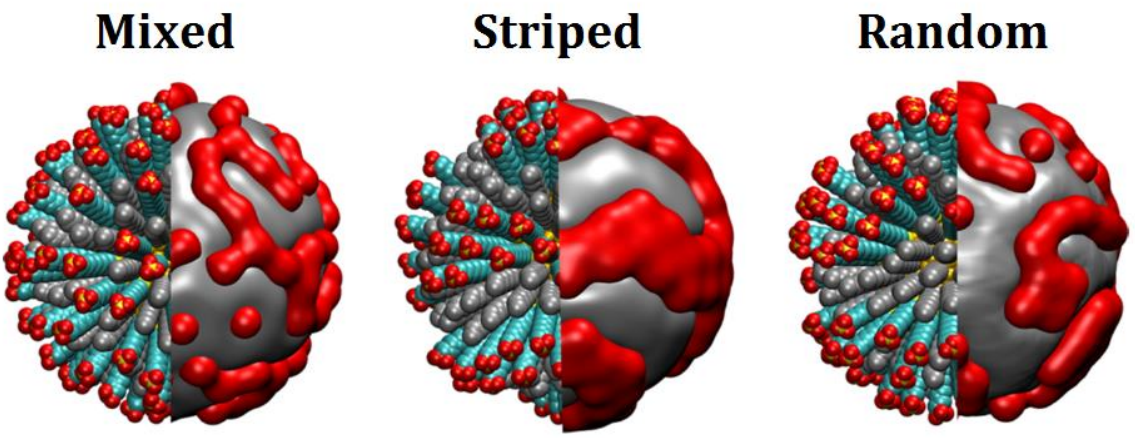

Figure 1.12 Three nanoscale morphologies corresponding to mixed, striped, and random surfaces. Hydrophilic (red) and hydrophobic (silver) ligands are partially drawn as surfaces to more clearly illustrate the difference between the nanoscale domains. The ligands represented the molecules 11-mercapto-1-undecanesulfonate (MUS) and 1-octanethiol (OT) as drawn, with 11 carbons in the backbone of the hydrophilic component and 8 carbons in the backbone of the hydrocarbon component. Adapted from reference 125.

Coarse-grained studies of functionalized AuNPs have gained considerable interest due to their advantage at modelling larger systems. Glotzer and co-workers have been working on the stripe morphology forms using coarse-grained methods and Molecular Dynamics.[69d,126] These conclusions were supported by other simulations performed on cylindrical surfaces by Glotzer[127,128] and others.[76,77] Glotzer's earliest work on patchy nanoparticles explains the minimalistic approach on these systems.[129] They modelled the AuNP surface as a sphere and simulated the AuNPs capped with alkanethiols, varying the length and the functional terminal group of the ligands, and the AuNP size. Gkeka *et al.* also used a coarse-grained model for AuNPs capped with hydrophilic and hydrophobic ligands.[130] They investigated nanoparticle membrane interactions as well as domains on these nanoparticles.[131,132] They demonstrated flexible hydrophobic and hydrophilic ligands arranged into striped domains in their simulations. The authors found that even when a stripe-like arrangement of the coarse-grained beads was imparted to the initial structure, the hydrophilic and hydrophobic areas tended to reorganize into homogeneous patterns. Şologan *et al.* recently published their work on coarse-grained

molecular simulations on large sets of mixed monolayer protected AuNPs.[133] The size of the nanoparticle is a determining factor in these systems. They stated that Janus domains are formed below 2 nm, whereas stripe-like domains spontaneously form for larger nanoparticles.[134]

1.5 References

1. R. P. Feynman, *Eng. Sci.* **1960**, *23*, 22-35.

2. N. Taniguchi, *On the Basic Concept of 'Nano-Technology'*, International Conference on Production Engineering, Tokyo, Japan, **1974**.

3. T.N.N. Initiative, Strategic Plan, **2004**.

4. G. Binnig, H. Rohrer, *IBM J. Res. Dev.* **1986**, *30*, 355-369.

5. G. Binnig, C. F. Quate, C. Gerber, *Phys. Rev. Lett.* **1986**, *56*, 930-933.

6. I. Freestone, N. Meeks, M. Sax, C. Higgitt, *Gold bull.* **2007**, *40*, 270-277.

7. U. Leonhardt, *Nat. Photon.* **2007**, *1*, 207-208.

8. P. Sciau, C. Mirguet, C. Roucau, D. Chabanne, M. Schvoerer, *JNanoR* **2009**, *8*, 133-139.

9. M. Vilarigues, P. Fernandes, L. C. Alves, R. C. da Silva, *Nucl. Instr. Meth. Phys. Res. B* **2009**, *267*, 2260-2264.

10. G. A. Ozin, *Adv. Mater.* **1992**, *4*, 612-649.

11. K. Ariga, M. Li, G. J. Richards, J. P. Hill, *J. Nanosci. Nanotechnol.* **2011**, *11*, 1-13.

12. W. McConnell, *J. Phys Chem. B* **2000**, *104*, 8925-8930.

13. K. L. Kelly, E. Coronado, L. L. Zhao, G. C. Schatz, *J. Phys Chem. B* **2003**, *107*, 668-677.

14. S. Link, M. A. El-Sayed, *Annu. Rev. Phys. Chem.* **2003**, *54*, 331-366.

15. J. D. Aiken, R. G. Finke, *J. Mol. Catal. A: Chem.* **1999**, *145*, 1-44.

16. C. Louis, O. Pluchery, *Gold Nanoparticles for Physics, Chemistry and Biology*, Imperial College Press, London, UK **2012**, pp. 1-4.

17. S. La Niece, *Gold*, Harvard University Press, Cambridge, Mass, United States **2012**, p. 10.

18. M. C. Daniel, D. Astruc, *Chem. Rev.* **2004**, *104*, 293-346.

19. J. M. de la Fuente, V. Grazu, *Nanobiotechnology: Inorganic Nanoparticles vs Organic Nanoparticles*, Elsevier, Amsterdam, Netherlands **2012**.

20. M. Faraday, *Philos. Trans.* **1857**, *147*, 145-181.

21. C. Lange, *Zeitschr. f. Chemotherap.* **1912**, *1*, 44.

22. J. Cruickshank, *Br J Exp Pathol.* **1920**, *1*, 71-88.

23. J. Patterson, *Br J Exp Pathol.* **1931**, *12*, 143-146.

24. J. Turkevich, P. C. Stevenson, J. Hillier, *Discuss. Faraday Soc.* **1951**, *11*, 55-75.

25. E. A. Hauser, J. E. Lynn, *Experiments in Colloid Chemistry*, McGraw-Hill, New York, United States **1940**.

26. G. Frens, *Colloid Polym. Sci.* **1972**, *250*, 736.

27. G. Frens, *Nature (London), Phys. Sci.* **1973**, *241*, 20.

28. J. Kimling, M. Maier, B. Okenve, V. Kotaidis, H. Ballot, A. Plech, *J. Phys. Chem. B* **2006**, *110*, 5700-5707.

29. N. G. Bastús, E. Sanchez-Tillo, S. Pujals, C. Farrera, C. Lopez, E. Giralt, A. Celada, J. Lloberas, V. Puntes, *ACS Nano* **2009**, *3*, 1335-1344.

30. E. Harrison, J. A Coulter, D. Dixon, *Nanomedicine* **2016**, *11*, 851-865.

31. M. Giersig, P. Mulvaney, *Langmuir* **1993**, *9*, 3408-3413.

32. M. Brust, M. Walker, D. Bethell, D. J. Schiffrin, R. J. Whyman, *J. Chem. Soc., Chem. Commun.* **1994**, 801-802.

33. M. Brust, J. Fink, D. Bethell, D. J. Schiffrin, C. Kiely, *J. Chem. Soc., Chem. Commun.* **1995**, 1655.

34. M. J. Hostetler, S. J. Green, J. J. Stokes, R. W. Murray, *J. Am. Chem. Soc.* **1996**, *118*, 4212.

35. A. C. Templeton, M. J. Hostetler, C. T. Kraft, R. W. Murray, *J. Am. Chem. Soc.* **1998**, *120*, 1906.

36. M. J. Hostetler, A. C. Templeton, R. W. Murray, *Langmuir* **1999**, *15*, 3782.

37. S. Banerjee, S. S. Wong, *Nano. Lett.* **2002**, *2*, 195.

38. T. K. Mandal, M. S. Fleming, D. R. Watt, *Nano. Lett.* **2002**, *2*, 3.

39. J. Kolny, A. Kornowski, H. Weller, *Nano. Lett.* **2002**, *2*, 361.

40. D. A. Giljohann, D. S. Seferos, W. L. Daniel, M. D. Massich, P. C. Patel, C. A. Mirkin, *Angew. Chem. Int. Ed.* **2010**, *49*, 3280.

41. C. Louis, O. Pluchery, *Gold Nanoparticles for Physics, Chemistry and Biology*, Imperial College Press, London, UK **2012**, p. 129.

42. E. Boisselier, D. Astruc, *Chem. Soc. Rev.* **2009**, *38*, 1759.

43. H. Haick, *J. Phys. D: Appl. Phys* **2007**, *40*, 7173.

44. A. Laguna, *Modern supramolecular gold chemistry: gold-metal interactions and applications*, John Wiley & Sons, Weinheim, Germany **2008**.

45. M. B. Cortie, *Gold bull.* **2004**, *37*, 12-19.

46. E. E. Connor, J. Mwamuka, A. Gole, C. J. Murphy, M. D. Wyatt, *Small* **2005**, *1*, 325.

47. A. M. Alkilany, C. J. Murphy, *J. Nanopart. Res.* **2010**, *12*, 2313-2333.

48. R. Elghanian, J. J. Storhoff, R. C. Mucic, R. L. Letsinger, C. A. Mirkin, *Science* **1997**, *277*, 1078-1081.

49. E. Casals, V. F. Puntes, *Nanomedicine* **2012**, *7*, 1917-1930.

50. R. A. Sperling, W. J. Parak, *Phil. Trans. R. Soc.* **2010**, *A368*, 1333-1383.

51. T. L. Moore, L. Rodriguez-Lorenzo, V. Hirsch, S. Balog, D. Urban, C. Jud, B. Rothen-Rutishauser, M. Lattuada, A. Petri-Fink, *Chem. Soc. Rev.* **2015**, *44*, 6287.

52. M. A. Dobrovolskaia, S. E. McNeil, *Nat Nanotechnol* **2007**, *2*, 469-478.

53. A. C. Templeton, W. P. Wuelfing, R. W. Murray, *Acc. Chem. Res.* **2000**, *33*, 27-36.

54. P. Ghosh, G. Han, M. De, C. K. Kim, V. M. Rotello, *Adv. Drug Deliv. Rev.* **2008**, *60*, 1307-1315.

55. C. D. Medley, J. E. Smith, Z. Tang, Y. Wu, S. Bamrungsap, W. H. Tan, *Anal. Chem.* **2008**, *80*, 1067.

56. P. Sharma, S. Brown, G. Walter, S. Santra, B. Moudgil, *Adv. Colloid Interface Sci.* **2006**, *123-126*, 471-485.

57. P. V. Baptista, M. Koziol-Montewka, J. Paluch-Oles, G. Doria, R. Franco, *Clin. Chem.* **2006**, *52*, 1433-1434.

58. R. Sperling, P. Gil, F. Zhang, *Chem. Soc. Rev.* **2008**, *37*, 1896-1908.

59. J. Gbadamosi, A. Hunter,S. Moghimi, *FEBS Lett*. **2002**, *532*, 339.

60. J. M. Bergen, H. A. Von Recum, T. T. Goodman, A. P. Massey, S. H. Pun, *Macromol. Biosci.* **2006**, *6*, 506-516.

61. G. F. Paciotti, L. Myer, D. Weinreich, D. Goia, N. Pavel, R. E. McLaughlin, L. Tamarkin, *Drug Deliv.* **2004**, 11, 169-183.

62. J. Comenge, V. F. Puntes, *ScienceOpen Research* **2015**, 1-10.

63. K. Avgoustakis, A. Beletsi, Z. Panagi, P. Klepetsanis, A. G. Karydas, D. S. Ithakissios, *J. Control. Release* **2002**, *79*, 123-135.

64. X. Xia, M. Yang, Y. Wang, Y. Zheng, Q. Li, J. Chen, Y. Xia, *ACS Nano* **2011**, *6*, 512-522.

65. V. Puntes, *Br J Radiol* **2015**, *89*.

66. J. C. Love, L. A. Estroff, J. K. Kriebel, R. G. Nuzzo, G. M. Whitesides, *Chem. Rev.* **2005**, *105*, 1103-1169.

67. E. Colangelo, J. Comenge, D. Paramelle, M. Volk, Q. Chen, R. Lévy, *Bioconjug. Chem.* **2016**, acs.bioconjchem.6b00587.

68. A. M. Jackson, J. W. Myerson, F. Stellacci, *Nat. Mater.* **2004**, *3*, 330-336.

69. **a.** A. M. Jackson, Y. Hu, P. J. Silva, F. Stellacci, *J. Am. Chem. Soc.* **2006**, *128*, 11135-11149. **b.** A. Centrone, Y. Hu, A. M. Jackson, G. Zerbi, F. Stellacci, *Small* **2007**, *3*, 814-817. **c.** G. A. DeVries, M. Brunnbauer, Y. Hu, A. M. Jackson, B. Long, B. T. Neltner, O. Uzun, B. H. Wunsch, F. Stellacci, *Science* **2007**, *315*, 358-361. **d.** C. Singh, P. K. Ghorai, M. A. Horsch, A. M. Jackson, R. G. Larson, F. Stellacci, S. C. Glotzer, *Phys. Rev. Lett.* **2007**, *99*, 226106. **e.** R. P. Carney, G. A. DeVries, C. Dubois, H. Kim, J. Y. Kim, C. Singh, P. K. Ghorai, J. B. Tracy, R. L. Stiles, R. W. Murray, S. C. Glotzer, F. Stellacci, *J. Am. Chem. Soc.* **2008**, *130*, 798-799. **f.** A. Centrone, E. Penzo, M. Sharma, J. W. Myerson, A. M. Jackson, N. Marzari, F. Stellacci, *Proc. Natl. Acad. Sci. USA* **2008**, *105*, 9886-9891. **g.** G. A. DeVries, F. R. Talley, R. P. Carney, F. Stellacci, *Adv. Mater.* **2008**, *20*, 4243-4247. **h.** Y. Hu, O. Uzun, C. Dubois, F. Stellacci, *J. Phys. Chem. C* **2008**, *112*, 6279-6284. **i.** O. Uzun, Y. Hu, A. Verma, S. Chen, A. Centrone, F. Stellacci, *Chem. Commun.* **2008**, 196-198. **j.** A. Verma, O. Uzun, Y. H. Hu, Y. Hu, H. S. Han, N. Watson, S. L. Chen, D. J. Irvine, F. Stellacci, *Nat. Mater.* **2008**, *7*, 588-595. **k.** Y. Hu, B. H. Wunsch, S. Sahni, F. Stellacci, *J. Scanning Probe Microsc.* **2009**, *4*, 24. **l.** J. K. Kuna, K. Voitchovsky, C. Singh, H. Jiang, S. Mwenifumbo, P. K. Ghorai, M. M. Stevens, S. C. Glotzer, F. Stellacci, *Nat. Mater.* **2009**, *8*, 837-842. **m.** C. M. Jewell, J. M. Jung, P. U. Atukorale, R. P. Carney, F. Stellacci, D. J. Irvine, *Angew. Chem. Int. Ed.* **2011**, *50*, 12312-12315. **o.** E. S. Cho, J. Kim, B. Tejerina, T. M. Hermans, H. Jiang, H. Nakanishi,

M. Yu, A. Z. Patashinski, S. C. Glotzer, F. Stellacci, B. A. Grzybowski, *Nat. Mater.* **2012**, *11*, 978-985.

70. Y. Cesbron, C. P. Shaw, J. P. Birchall, P. Free, R. Lévy, *Small* **2012**, *8*, 3714-3719.

71. J. Stirling, I. Lekkas, A. Sweetman, P. Djuranovic, Q. Guo, B. Pauw, J. Granwehr, R. Lévy, P. Moriarty, *PLoS One* **2014**, *9*, e108482.

72. R. Zhachuk, S. Pereira, *Phys. Rev. B* **2009**, *79*.

73. R. Toomes, J. Kang, D. Woodruff, M. Polcik, M. Kittel, J. T. Hoeft, *Surf. Sci.* **2003**, *522*,1-3.

74. M. Yu, F. Stellacci, Small **2012**, *8*, 3720-3726.

75. Q. K. Ong, F. Stellacci, *PLoS One* **2015**, *10*, e0135594.

76. S. A. Egorov, *Soft Matters* **2012**, *8*, 3971-3979.

77. W. L. Miller, B. Bozorgui, K. Klymko, A. Cacciuto, *J. Chem. Phys.* **2011**, *135*, 244902-244905.

78. E. Edlund, O. Lindgren, M. N. Jacobi, *Soft Matter* **2014**, *10*, 2955-2960.

79. M. Azubel, J. Koivisto, S. Malola, D. Bushnell, G. L. Hura, A. L. Koh, H. Tsunoyama, T. Tsukuda, M. Pettersson, H. Häkkinen, R. D. Kornberg, *Science* **2014**, *345*, 909.

80. https://plato.stanford.edu/entries/simulations-science/#EpiComSim

81. A. Leifert, Y. Pan-Bartnek, U. Simon, W. Jahnen-Dechent, *Nanoscale* **2013**, *5*, 6224.

82. P. Charchar, A. J. Christofferson, N. Todorova, I. Yarovsky, *Small* **2016**, *12*, 2395-2418.

83. Z. Wu, J. Liu, Y. Li, Z. Cheng, T. Li, H. Zhang, Z. Lu, B. Yang, *ACS Nano* **2015**, *9* ,6315.

84. S. M. Neidhart, B. M. Barngrover, C. M. Aikens, *ChemPhysChem* **2015**, *17*, 7676.

85. H. Yang, Y. Wang, J. Lei, L. Shi, X. Wu, V. Mäkinen, S. Lin, Z. Tang, J. He, H. Häkkinen, L. Zheng, N. Zheng, *J. Am. Chem. Soc.* **2013**, *135*, 9568.

86. V. G. Yarzhemsky, M. A. Kazaryan, N. A. Bulychev, E. N. Muraviev, Y. A. Dyakov, O. K. Kosheleva, C. H. Chen, *J. Nanotechnol. Diagn. Treat.* **2014**, *2*, 27.

87. A. Trinchero, S. Klacar, L. O. Paz-Borbón, A. Hellman, H. Grönbeck, *J. Phys. Chem. C* **2015**, *119*, 10797.

88. C. L. Heinecke, T. W. Ni, S. Malola, V. Mäkinen, O. A. Wong, H. Häkkinen, C. J. Ackerson, *J. Am. Chem. Soc.* **2012**, *134*, 13316.

89. J. Zhong, X. Tang, J. Tang, J. Su, Y. Pei, *J. Phys. Chem. C* **2015**, *119*, 9205.

90. N. Takagi, K. Ishimura, M. Matsui, R. Fukuda, T. Matsui, T. Nakajima, M. Ehara, S. Sakaki, *J. Am. Chem. Soc.* **2015**, *137*, 8593.

91. E. Fertitta, E. Voloshina, B. Paulus, *J. Comput. Chem.* **2014**, *35*, 204.

92. D. Mollenhauer, N. Gaston, E. Voloshina, B. Paulus, *J. Phys. Chem. C* **2013**, *117*, 4470.

93. R. Ouyang, J. Yan, P. S. Jensen, E. Ascic, S. Gan, D. Tanner, B. Mao, L. Niu, J. Zhang, C. Tang, N. S. Hush, J. R. Reimers, J. Ulstrup, *ChemPhysChem* **2015**, *16*, 928.

94. S. J. Marrink, A. H. de Vries, A. E. Mark, *J. Phys. Chem. B* **2004**, *108*, 750-760.

95. S. J. Marrink, H. J. Risselada, S. Yefimov, D. P. Tieleman, A. H. de Vries, *J. Phys. Chem. B* **2007**, *111*, 7812-7824.

96. J. Dong, J. Li, J. Zhou, *Langmuir* **2014**, *30*, 5599.

97. H. Chan, P. Král, *Nanoscale* **2011**, *3*, 1881.

98. F. Simonelli, D. Bochicchio, R. Ferrando, G. Rossi, *J. Phys. Chem. Lett.* **2015**, *6*, 3175.

99. J. Q. Lin, Y. G. Zheng, H. W. Zhang, Z. Chen, *Langmuir* **2011**, *27*, 8323.

100. B. Song, H. J. Yuan, S. V. Pham, C. J. Jameson, S. Murad, *Langmuir* **2012**, *28*, 16989.

101. E. L. da Rocha, G. F. Caramori, C. R. Rambo, *Phys. Chem. Chem. Phys.* **2013**, *15*, 2282.

102. J. Lin, A. Alexander-Katz, *ACS Nano* **2013**, *7*, 10799.

103. R. C. Van Lehn, A. Alexander-Katz, *Soft Matter* **2011**, *7*, 11392.

104. F. Tavanti, A. Pedone, M. C. Menziani, *New J. Chem.* **2015**, *39*, 2474.

105. F. Tavanti, A. Pedone, M. C. Menziani, *J. Phys. Chem. C* **2015**, *119*, 22172.

106. P. A. Oroskar, C. J. Jameson, S. Murad, *Langmuir* **2015**, *31*, 1074.

107. M. Levitt, A. Warshel, *Nature* **1975**, *253*, 694-698.

108. A. Warshel, M. Levitt, *J. Mol. Biol.* **1976**, *103*, 227-249.

109. M. Levitt, *Angew. Chem. Int. Ed.* **2014**, *53*, 10006-10018.

110. F. De Proft, P. Geerlings, *Chem. Rev.* **2001**, *101*, 1451.

111. S. Malola, H. Häkkinen, *Europhys. News* **2015**, *46*, 23.

112. H. Häkkinen, *Chem. Soc. Rev.* **2008**, *37*, 1847-1859.

113. C. Louis, O. Pluchery, *Gold Nanoparticles for Physics, Chemistry and Biology*, Imperial College Press, London, UK **2012**, p. 235.

114. H. Häkkinen, *Nat. Chem.* **2012**, *4*, 443-455.

115. S. Letardi, F. Cleri, *J. Chem. Phys.* **2004**, *120*, 10062-10068.

116. J. R. Reimers, M. J. Ford, S. M. Marcuccio, J. Ulstrup, *Nat. Rev. Chem.* **2017**, *1*, 0017.

117. J. R. Reimers, M. J. Ford, A. Halder, J. Ulstrup, N. S. Hush, *Proc. Natl Acad. Sci. USA* **2016**, *113*, E1424-E1433.

118. B. M. Barngrover, C. M. Aikens, *J. Phys. Chem. A* **2013**, *117*, 5377.

119. V. Rojas-Cervellera, E. Giralt, C. Rovira, *Inorg. Chem.* **2012**, *51*, 11422.

120. M. Askerka, D. Pichugina, N. Kuz'menko, A. Shestakov, *J. Phys. Chem. A* **2012**, *116*, 7686.

121. D. E. Jiang, *Nanoscale* **2013**, *5*, 7149.

122. J. R. Reimers, Y. Wang, B. O. Cankurtaran, M. J. Ford, *J. Am. Chem. Soc.* **2010**, *132*, 8378.

123. J. Yan, R. Ouyang, P. S. Jensen, E. Ascic, D. Tanner, B. Mao, J. Zhang, C. Tang, N. S. Hush, J. Ulstrup, J. R. Reimers, *J. Am. Chem. Soc.* **2014**, *136*, 17087.

124. V. Velachi, D. Bhandary, J. K. Singh, M. N. D. S. Cordeiro, *J. Phys. Chem. C* **2015**, *119*, 3199-3209.

125. R. C. Ran Lehn, A. Alexander-Katz, *J. Phys. Chem. C* **2013**, *117*, 20104-20115.

126. S. C. Glotzer, M. Solomon, *Nat. Mater.* **2007**, *6*, 557-562.

127. C. Singh, Y. Hu, B. P. Khanal, E. R. Zubarev, F. Stellacci, S. C. Glotzer, *Nanoscale* **2011**, *3*, 3244-3250.

128. P. K. Ghorai, S. C. Glotzer, *J. Phys. Chem. C* **2010**, *114*, 19182-19187.

129. Z. Zhang, S. C. Glotzer, *Nano Lett.* **2004**, *4*, 1407-1413.

130. P. Gkeka, L. Sarkisov, P. Angelikopoulos, *J. Phys. Chem. Lett.* **2013**, *4*, 1907-1912.

131. J. P. P. Ramalho, P. Gkeka, L. Sarkisov, *Langmuir* **2011**, *27*, 3723-3730.

132. P. Gkeka, P. Angelikopoulos, *Curr. Nanosci.* **2011**, *7*, 690-698.

133. M. Şologan, D. Marson, S. Polizzi, P. Pengo, S. Boccardo, S. Pricl, P. Posocco, L. Pasquato, *ACS Nano* **2016**, *10*, 9316-9325.

134. P. Posocco, C. Gentilini, S. Bidoggia, A. Pace, P. Franchi, M. Lucarini, M. Fermeglia, S. Pricl, L. Pasquato, *ACS Nano* **2012**, *6*, 7243-7253.

Chapter 2

OBJECTIVES

Chapter 2

OBJECTIVES

As explained in the introduction, a better understanding of the interactions happening on the surface of gold at nanoscale is needed. Despite the significant recent advancements, current experimental techniques have their own limitations. The work done so far by different research groups has had controversial reactions from the field. Our aim is to find a different approach to investigate this problem.

The main objectives of this dissertation are listed below:

- To gain a basic knowledge of computational chemistry;
- To adapt an in house mesoscopic method using Dissipative Particle Dynamics (DPD), to be able to work with nanomaterials;
- To investigate possible coarse-grained methods for simulating large scale events, such as gold nanoparticles caped with ligands, which has its limitations with other methods;
- To gain a deeper understanding on gold nanoparticle conjugates by computational studies with the help of working closely with several experimental groups;
- To simulate gold nanoparticle conjugates and to understand the reason of the conformational changes happening on their surface.

Chapter 3

MESOSCOPIC MODEL AND SIMULATION METHODS

Chapter 3

MESOSCOPIC MODEL AND SIMULATION METHODS

Theoretical and computational approaches are complementing experiments at multiple time scales, length scales and levels of detail that is not achievable in the laboratory. In this direction, computational chemistry is expanding dramatically over the years. The rapid evolution of computers has a big impact on this expansion.

The use of computational methods in a variety of simulation techniques has proven to be a valuable tool in chemistry. Moreover, they can be compared to experimental data to verify the theory. We need to keep in mind that it is crucial to choose the right method based on the problem addressed.

Of the computational approaches available, those based on Quantum Mechanics provide information about molecular systems via their explicit consideration of the electronic structure, and include the wave function[1] and density functional theory (DFT).[2] These methods can be used to accurately calculate electronic and chemical properties including binding energies and chemical reaction barriers. However, these techniques are computationally demanding, and their applications are, therefore, limited by the system size.

On the contrary, those approaches based on Classical Mechanics create a molecular model based on spheres and springs.[3] This simplification of the reality needs the use of equations based on classical mechanics to obtain the energy associated to the

structure, which in turn need lots of parameters. Nevertheless, these methods allow to conformationally study much larger systems but reactivity and reaction barriers are out of their scope. Among these methods, probably Molecular Dynamics and Monte Carlo are the most widely used. The big advantage of Molecular Dynamics over Monte Carlo is that it gives a route to dynamical properties of the system: transport coefficients, time-dependent responses to perturbations, rheological properties and spectra.[4]

Additionally, there is a whole range of hybrid techniques which combine features from both, quantum and classical. These hybrid methods use quantum chemistry to study the reactive zone, or that zone that contains important electronic effects, and molecular mechanics to study the rest of the system. Figure 1 describes the differences between all these methods and shows the properties that can be achieved by each method.

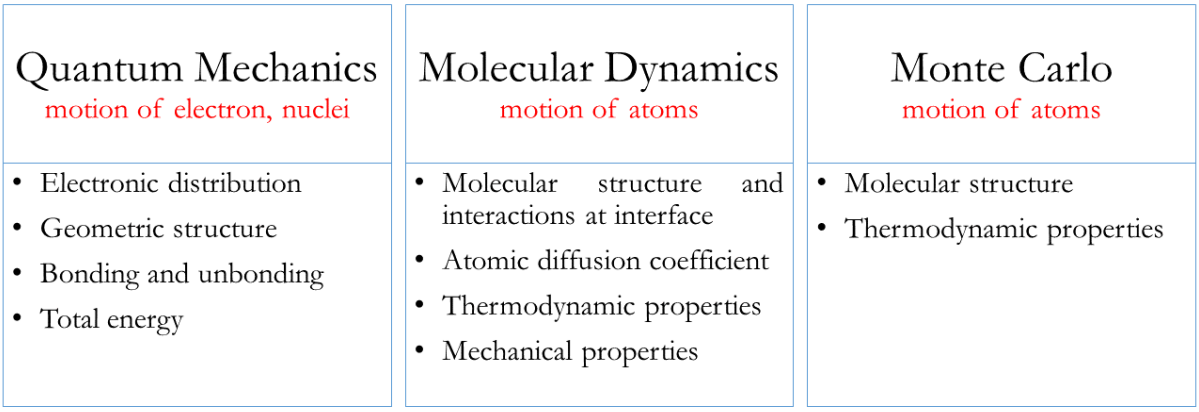

Figure 3.1 Most commonly used simulation methods and typical properties predicted from each of them.

Also, the coarse-gained model that was used in our simulation studies is introduced in this chapter. Coarse-grained methods provide an alternative route to deal with the length and time scale issues. In coarse-grained simulations, sets of atoms are simplified which allows much faster and cheaper simulations.

Current computational techniques have all been used to gain better understanding of the interactions and dynamics of nanoparticles within biological systems.[5] Working

side by side with experimentalist, computational methods are here to improve our knowledge. We are going to explore these methods deeply in this section.

3.1 Molecular Dynamics Simulations

Computer simulations are very popular in the hope of understanding the properties of complex systems. They serve as a complement to conventional experiments, enabling us to learn something new and something that cannot be found out in other ways. It has been a long time since the first article on Molecular Dynamics of a macromolecule of biological interest has been published.[6] Since then, the realm of Molecular Dynamics has grown tremendously.

In Molecular Dynamics, the time evolution of a system is simulated by numerically integrating Newton's equations of motion. To have an idea of how Molecular Dynamics works there is no better way than following Frenkel and Smit's description:

"Molecular Dynamics simulations are in many respects very similar to real experiments. When we perform a real experiment, we proceed as follows. We prepare a sample of the material that we wish to study. We connect this sample to a measuring instrument (e.g., a thermometer, manometer, or viscosimeter), and we measure the property of interest during a certain time interval. If our measurements are subject to statistical noise (as most measurements are), then the longer we average, the more accurate our measurement becomes. In a Molecular Dynamics simulation, we follow exactly the same approach. First, we prepare a sample: we select a model system consisting of N particles and we solve Newton's equations of motion for this system until the properties of the system no longer change with time (we equilibrate the system). After equilibration, we perform the actual measurement. In fact, some of the most common mistakes that can be made when performing a computer experiment are very similar to the mistakes that can be made in real experiments (e.g., the sample is not prepared correctly, the measurement is too short, the system undergoes an irreversible change during the experiment, or we do not measure what we think)."[7]

Molecular Dynamics simulations are based on Newton's equations of motion by solving the differential equations embodied in Newton's second law.[8] It is possible to obtain a trajectory that describes the atomic positions as they progress over time. All-atom simulations rely on the fundamental forces that govern atomic motion. Forces between atoms are defined by a force field, adhering to the chemical interactions of the specific atoms involved. These force fields describe bond stretching, bending and rotation as well as the non-bonded interactions, including electrostatic and van der Waals interactions.[9] It is crucial to choose the right force field as they determine the end result.[10]

To bridge the gap between atomistic simulations and large scale macroscopic network simulations, an intermediate simulation technique aimed at a length scale larger than the atomistic scale, but smaller than the network connection scale is the key to overcome the difficulties faced by conventional methods (Figure 3.2).[11] One possible method of bridging this gap is the use of mesoscopic models. Coarse-grained models treat sets of atoms as one group and waive the atomistic detail in favour of reducing the number of degrees of freedom.[12] Properties defined on a smaller length-scale than an effective cross-link, like how many chains are joined together in a micelle, cannot be predicted in on larger length-scales. Besides, hydrodynamic interactions are not accounted for while in mesoscopic simulations the hydrodynamic behaviours are captured easily using continuum methods. Dissipative Particle Dynamics (DPD) is a promising technique to overcome these problems. DPD is a potentially powerful and simple mesoscopic approach, which facilitates the simulation of the statics and dynamics of complex fluids and soft matter systems at physically interesting length and time scales.

The advantage of Molecular Dynamics methods is the ability to determine the structure and dynamics of complex systems with atomic detail, but this takes a long time in larger systems. Many biological processes occur over longer periods of time and require modelling of larger systems, thus more simplistic techniques, such as the coarse-grained methods need to be applied.

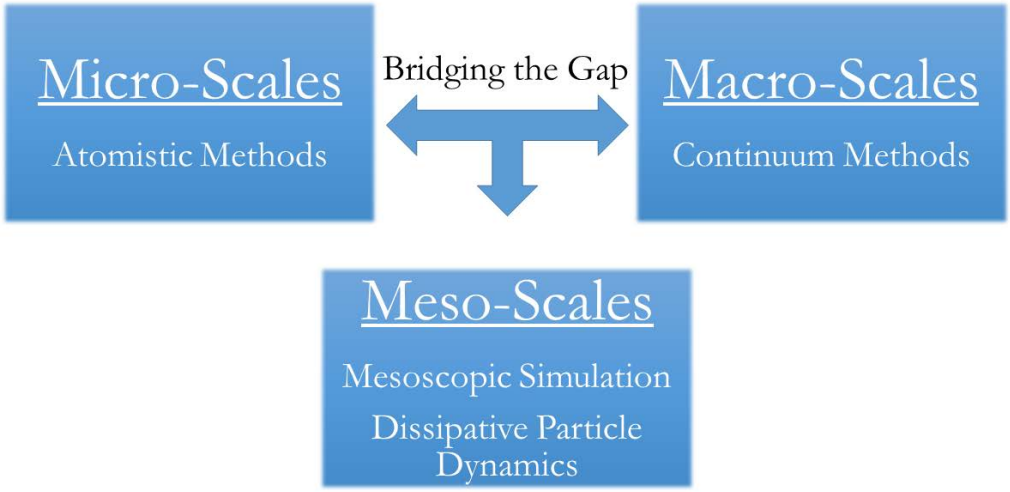

Figure 3.2 Dissipative Particle Dynamics is a mesoscale technique for bridging the gap between the micro- and macro-scales.

3.2 Coarse-Grained Model

Traditional all-atom models are inadequate to simulate large systems. Coarse-grained models neglect some of the atomistic degrees of freedom and allow for a significant increase over the limitations of all-atom models.[13,14] A reduction of the degrees of freedom for particles leads to an acceleration of computation times. However, it can be interpreted as an oversimplification of the system because of neglecting atomistic details.

A general procedure in coarse-graining usually involves:

1. Defining the goal and determining the degree of coarse-graining;

2. Mapping an atomistic model to a coarse-grained model;

3. Interaction between the coarse-grained particles;

4. Reproducing target functions by the coarse-grained model;

5. Optimizing parameters/functions in the coarse-grained model;

6. Conducting coarse-grained simulations.

Mapping an atomistic model to a coarse-grained model is very important in defining the positions of coarse-grained particles and it directly influences the parameterization.

Replacing atomistic details with lower resolution, coarse-grained, beads has opened a new way to simulate large-scale biomolecular processes on time scales inaccessible to all-atom models.[15] In coarse-grained simulations, sets of atoms are grouped together to one bead, which allows faster computation, and this has been used to probe biologically relevant time and length scales.[16,17,18] Roughly three heavy atoms are considered as one bead in our simulations. It is shown that these models were successful in predicting bulk material properties as well as in describing molecular level phenomena.[19,20,21] Coarse-grained particles or beads are defined as groups of atoms of common chemistries, like methyl or carbonyl groups where the bead composition, topology and interaction parameters are chosen to mimic the inherent chemistry of the atoms (Figure 3.3).

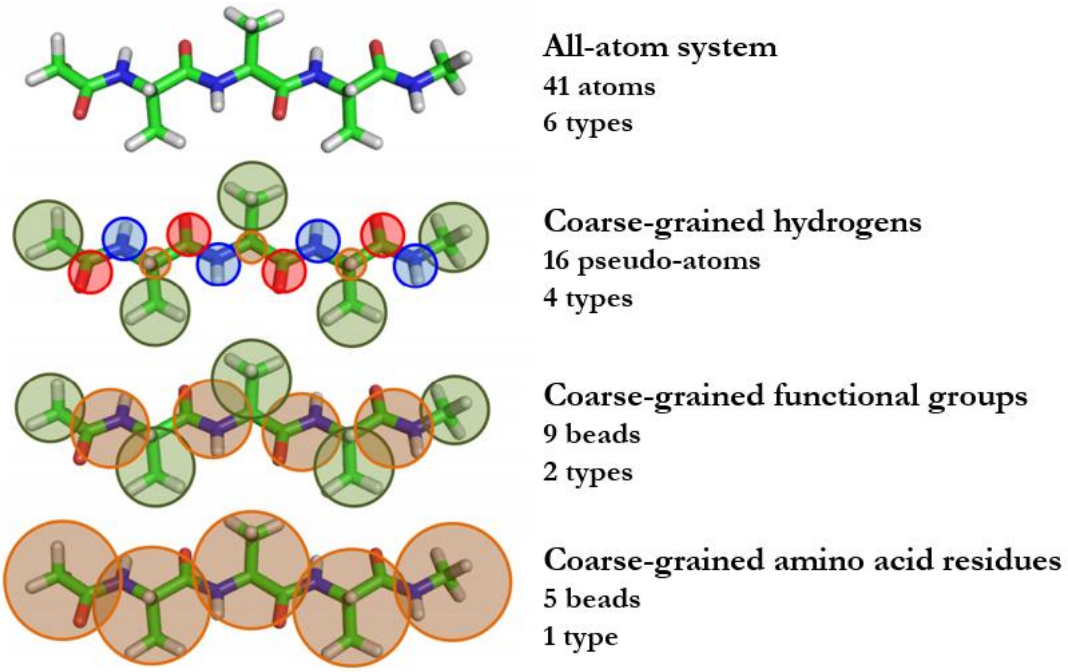

Figure 3.3 Example of polyalanine showing the different approaches of coarse-grained particles as beads comparing to all-atom method. Adapted from reference 22.

The coarse-grained model used in this study is developed by Berend Smit's team for simple bilayer systems[23,24] and later improved by de Meyer *et al.*[25] and Benjamini & Smit[26] for bilayer inclusions such as cholesterol and transmembrane proteins. The model originally works with soft and purely repulsive potentials for lipid bilayer systems. In their article where they explain the effect of cholesterol on lipid-mediated protein-protein interactions[25], two kinds of beads are designed to construct lipids; a hydrophilic bead that has relatively favourable interactions with a solvent, and a hydrophobic bead that has relatively unfavourable interactions with a solvent (Figure 3.4.a). This model represents the simplest of design principles required to assemble a lipid bilayer and other surfactant assemblies. One water bead comprises three water molecules. Coarse-grained models of phospholipid and cholesterol are shown in Figure 3.4 b and c where each bead represents an average of three heavy atoms. The phospholipid model contains hydrophilic head beads and a hydrophobic tail whereas the cholesterol model contains a hydrophilic head bead and a hydrophobic ring to which a tail of two hydrophobic beads is attached. The non-bonded interactions between beads are described with soft-repulsive interactions, in Figure 3.4.d a full table of the repulsion values are shown. Non-bonded and bonded interactions will be discussed in the following subsections.

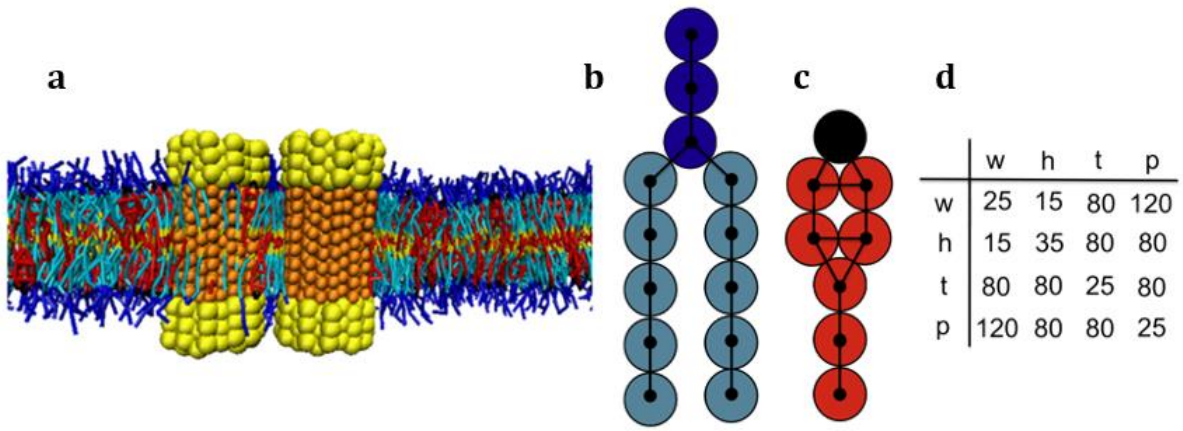

	w	h	t	p
w	25	15	80	120
h	15	35	80	80
t	80	80	25	80
p	120	80	80	25

Figure 3.4 The Coarse-grained model and soft-repulsive interaction parameters from Smit's article. **a.** Snapshot of a model bilayer containing phospholipids and cholesterol. Hydrophilic (type h) and hydrophobic (type p) beads are in yellow and orange respectively. **b.** Coarse-grained model of phospholipid. Hydrophilic head beads (type h) are in dark blue and hydrophobic tail beads (type t) are in light blue. **c.** Coarse-grained model of cholesterol. Hydrophilic head beads (type h) are in black hydrophobic

tail beads (type t) red. **d.** Table with the soft-repulsive interaction parameters between the four types of beads: water (w), hydrophilic (h), hydrophobic (t), hydrophobic protein bead (p). Adapted from reference 25.

The model we use in our laboratory is based on Smit's model with some adaptations to specific needs. Certain modifications are needed to adjust the hydrophilic and hydrophobic character of the different beads in our system. The detailed description of our model is explained in Chapter 4.

3.3 The MARTINI Force Field

One of the most popular coarse-grained modelling technique is the famous MARTINI force field model developed by the groups of Marrink and Tieleman.[27,28,29] The name "Martini" was coined in 2007.[28] Martini is the nickname of the city of Groningen in the Netherlands where the force field was developed and where its development continues to date. The nickname is coming from the famous landmark in the city; the 100m high Martini tower.

The MARTINI model is based on a four-to-one mapping, i.e., on average four heavy atoms are represented by a single coarse-grained bead, with an exception for ring-like molecules.[28] The four-to-one mapping was chosen as an optimum between computational efficiency and chemical representability. Ring-like molecules are mapped with higher resolution up to two non-hydrogen atoms to one bead. The model considers four main types of interaction sites: polar, non- polar, apolar, and charged. Within these categories, the particles differ based on hydrogen bonding capability and/or degree of polarity. The mapping of representative biomolecules is shown in Figure 3.5.

The beads have a fixed size and interact using an interaction map with 10 different strengths.[15] Both van der Walls and electrostatic interactions are described using shifted Lennard-Jones potentials and the electrostatics is screened with a relative dielectric constant. Bonds and bond angles are described with harmonic potentials. Parameters were tuned to match thermodynamic and structural data from experimental as well as atomistic simulations of several systems.

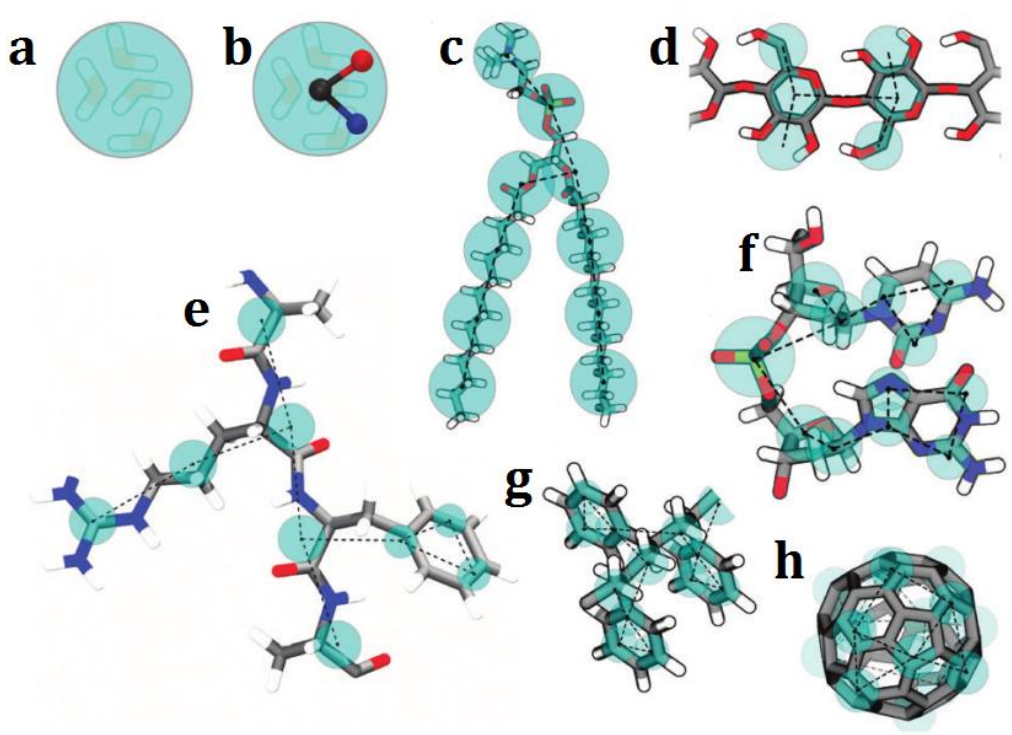

Figure 3.5 MARTINI mapping of coarse-grained particles shown as cyan transparent beads overlaying **a**. Standard water particle representing four water molecules. **b.** Polarizable water molecule with embedded charges. **c.** A dimyristoyl phosphatidylcholine molecule. **d.** Polysaccharide fragment. **e.** Peptide. **f.** DNA fragment. **g.** Polystyrene fragment. **h.** Fullerene molecule. Adapted from reference 30.

The overall aim of the MARTINI coarse-graining approach is to provide a simple model that is computationally fast and easy to use, yet flexible enough to be applicable to a large range of biomolecular systems. The MARTINI model has developed from a model for simulations of lipids and surfactants to the most widely-used coarse-grained force field for biomolecular simulations and increasingly in synthetic biology.[30]

3.4 Dissipative Particle Dynamics

DPD is an alternative method to the mesoscopic complex fluid simulation method developed by Hoogerbrugge and Koelman[31] at 1992 for simulating hydrodynamic

behaviour. They demonstrated that their original DPD scheme obeys the Navier–Stokes equations.[32,33] This technique was conceived as an improvement over conventional Molecular Dynamics in order to describe complex hydrodynamic behaviour with computational efficiency. Important contributions to the methodology were added by Español and Warren,[34,35] such as describing relationship between the magnitude of the dissipative and random forces. They studied the fluctuation dissipation theorem and its connection with this method. DPD has several advantages: Firstly, it exhibits hydrodynamic behaviour. Secondly, it has thermal fluctuations that can drive Brownian motions. Thirdly, it is cheap to simulate. We should also keep in mind that DPD is suitable for simulating systems that contain a large number of atoms in nanosecond time and nanometer length scales.[11,36]

The original DPD simulations consist of a collection of soft repelling frictional and noisy balls. In this direction, we can say that DPD is a coarse-grained method of Molecular Dynamics where atoms are grouped together up to one mesoscopic bead, defined as groups of atoms of common chemistries like methyl or carbonyl groups. The beads allow large time scale simulations as they are a simplification of the overall system. By coarse graining of each bead, one can reach larger time and length scales in DPD compared with regular Molecular Dynamics.

The basic elements of the DPD algorithm are very similar to the Molecular Dynamics algorithm. In addition to the conservative force acting between particles, the total force on a particle *i* also contains a dissipative force and a random force (Figure 3.6). The reason behind introducing dissipation and random forces into a Molecular Dynamics simulation is to conserve momentum locally and ensure correct hydrodynamic behaviour. The dissipative force and random force act together to maintain an essentially constant temperature with small fluctuations around the nominal temperature.

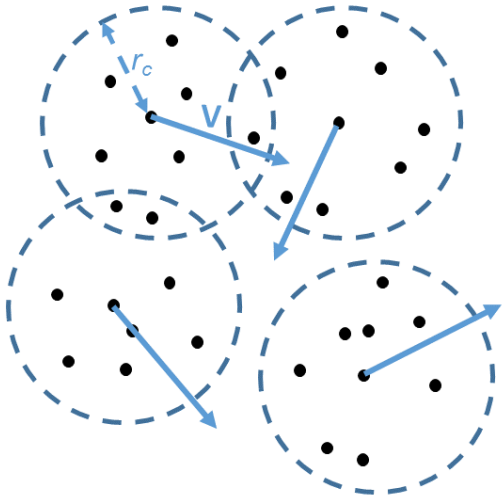

Figure 3.6 The particles have continuous positions and interact through pairwise forces that contain a conservative, a dissipative and a random part in DPD method.

The system consists of a set of particles, whose time evolution is described by Newton's equations of motion

$$\frac{d\boldsymbol{r}_i}{dt} = \boldsymbol{V}_i, \frac{d\boldsymbol{V}_i}{dt} = \boldsymbol{f}_i \,. \tag{3.1}$$

Up to this point, there is no difference to conventional Molecular Dynamics. It is the definition of the forces that makes DPD different from Molecular Dynamics. The masses of the particles are put at one for simplicity. In this way, the force acting on a particle equals its acceleration. Forces acting on each bead are defined as following

$$\boldsymbol{f}_i = \sum_{i \neq j} (\mathbf{F}_{ij}^C + \mathbf{F}_{ij}^D + \mathbf{F}_{ij}^R) \,, \tag{3.2}$$

where the sum runs over all other particles within a certain cutoff radius r_c. $\mathbf{F}_{ij}^C$ is the conservative force and is linear in the bead–bead separation which is usually chosen to be a pair potential between particles for non-bonded and bonded interactions that only

depends on the position of atoms relative to each other and not their velocities. The remaining two forces are a dissipative force and a random force. $\boldsymbol{F}_{ij}^{D}$ is the dissipative force and is proportional to the relative velocity of beads *i* and *j*; and $\mathbf{F}_{ij}^{R}$ is the random force between bead *i* and its neighboring bead *j*. The dissipative force represents a viscous force that depends on both the positions and velocities, while the random force adds thermal fluctuations to the system and depends solely on particle positions. The random force $\mathbf{F}_{ij}^{R}$ compensates the loss of kinetic energy due to the dissipative force. It provides random 'kicks' in the radial direction $\hat{\mathbf{r}}_{ij}$ that keep the particles in thermal motion. They are given by

$$\mathbf{F}_{ij}^{C} = -\nabla_{\boldsymbol{r}_{ij}} V_{ij}(r_{ij}) ,$$

$$\mathbf{F}_{ij}^{D} = -\gamma \omega_D(r_{ij})(\hat{\mathbf{r}}_{ij}.\boldsymbol{V}_{ij})\hat{\mathbf{r}}_{ij} ,$$

$$\mathbf{F}_{ij}^{R} = \sigma \omega_R(r_{ij})\zeta_{ij}\hat{\mathbf{r}}_{ij} , \qquad (3.3)$$

where r_{ij} is the vector between two particles i and j while $\boldsymbol{V}_{ij} = \boldsymbol{V}_i - \boldsymbol{V}_j$. γ and σ determine the strength of the dissipative force and random forces between the particles respectively. $\omega_D(r_{ij})$ and $\omega_R(r_{ij})$ are weight functions that describe the variation with distance of the dissipative force and random forces respectively. $\hat{\mathbf{r}}_{ij}$ is the unit vector in the direction of r_{ij}. The term ζ_{ij} is Gaussian white noise which is a random variable normally distributed mean 0 and variance 1. The conservation of momentum required to produce correct hydrodynamic behaviour requires that $\mathbf{F}_i = -\mathbf{F}_j$ and therefore $\zeta_{ij} = \zeta_{ji}$.

The weighting functions ω_D and ω_R are not specified by the original model. Español and Warren showed that the correct equilibrium density of states that corresponds to the application of the conservative force may be recovered, with a well-defined temperature. The algorithm ensures the fluctuation-dissipation theorem and generates Boltzmann-weighted configurations when the dissipative and random forces are related as

$$\omega_D(r_{ij}) = [\omega_R(r_{ij})]^2 , \tag{3.4}$$

while σ and γ are related as

$$\sigma^2 = 2\gamma k_B T . \tag{3.5}$$

In DPD, the particular functional forms of the frictional and random forces make certain that all forces obey action equals reaction and hence the model conserves momentum. This is essential for recovering the correct hydrodynamic behaviour on large length and time scales.[37]

In our simulations, $\omega_R(r_{ij})$ is the same function as in the conservative force. Therefore, it has the same dependence on r_{ij} as the conservative force. As a simple choice for computational convenience we take:

$$\omega_R = \begin{cases} (1 - |r_{ij}|/r_c)\hat{\mathbf{r}}_{ij} & (|r_{ij}| < r_c) \\ 0 & (|r_{ij}| \geq r_c) \end{cases}, \tag{3.6}$$

and $\omega_D(r_{ij})$ set as:

$$\omega_D = \begin{cases} (1 - |r_{ij}|/r_c)^2 \hat{\mathbf{r}}_{ij} & (|r_{ij}| < r_c) \\ 0 & (|r_{ij}| \geq r_c) \end{cases}. \tag{3.7}$$

The amplitude of the random force is set to $\sigma = 3.0$, and the friction coefficient is set accordingly to maintain this requirement.

In classical Molecular Dynamics, the force on a given particle depends only on the positions of the particles surrounding it. This allows for a separate integration of the force and velocity on a given particle. In DPD, however, since the dissipative force depends on particle positions as well as velocities, the force on a given particle depends on the positions and the velocities of the particles surrounding it. The equations are identical to the original Velocity-Verlet algorithm[38] for $\lambda = 0.5$ with forces independent of velocities.

3.4.1 Non-bonded Interactions

The basic interactions between different bead types are defined by non-bonded interactions. For example, these interactions should reproduce that hydrophilic groups attract water while hydrophobic groups repel water. The non-bonded interactions between two particles *i* and *j* in this model are soft, purely repulsive, conservative forces described as

$$\mathbf{F}_{ij}^{C} = \begin{cases} a_{ij}(1 - r_{ij}/r_c)\hat{\boldsymbol{r}}_{ij} & (r_{ij} < r_c) \\ 0 & (r_{ij} \geq r_c) \end{cases}, \tag{3.8}$$

where a_{ij} is the maximum repulsion between particle *i* and *j*, and r_{ij} is the distance between beads $r_{ij} = r_i - r_j$, $r_{ij} = |r_{ij}|$, $\hat{\boldsymbol{r}}_{ij} = r_{ij}/|r_{ij}|$, $\hat{\boldsymbol{r}}_{ij}$ is a unit vector connecting particle *j* and particle *i* and r_c is the cutoff radius for the soft repulsive interaction. r_c is set to 1.0 d_0, where d_0 is the reduced unit for length, in our simulations. The strength of the repulsion is set by the repulsion parameter, $a_{ij} > 0$.

Groot *et al.* introduced a typical value for repulsion parameter water–water interactions by reproducing the radial distribution functions and isothermal compressibility of water at room temperature, the repulsion parameter between two identical water-like beads, to be $a_{ij} = 25\varepsilon_0$ where ε_0 is the reduced unit of energy.[11]

The repulsion parameters used in our work is based on Smit's model and the complete matrix of non-bonded parameters are given in Figure 2.d. The adaptation of Smit's model to our work will be explained in detail in Chapter 4.

3.4.2 Bonded Interactions

The bonded interactions are described using a harmonic force to constrain the bond lengths described by

$$\mathbf{F}_{\text{bond}} = -K_{\text{bond}}(r_{ij} - R_{\text{bond}}), \tag{3.9}$$

where typically the force constant $K_{\text{bond}} = 100\varepsilon_0$ and the equilibrium bond distance $R_{\text{bond}} = 0.7d_0$. A harmonic force for the bond deformation is defined similarly as

$$\mathbf{F}_{\text{angle}} = -\nabla\left(\frac{1}{2}K_{\text{angle}}(\theta_{ij} - \theta_0)^2\right). \tag{3.10}$$

The typical bond constant $K_{\text{angle}} = 6\varepsilon_0\text{rad}^{-2}$ and the equilibrium angle $\theta_0 = \pi$ rad for the hydrophobic bonded beads. Values can change to properly reproduce the geometry of the system.

3.5 Reduced Units

It is very typical to use reduced units it the Molecular Dynamics realm.[7] Quantities such as temperature, density, pressure, etc. are expressed in terms of convenient units of energy, length, and mass. The main advantages of using reduced units in Molecular Dynamics simulations are the possibility to work with numerical values of the order of unity, instead of the typically very small values associated with the atomic scale; the

simplification of the equations of motion, due to the absorption of the parameters defining the model into the units and the possibility of scaling the results for a whole class of systems described by the same model.

Reduced units used in our DPD simulations:

Mass: It is assumed that all beads in the system have unit mass and the reduced unit for mass is set to be the mass of one bead. The standard bead represents $N_m = 3$ water molecules. This sets the reduced unit of mass, m^* to be $N_m m_{H_2O} = 9.10^{-26}$kg.

Length: The length scale for the simulation is determined by the volume occupied by the beads at a fixed temperature where $T^* = 1.0$. The cut-off diameter r_c is used as the basic length unit d_0, which means $r_c \equiv d_0$. This length can be related to a physical length by comparing a coarse-grained solvent particle to three water molecules as one bead in our coarse-grained model is formed by three water molecules. Therefore, a cube of unit volume ${r_c}^3$ holds an average of three beads, which makes approximately nine water molecules. If the volume of the water molecule is taken to be approximately 30Å^3, then we have $d_0 = 6.46$Å.

Time: Groot *et al.* used the experimental value for the self-diffusion of water to set the time unit.[11] The simulation time can be related to real time by comparing transport coefficients in the system to those in atomistic simulations or experiments. Comparing the diffusion coefficient of water yields a reduced time unit of 5 ps.

Temperature: Berend Smit's group[39] indicates that there are different methods to derive mapping of reduced temperatures to a physical units scale. They were interested in the qualitative description of biological bilayers, thus mapping the temperature scale to the thermodynamics properties of bilayers would be the best

approach. Assuming linear scaling between the reduced and physical temperatures, and using the values for the main and pre-transition temperatures (24ºC and 15.3ºC, respectively)[25] of the bilayer formed by 1,2-Dimyristoyl-sn-glycero-3-phosphocholine (DMPC), the temperature scale results to be: T(ºC) = 116 T* - 25.3.

Our simulations were performed at T* = 0.42, which corresponds to 23.5ºC, an intermediate value between the room temperature T and the normal conditions T. We do not expect quantitative agreements but our results should be close to those from experiments run at room temperature.

3.6 Monte Carlo Approach

The Monte Carlo technique, also called Metropolis method,[40] is a method that uses random numbers to generate a sample population of the system from which one can calculate the properties of interest. Monte Carlo approach is used in various endeavours, such as studying biological systems like proteins,[41] or membranes.[42]

Smit's group introduced the combination of DPD with a Monte Carlo scheme to ensure a constant surface tension (γ) in lipid membranes.[43] They demonstrated that within 100-300 Monte Carlo cycles the surface area reached equilibrium. This hybrid simulation scheme uses DPD to move the positions of the particles and Monte Carlo to change the simulation box shape.[44] Accordingly, in our simulations Monte Carlo helps to achieve a tensionless ($\gamma = 0$) state.

We wish to simulate our system in an ensemble that allows for both changes in area as well as in volume, such that the equilibration would mimic natural conditions. This is achieved using the $NP\gamma T$ ensemble where N is the total number of particles in the system, P is the pressure of the system, γ is the surface tension, and T is the temperature maintained by the dissipative and random forces.

3.7 References

1. J. A. Pople, *Angew. Chem. Int. Ed.* **1999**, *38*, 1894.

2. F. De Proft, P. Geerlings, *Chem. Rev.* **2001**, *101*, 1451.

3. N. L. Allinger, *Molecular structure: understanding steric and electronic effects from molecular mechanics*, John Wiley & Sons, New Jersey, United States **2010**.

4. M. P. Allen, *Introduction to molecular dynamics simulation*, In N. Attig, K. Binder, H. Grubmüller, K. Kremer, Computational soft matter: from synthetic polymers to proteins, *23*, pp. 1-27, Jülich, **2004**. John von Neumann Institute for Computing, NIC-Directors.

5. P. Charchar, A. J. Christofferson, N. Todorova, I. Yarovsky, *Small* **2016**, *12*, 2395-2418.

6. J. A. McCammon, B. R. Gelin, M. Karplus, *Nature* **1977**, *267*, 585-590.

7. D. Frenkel, B. Smit, *Understanding Molecular Simulations*, 2nd ed., Academic Press, San Diego, United States **2002**, pp. 63-64.

8. D. C. C. Rapaport, *The Art of Molecular Dynamics Simulation*, 2nd ed., Cambridge University Press, Cambridge, UK **2004**.

9. A. R. Leach, *Molecular Modelling: Principles and Applications*, 2nd ed., Pearson education, Harlow, UK **2002**.

10. N. Todorova, F. S. Legge, H. Treutlein, I. Yarovsky, *J. Phys. Chem. B* **2008**, *112*, 11137-11146.

11. R. D. Groot, P. B. Warren, *J. Chem. Phys* **1997**, *107*, 4423.

12. S. O. Nielsen, C. F. Lopez, G. Srinivas, M. L. Klein, *J. Phys* **2004**, *16*, R481-R512.

13. G. A. Voth, *Coarse-Graining of Condensed Phase and Biomolecular Systems*, CRC Press, Boca Raton, United States **2008**.

14. P. J. Bond, J. Holyoake, A. Ivetac, S. Khalid, M. S. P. Sansom, *J. Struct. Biol.* **2007**, *157*, 593-605.

15. H. I. Ingólfsson, C. A. Lopez, J. J. Uusitalo, D. H. de Jong, S. M. Gopal, X. Periole, S. J. Marrink, *WIREs Comput Mol Sci* **2014**, *4*, 225-248.

16. L. Monticelli, S. K. Kandasamy, X. Periole, R. G. Larson, D. P. Tieleman, S. J. Marrink, *J. Chem. Theory Comput.* **2008**, *4*, 819-834.

17. F. J. M. de Meyer, M. Venturoli, B. Smit, *Biophys. J.* **2008**, *95*, 1851-1865.

18. S. J. Marrink, H. J. Risselada, S. Yefimov, D. P. Tieleman, A. H. de Vries, *J. Phys. Chem. B* **2007**, *111*, 7812-7824.

19. S. J. Marrink, A. H. de Vries, D. P. Tieleman, *Biochim. Biophys. Acta, Biomembr.* **2009**, *1788*, 149-168.

20. J. Wong-Ekkabut, S. Baoukina, W. Triampo, I. M. Tang, D. P. Tieleman, L. Monticelli, *Nat. Nanotechnol.* **2008**, *3*, 363-368.

21. J. Gumbart, K. Schulten, *Biochemistry* **2007**, *46*, 11147-11157.

22. M. S. Shell, *Coarse graining and multiscale techniques* **2009**. Available at: https://engineering.ucsb.edu/~shell/che210d/Multiscale.pdf

23. M. Venturoli, B. Smit, *Phys. Chem. Comm.* **1999**, *2*, 45-49.

24. M. Kranenburg, B. Smit., *J. Phys. Chem. B* **2005**, *109*, 6553-6563.

25. F. J. M. De Meyer, J. M. Rodgers, T. F. Willems, B. Smit, *Biophys. J.* **2010**, *99*, 3629-3638.

26. A. Benjamini, B. Smit, *Biophys. J.* **2012**, *103*, 1227-1235.

27. S. J. Marrink, A. H. de Vries, A. E. Mark, *J. Phys. Chem. B* **2004**, *108*, 750.

28. S. J. Marrink, H. J. Risselada, S. Yefimov, D. P. Tieleman, A. H. De Vries, *J. Phys. Chem. B* **2007**, *111*, 7812-7824.

29. L. Monticelli, S. K. Kandasamy, X. Periole, R. G. Larson, D. P. Tieleman, S. J. Marrink, *J. Chem. Theor. Comput.* **2008**, *4*, 819.

30. S. J. Marrink, D. P. Tieleman, *Chem. Soc. Rev.* **2013**, *42*, 6801-6822.

31. P. J. Hoogerbrugge, J. M. V. A. Koelman, *EPL* **1992**, *19*, 155-160.

32. R. Temam, *Navier–Stokes Equations: Theory and Numerical Analysis*, AMS Chelsea Publishing, Amsterdam, North-Holland **1984**.

33. A. N. Gorban, I. V. Karlin, *Contemp. Phys.* **2016**, 1-21.

34. P. Espanol, *Handbook of Materials Modeling* **2005**, 2503-2512.

35. P. Espanol, P. Warren, *EPL (Europhysics Letters)* **1995**, *30*, 191-196.

36. R. D. Groot, T. J. Madden, *J. Chem. Phys* **1998**, *108*, 8713.

37. O. K. Rice, *J. Chem. Phys* **1944**, *12*, 1-18.

38. W. C. Swope, H. C. Andersen, P. H. Berens, K. R. Wilson, *J. Chem. Phys.* **1982**, *76*, 637-649.

39. M. Venturoli, B. Smit, M. M. Sperotto, *Biophys. J.* **2005**, *88*, 1778-1798.

40. N. Metropolis, A. W. Rosenbluth, N. Marshall, M. N. Rosenbluth, A. T. Teller, *J. Chem. Phys.* **1953**, *21*, 1087-1092.

41. P. Ojeda, M. E. Garcia, A. Londoño, N. -Y. Chen, *Biophys. J.* **2009**, *96*, 1076-1082.

42. M. Milik, J. Skolnick, *Biophys. J.* **1995**, *69*, 1382-1386.

43. M. Venturoli, B. Smit, *Phys. Chem. Comm.* **1999**, *10*, 1-5.

44. M. Kranenburg, M. Venturoli, B. Smit, *J. Phys. Chem. B* **2003**, *107*, 11491-11501.

Chapter 4

CONFORMATIONAL CHANGES ON GOLD NANOPARTICLE CONJUGATES

Chapter 4

CONFORMATIONAL CHANGES ON GOLD NANOPARTICLE CONJUGATES

Colloidal nanoparticles encounter the environment in which they are immersed *via* their surfaces. Therefore, the successful development of their applications requires not only the production of nanoparticles with well-defined physicochemical properties but also the study and understanding of their surface state chemistry. This becomes very important in the biological context,[1] where the surface properties of nanoparticles play a key role in the extent of the interaction between nanoparticles and biological systems. One of the most significant properties of nanoparticles is that their high surface energies tend to be minimized *via* homo (particle-particle) and hetero (particle-molecule) interactions. This property is employed to control both aggregation and functionalization.[2] Hence, surface modification methods *via* functionalization of nanoparticles with relevant biomolecules have been used to improve the colloidal stability of nanoparticles in biological systems,[3] increase circulation times and targeting,[4] as well as to reduce overall toxicity and aggregation.[5] In these processes, the ligand molecules on the surface remaining after the synthesis are exchanged by others able to provide new properties or functionalities to the particles.[6]

A well-known example in synthesis of gold nanoparticles (AuNPs) is by citrate reduction.[2] The citrate layer can be easily replaced by ligands which have higher affinity for the particle surface, such as thiol- and amine- containing ligand molecules. Thus, thanks to functionalization, AuNPs have been selectively delivered to target regions, providing enhanced opportunities for controlled drug delivery,[7] cancer treatment,[8] biomedical imaging[9] and diagnosis.[10]

4.1 Introduction to the Gold Nanoparticle Conjugates Used in This Study

The unique physicochemical properties of AuNPs have been extensively studied, and are precisely controlled by tuning their size and morphology. On the other hand, the control of their interactions with their surrounding environment *via* surface modifications is still challenging. The compatibility of these systems with the immune system is largely determined by their surface chemistry.[11] Small nanoparticles show high surface energies and have the possibility to aggregate, which would dramatically affect cellular and molecular responses. Modifying the surface chemistry can reduce the immunotoxicity of nanoparticles and improve the drug delivery process.

The composition of the layer determines the physicochemical properties of the AuNPs. Additionally, the composition and distribution of the different molecules on the nanoparticle surface has been found of paramount importance. It has been reported how subtle conformational changes of the molecules alter the final properties of the conjugate, which translates into variations in their biodistribution and toxicity.[12] In a context where nano-biointeractions are determined by the nature of the nanoparticle surface, the composition or the coating layer, and more importantly, its structure, define the final identity of the particle. This affects not only the properties of the nanoparticle, but also its stability, interactions with other biological entities, particularly proteins,[13] and biodistribution.[14] All these factors are responsible for obtaining the desired effect on cellular and molecular responses.[15] In this sense, the precise control of the surface chemistry[11] represents a crucial aspect not only in the efficient development of

nanoparticle based medical technologies but also in the full exploitation of the potential differential benefits of nanoparticles.

In this chapter, the computational study of the distribution and conformational changes of two relevant molecules, 11-mercaptoundecanoic acid (MUA), and thiolated polyethylene glycol (SH-PEG), after their attachment to the surface of AuNPs in the liquid phase, forming a coating mixed layer is reviewed.

PEG is a regular coating of nanomedicines.[16,17] Conformational changes of the thiolated PEG attached to the nanoparticle have been correlated to altered biodistribution and appearance of toxicity.[12] Remarkably, SH-PEG can be adsorbed on the nanoparticle surface in a flat or radial configuration. Only the radial conformation stabilizes nanoparticles against aggregation or opsonization.[18]

MUA is a typical surfactant molecule employed in several nanoparticle systems.[19] MUA provides colloidal stability to the nanoparticles at physiological pH by electrostatic repulsion. In addition to that, its carboxylic acid functional group has been used to bond and transport drugs.[20]

Mixture of ligands helps to combine different functionalities. In this case, MUA provides electrostatic repulsion while SH-PEG provides steric repulsion.[21] These are the two existing strategies to provide repulsion forces to avoid nanoparticle aggregation.

Experimental results[21] on the formation of mixed layers of MUA and SH-PEG on AuNPs describe a change in the conformation of SH-PEG molecules depending on the relative MUA/SH-PEG ratio at the nanoparticle surface. This indicates how the competition between MUA and SH-PEG for the nanoparticle surface is a key point to understand these systems. Interestingly, the exposition of AuNPs to different mixtures of MUA and SH-PEG results in different conformational organizations of SH-PEG molecules onto the nanoparticle surface. Thus, while at low SH-PEG concentrations, SH-PEG tend to lay flat on the surface, as the SH-PEG concentration increases, it approaches a threshold concentration (About the 60% of the nanoparticle surface coverage) where the SH-PEG molecules stretch out and display a radial conformation.

In previous studies by Jackson *et al.*,[22] it was suggested that different molecules tend to form striped domains when conjugated to a nanoparticle surface. They suggested

that this opens the opportunity to make polarized multifunctional nanoparticles. However, the systematic evaluation of these aspects is greatly limited by the experimental techniques and resources available to study the distribution and conformation of two different molecules attached to a nanoparticle surface in the liquid phase.

In the following sections, computational studies on systems containing AuNPs functionalized with MUA, and SH-PEG are shown. Firstly, the coarse-grained model and the simulation technique are explained in detail. Secondly, the behaviour of each component alone in water is examined. After that, the description of how MUA or SH-PEG occupy the AuNP surface follows. Later, the competition between both thiolated compounds is demonstrated. Lastly, the effect of the order of addition on the AuNP (First MUA then SH-PEG or vice versa) is studied. Our final aim is to understand the change of the conformation in the mixed monolayer, which will allow further engineering of the nanoparticle surface.

4.2 Coarse-grained Model

As mentioned in the Chapter 1, atomistic models can be complemented with lower-resolution coarse-grained methods that use groups of atoms as single interaction sites. This allows for both a reduction in the system's degrees of freedom as well as faster simulations. This section focuses on the study of a AuNP conjugate formed by a gold core surrounded by MUA and SH-PEG. These two compounds compete to occupy the AuNP surface and, in addition, the conformation adopted by SH-PEG is influenced by the number of MUA present on the surface.

In our model, one bead consists of roughly three heavy atoms. One water bead comprises three water molecules and one gold bead comprises three gold atoms. MUA was considered as to have four beads of three types and SH-PEG was considered to have fifteen beads of two types (Figure 4.1). Both have the same thiol group which lets them bond to the gold surface with the same strength. This assumption may seem too simple, but Density Functional Theory (DFT) studies on $(RSAu)_4$ clusters[23] show that ligand

exchange modifies the cluster electronic structure, which gives rise to large changes on electronic spectrums; however, it has very minor effects on structural and energetic data, reinforcing our approach.

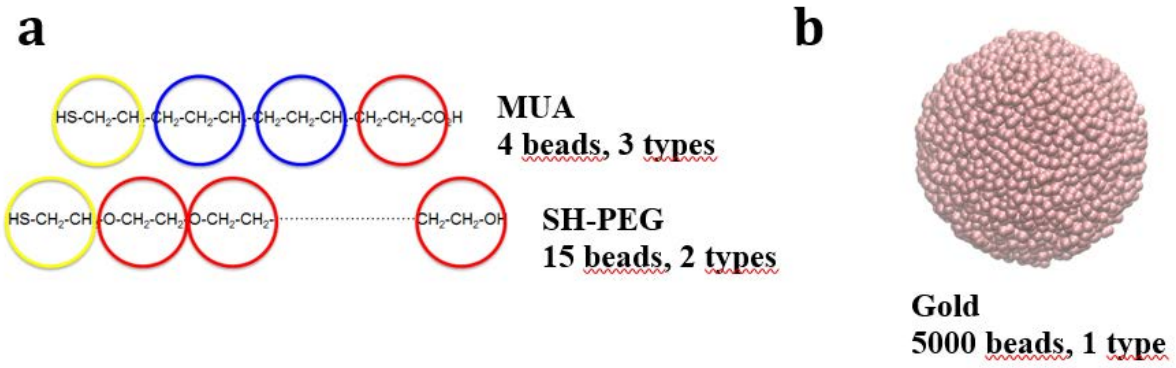

Figure 4.1 Coarse-grained model of the system. **a.** Coarse-grained representation of MUA and SH-PEG, beads including thiol group (Type S) are depicted in yellow, while the hydrophobic beads (Type P) are depicted in blue and hydrophilic beads (Type H_{MUA}, $H_{SH\text{-}PEG}$) are depicted in red. **b.** Snapshot of a model of AuNP (Water particles were removed for clarity).

4.3 Simulation Technique

The behavior of AuNPs was studied using a hybrid model of Dissipative Particle Dynamics - Monte Carlo (DPD-MC) simulation technique. Monte Carlo moves were used with the $NP\gamma T$ ensemble, with $\gamma = 0$. Reduced units were used to measure energy and length: $\varepsilon_0 = 1 \kappa_B T$, $d_0 = 0.646$ nm, respectively.[26c] Almost all simulations were performed in a cubic water box of size 30x30x30 d_0^3 where the cut off for non-bonded interactions is defined as $R_C \equiv 1\ d_0$ and with $\Delta t = 0.03$. Periodic boundary conditions were applied. The dimensionless temperature used throughout the simulations was 0.42 (*ca*. 35ºC). The systems were simulated for 18 x 10^4 cycles, equivalent to ~ 270 ns, only with the exception for the short cycle runs to test all the parameters. Systems were considered to be equilibrated when total energy was stable during more than 200 ns.

To simulate a system, the non-bonded interactions between beads should be described with soft-repulsive interactions.[24,25] The repulsive parameters are obtained

considering a large value indicates strong repulsive interaction between beads, and are closely based on those used by Smit[26] which in turn are based on those determined by Groot.[24] Table 4.1 gathers all the soft-repulsive interaction parameters between the six types of beads used in this study: water (W), gold (Au), thiol group (S), hydrophobic bead (P), hydrophilic bead for MUA (H_{MUA}), and hydrophilic bead for SH-PEG ($H_{SH\text{-}PEG}$).

Table 4.1 Soft-repulsive interaction parameters used in this study.

	W	**Au**	**S**	**P**	**H_{MUA}**	**$H_{SH\text{-}PEG}$**
W	25	120	15	120	15	30
Au	120	20	1	120	20	80
S	15	1	35	80	35	40
P	120	120	80	25	80	80
H_{MUA}	15	20	35	80	35	45
$H_{SH\text{-}PEG}$	30	80	40	80	45	35

To set the interaction parameters between gold-gold and gold-water, we repeated the parameters from the work of Chen *et al.*[27] but, as indicated above, the use of 20 and 120, respectively, was decided based on considering the hydrophilicity of AuNPs. The repulsion parameter between gold and the thiol group bead was decided as 1. Figure 4.2 shows the effect of the repulsion parameter between thiol bead and gold bead. Only with repulsion constant of 1, we obtain all the thiol beads on the surface of the AuNP indicating a strong gold-thiolate bond. As one bead represents three heavy atoms, we considered the thiol bead as an ethanethiol, CH_3CH_2SH, which is shown in Figure 4.1.a as the bead type drawn in yellow.

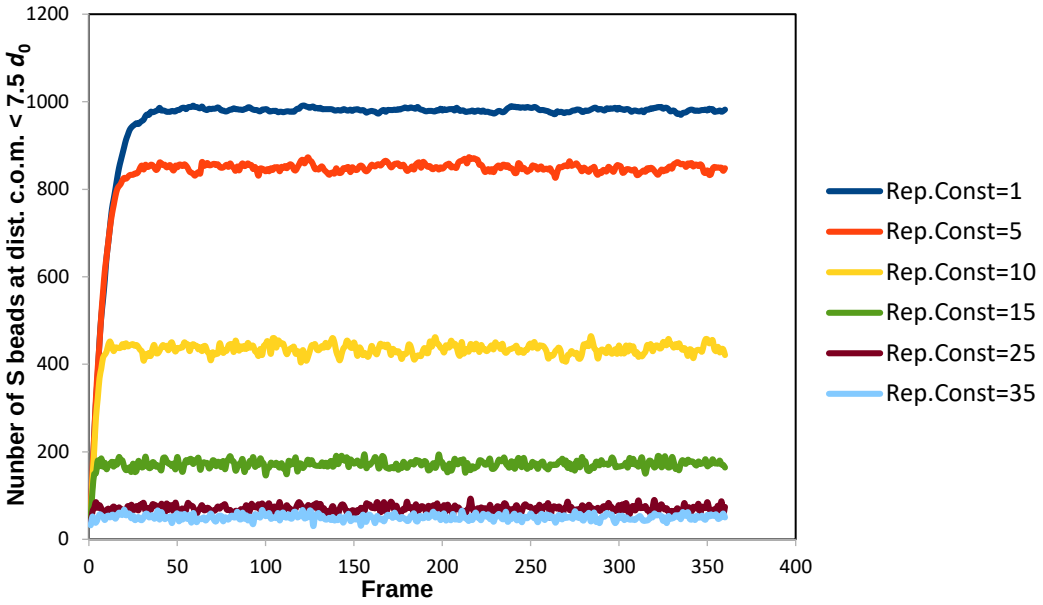

Figure 4.2 Distribution of thiol beads from the gold centre of mass for each frame graphed using 1000 thiol beads around a 2000 beads AuNP, changing the repulsion constant between Au and S from 1 to 35.

Most of the simulations were performed in a water box of 30x30x30 d_0^3 formed by 240 000 water molecules, which corresponds to 80 000 beads and 15 000 gold atoms, which corresponds to 5000 beads. In addition, 120 MUAs (480 beads) or/and 120 SH-PEGs (1800 beads) were added. Water boxes of 40x40x40 d_0^3 formed by 600 000 water molecules (200 000 beads) were used in the simulations on individual components of 120 MUAs, PEGs and SH-PEGs. All the simulations start at a random point. The dissipative and random forces act together as a thermostat which means the overall effect is a system simulated at constant temperature.

Systems were considered to be equilibrated when un-bonded energy was stable during more than 200 ns. Table 4.2 shows the average values for the non-bonded energy, temperature, pressure and volume, as well as their standard deviations, which represent small fluctuations of 0.1%, 1.2%, 0.1%, and 0.06%, respectively, along simulation time for the case of gold and 100 MUAs, as an example.

Table 4.2. Average values, standard deviations, and relative % for different variables (Expressed in the corresponding reduced units) of a AuNP with 100 MUA as an example.

	V(non-bonded)	**T**	**P**	**V**
Average	$3.49 \cdot 10^{5}$	0.41	22.3	$2.84 \cdot 10^{4}$
Standard Deviation	$5.01 \cdot 10^{2}$	$5.13 \cdot 10^{-3}$	0.02	17.0
%	0.14	1.25	0.13	0.06

4.4 Design of Individual Components

4.4.1 Gold Nanoparticle

AuNP was built using 15 000 gold atoms initially located randomly in a water box of 30x30x30 d_0^3 formed by 240 000 water molecules using values of 20 and 120 as the repulsion parameters for gold-gold and for water-gold. We started building the AuNP firstly running short cycle simulations with different box sizes and nanoparticle sizes. The main reason we have chosen the AuNP with 15 000 gold atoms is to be able to compare the results with the experimental data.[21]

A good result was obtained using a repulsion parameter for gold-gold equal to 20. Other runs using repulsion parameters of 5, 10 or 15, gave worse results in the sense of too compact AuNPs with atomic overlapping (Figure 4.3). The gold-gold repulsion value of 15 was taken from the work of Chen *et al.*[27] which gave similar results with repulsion value of 20 for gold-gold. As seen in the graphs below, the spherical shape and the compactness of the nanoparticle was kept better with the repulsion value of 20 for gold-gold interaction. Besides, these authors used a water-gold repulsion of 97.5, value substantially smaller than the value of 120 used in for the hydrophobic part of proteins in all the works from Berend Smit's group.[26c] In this work, we considered that an AuNP must be at least as hydrophobic as a protein, which contain many polar groups even in its

hydrophobic moiety. Therefore, we have chosen 20 for the repulsion value of gold-gold and 120 for the repulsion value of water-gold.

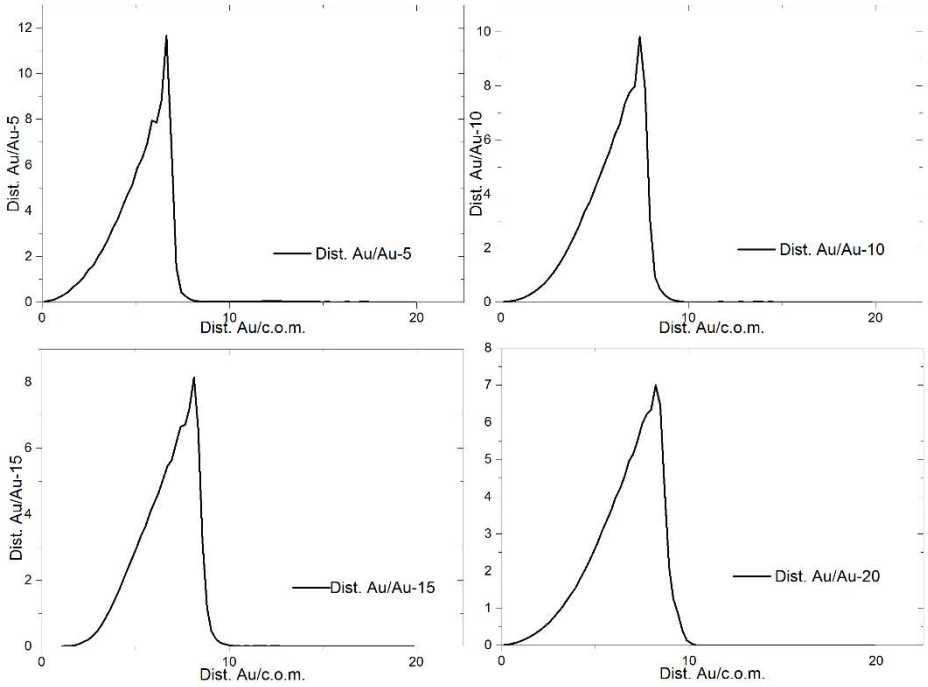

Figure 4.3 Distribution of gold beads from the centre of mass graphed for the four different repulsion values for gold-gold; using 5, 10, 15, and 20. The distances are shown in reduced units.

The results of the simulation produced a compact and spherical AuNP with an average diameter of 8.9 nm. The average size for the AuNP radius 6.9 d_0 was obtained by computing for each frame the average distance from the AuNP centre of mass to the farthest 666 gold beads. The "magic" number of 666 was deduced by considering a close-packed spherical arrangement (26% of unoccupied space)[28] of gold beads.

4.4.2 11-Mercaptoundecanoic Acid

MUA was studied in a water box of 40x40x40 d_0^3 formed by 600 000 water molecules without other components, using a total of 120 MUAs for the simulation. They formed micelles in water from the very early moments of the simulation (Figure 4.4.a).

This is consistent with the fact that MUA is a hydrophobic linear molecule with both hydrophilic ends; therefore, by clamping together they protect their hydrophobic chains while exposing their hydrophilic ends. As a control experiment to avoid the patching of the MUAs, unrealistic repulsion values were introduced to observe if this behaviour continued. At the end, patches were seen even with these unrealistic values, indicating how the hydrophobicity was driving the formation of these micelles. The Radial Distribution Function (rdf) for the thiol group (S···S) was calculated to see the average distance between two MUAs along the simulation (Red line in Figure 4.4.b). Rdf is the conditional probability to find one object at a given distance (radius) from another object taken as the origin. In this case, the rdf provides information about the density of S atoms at a given radius from another S atom. Interestingly, rdf between SH groups indicates two zones of high probability of finding an S atom (A maximum at 0.61 nm and a shoulder at 1.5 nm) and a value of 1 for distances larger than 2.3 nm, distance which coincides with the total length of MUA. The integral below the curve (Blue line in Figure 4.4.b) indicates that a total of 4 S atoms can be found at a distance smaller of 2.3 nm from any other S atom, i.e., micelles with a total number of 5 units of MUA are formed.

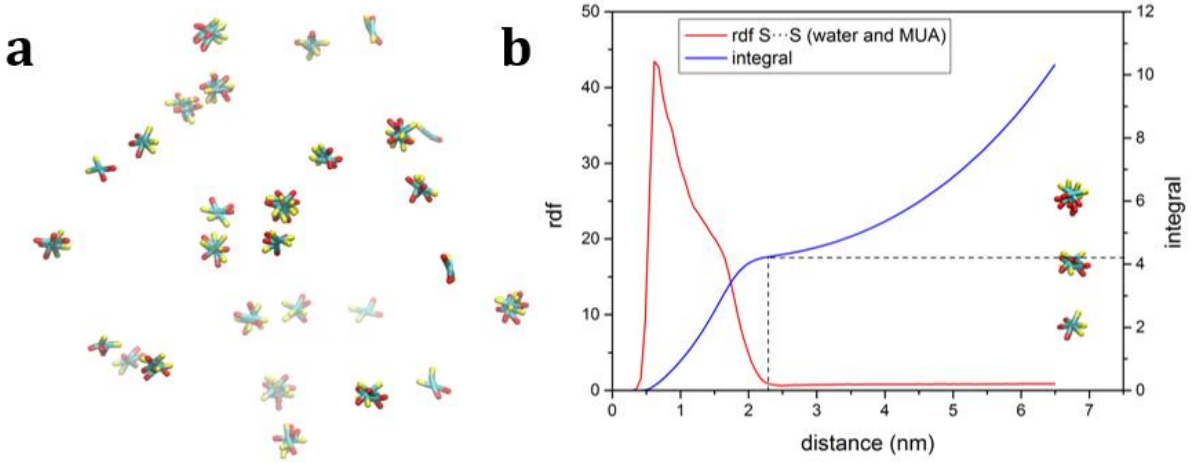

Figure 4.4 MUA simulated alone in a water box. **a.** Snapshots of MUA (Water particles were removed for clarity). **b.** Radial Distribution Function (In red) for S···S in MUA, and its integral (In blue); insets are micelles with 3, 5, and 7 S atoms.

4.4.3 Thiolated Polyethylene Glycol

PEG and SH-PEG were also studied in a water box of 40x40x40 d_0^3 formed by 600 000 water molecules without other components. The final result of the simulations was quite similar for both; as a consequence of their large hydrophilicity, PEG and SH-PEG occupy the entire box without adopting any clear arrangement in any case (Figure 4.5).

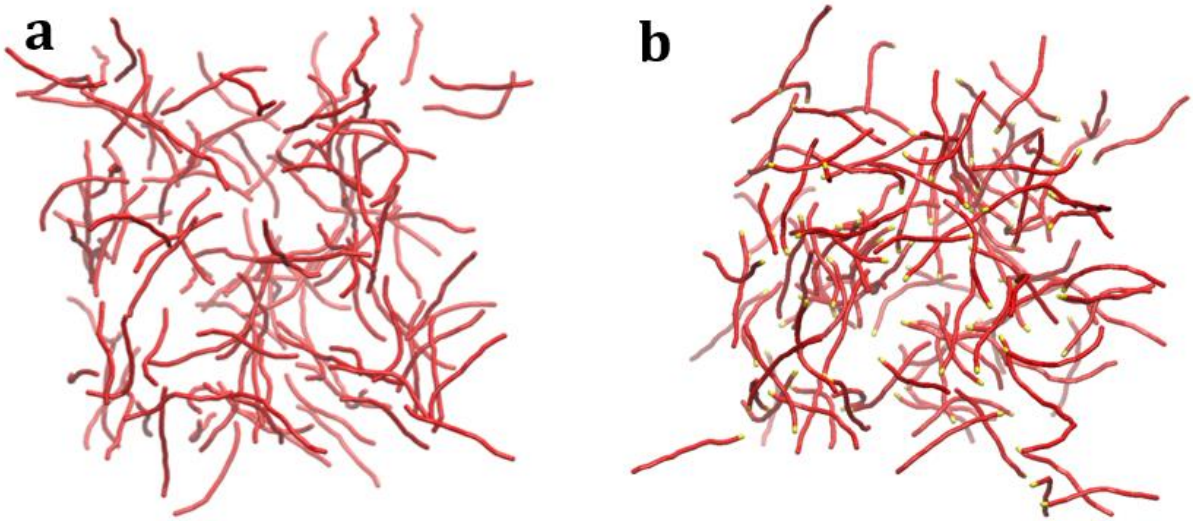

Figure 4.5 Snapshots of **a.** PEG and **b.** SH-PEG alone in water (Water particles were removed for clarity). Both snapshots were taken at 270 ns.

Rdf graphs of PEG and SH-PEG (Figure 4.6) show that there is a small difference, where SH-PEGs are slightly more ordered than PEG, especially at short distances (See Supporting Information for details), probably due to SH-SH interactions. The integral curves are practically overlapping indicating an identical behaviour despite the presence of the thiol group, the effect of which is minor until it reacts with the AuNP surface (vide infra). The integral curves are completely overlapping indicating an identical behaviour.

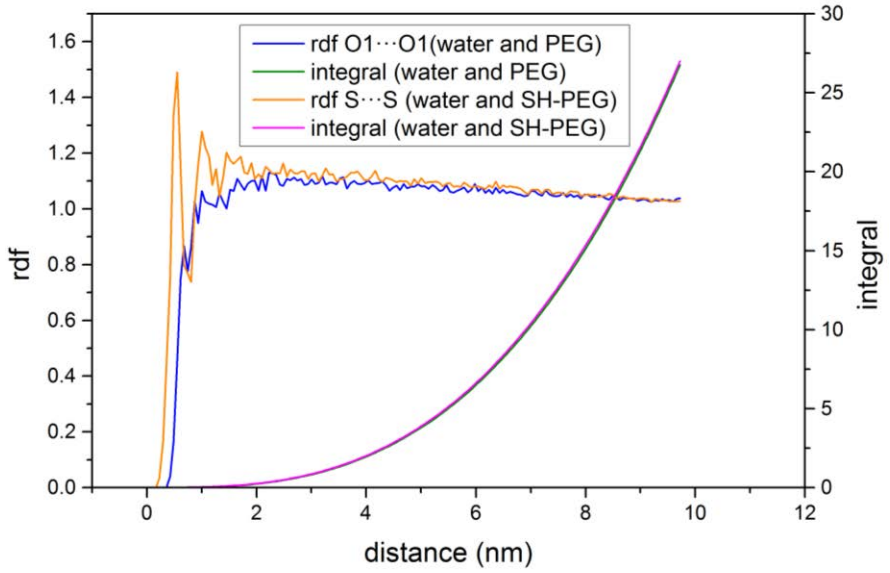

Figure 4.6 Radial distribution functions for O1···O1 in PEG (In blue), and for S···S in SH-PEG (In orange), as well as their integral (In green and pink, respectively).

4.5 Interactions between Gold and Other Components

4.5.1 Systems with Two Components

Interactions between MUA and gold were studied in several simulations performed in a water box of 30x30x30 d_0^3 formed by 240 000 water molecules with 15 000 gold atoms and 120 MUA molecules. It is observed that MUA has the tendency to make patches onto the gold surface (Figure 4.7.a). Like all the simulations done in our laboratory, the initial positions of MUAs were given randomly. However, it becomes visible that MUAs start to form patches on top of the nanoparticle surface from the very beginning (Early snapshots). The formation of segregated molecular domains is key to understand heterogeneous (mixed) functionalization and open the opportunity to make chemically polarized nanoparticles.[29] In this direction, it has been acknowledged that patchiness can define key properties to these nanoparticles.[30,31]

How MUAs are structured on the surface of the nanoparticle can be determined by analysing the S···S distances. Figure 4.7.b shows the evolution of the S···S distances, smaller than a certain value, along the simulation. In addition, the snapshot corresponding to the last saved structure of the simulation is shown as inset. As it can be appreciated in the inset, at the end of the simulation all the MUA molecules are on the gold surface and form patches of different sizes. Graphs indicate the variation of all S···S distances at each frame of the simulation filtered by different distances from 1.3 to 5.2 nm. Interestingly, one can observe three well defined regions. During the first 70 snapshots and at the last 120 ones, the number of S···S distances remains almost constant indicating somehow stable configurations, while a transition can be observed in the central part of the trajectory. At the beginning of the simulation, MUA forms small micelles, similar to those depicted in Figure 4.4. Those will have S···S distances of about 1.95 nm which corresponds to the overall length of a MUA molecule. Figure 4.7.b indicates that for distances < 1.95 nm, a total of about 500 S···S distances are obtained, indicating about 4 S atoms near each other S atom. On the contrary, at the end of the simulation, and for the same distance, the number of S···S distances has increased up to about 800, indicating a total amount of 7-8 S atoms near each other, which makes larger domains over the AuNP surface. When the analysis is performed at longer distances (Figure 4.7.b), much larger differences are observed. At the beginning of the simulation and for distances smaller than 5.2 nm, a total of about 1500 S···S contacts are obtained, indicating the existence of 12-13 S atoms around each other S; while at the end of the simulation, near 3000 S···S distances are observed, which gives 25 sulfurs near any other S atom. Both analyses correspond to the same structures although they look very different, giving a clear picture of how MUA is arranged. At the beginning of the simulation, we have 24 MUA small micelles formed by 5 MUAs and having only 2-3 micelles at a distance smaller than 5.2 nm (Which will give a total of 10-15 sulfur atoms around each other sulfur). On the contrary, at the end of the simulation we have less MUAs aggregations, about 5, but larger (About 25 sulfurs near each other sulfur) and more compact (Up to 8 sulfurs near any other sulfur at distances<1.92 nm), i.e. MUA forms patches on the AuNP that grow as more MUA is deposited.

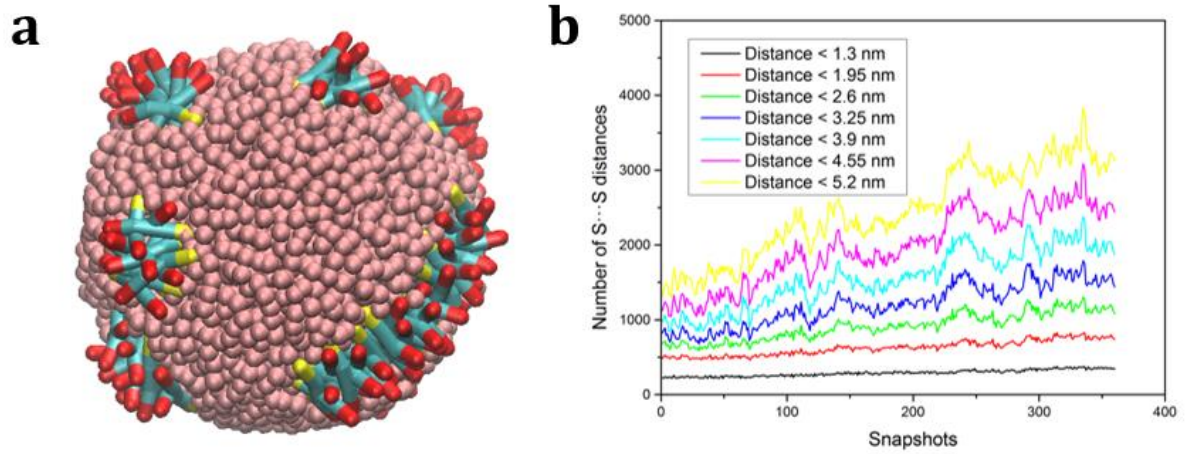

Figure 4.7 a. Example of one final distribution of the 120 MUA molecules onto the AuNP surface which corresponds to the last snapshot (270 ns) saved in the simulation (Water particles were removed for clarity). **b.** Variation of the number of S···S distances along the simulation of a model AuNP (Formed by 15 000 gold atoms) containing 120 MUA molecules. Graphs for different S···S distances are shown.

Subsequently, simulations of the behaviour of PEG and SH-PEG with the AuNPs were run. They were both studied in a water box of 30x30x30 d_0^3 formed by 240 000 water molecules with 15 000 gold atoms forming a single nanoparticle. A total of 120 PEG and 120 SH-PEG molecules were used for the simulations, the results of which are shown in Figure 4.8. The simulations were able to reproduce what was observed experimentally.[21] In the absence of the thiol group, PEG wrapped around the gold core; while in the presence of the thiol group, SH-PEG ended in a more radial conformation. The presence of the thiol group forces the SH-PEG to adopt a radial conformation over the AuNP surface because the thiol group has a stronger affinity for the AuNP surface than PEG chains do. An interesting study on how the gold–thiolate bonding in molecular complexes occurs is beautifully carried out by Hannu Häkkinen,[32] where it is explained how the pseudo covalent interaction between gold and sulfur forms, indicating that the gold-thiolate bond has strength close to the gold-gold bond. In our simulations, bond strength between two molecules is simulated by the help of the repulsion constants. However, as can be seen in the Table 4.1 of the Simulation Technique section, we are using very different repulsion values for gold-gold (20) and gold-thiol (1). Apart from this value, sulfur is treated as a standard hydrophilic unit with a water-sulfur repulsion

constant of 15 (See Simulation Technique section). If we had used 20 for the gold-sulfur repulsion, the sulfur would have never approached gold because it would have preferred to stay surrounded by water molecules; a value of just 1 forces sulfur to approach very fast to the AuNP. Since the SH-PEG also contains a sulfur unit in one end, the absolute value for the gold-sulfur repulsion is irrelevant as far as it is smaller than 15, because its effect will be the same over the MUA as over the SH-PEG. Differences in the behaviour of both components will come from the hydrodynamic characteristics of the rest of the MUA and SH-PEG molecules, being the first more hydrophobic than the second.

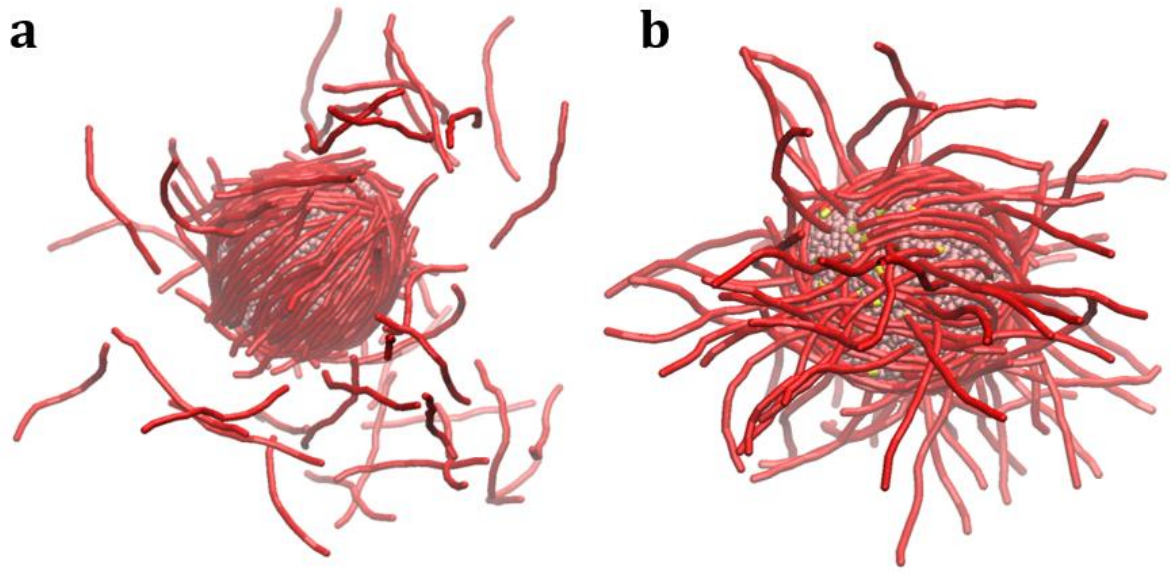

Figure 4.8 Snapshot of a model AuNP containing PEG or SH-PEG; **a.** PEG/AuNP; **b.** SH-PEG/AuNP (Water particles were removed for clarity). Both snapshots were taken at 270 ns.

4.5.2 Systems with Three Components

Lastly, all three components were studied in the same system to see how the distribution and conformation of the different molecules onto the AuNP surface takes place. The simulations were performed in the same water box of 30x30x30 d_0^3 formed by 240 000 water molecules with 15 000 gold atoms that form the nanoparticle, 120 MUA and 120 SH-PEG molecules. The results were quite interesting. At the end of the

simulation, we could observe that SH-PEGs adopt mainly the radial conformation and MUAs formed patches onto the gold surface although some of the micelles remained in the water solution (Figure 4.9). It was observed that MUA lands first on the AuNP's surface, very likely due to its smaller size and its higher hydrophobicity as compared with SH-PEG. As a consequence, SH-PEG occupies the AuNP surface not being initially occupied by MUA. These results are in agreement with those described by Hannu Häkkinen's[32] where it is pointed out that for low coverage adsorption and small molecules, it is common to observe a 'striped' phase. Besides, longer alkyl thiolates show a tangential configuration at low coverage rates where the alkyl chains oriented parallel to the surface, and for higher coverage, a radial phase is observed where all molecules are packed vertically (Named 'lying-down' and 'standing-up' respectively, in Häkkinen's paper).

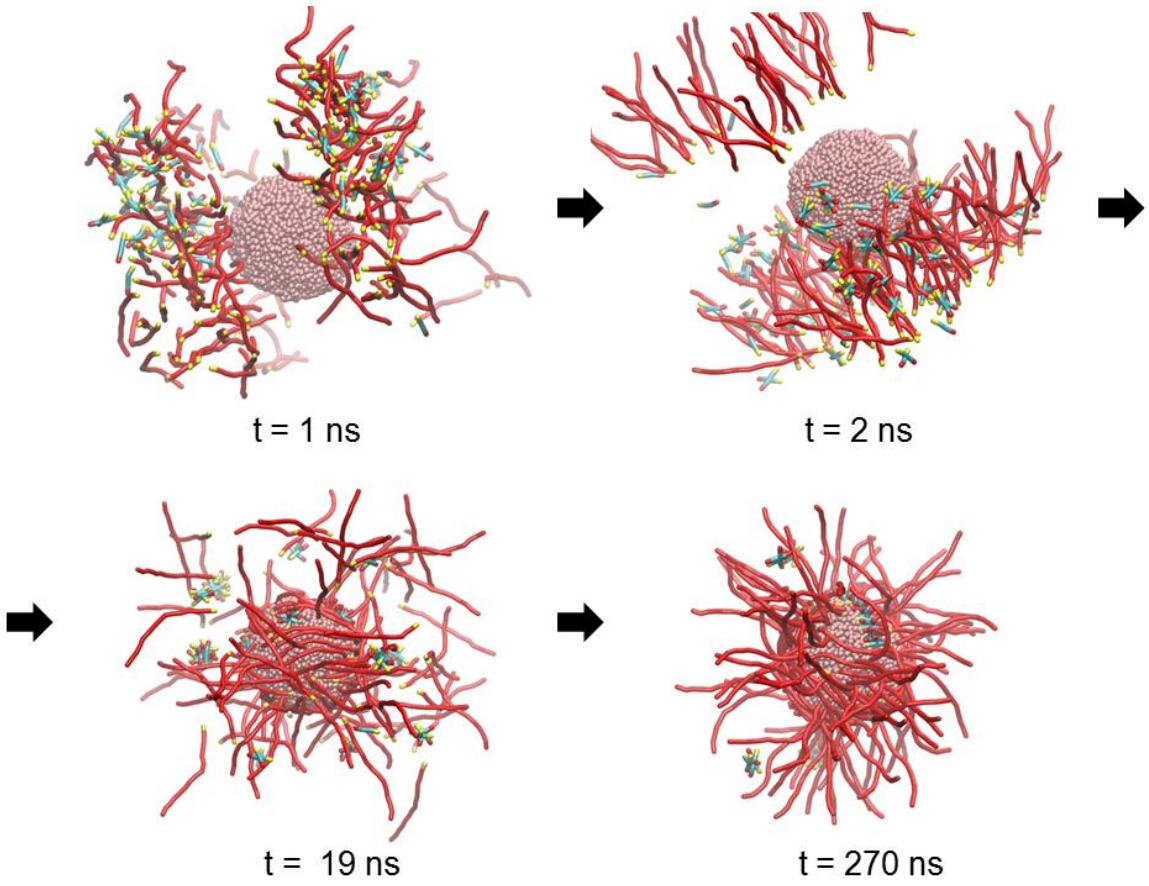

Figure 4.9 Snapshots of a model AuNP containing MUA and SH-PEG showing time resolved evolution of the system (Water particles were removed for clarity). Snapshots were taken between t = 1 ns and t = 270 ns.

An investigation on the behaviour of the conformation of PEG was done in the presence or absence of the thiol group and in the addition of MUA (Figure 4.10). All three simulations were carried out in equal cycles. The results were analysed using the distance from the last bead of SH-PEG, or from the first and last beads of PEG, to the centre of mass of the gold. As expected, the percentage of non-radial PEG is 100 % for the simulation done using PEG without the thiol group. There is an increment of radial SH-PEG when passing from the simulation using only SH-PEG (35 % wrapping) to the simulation using SH-PEG and MUA (25 % wrapping). According to this results, MUA forces SH-PEG to be more radial. The results are in agreement with the observations from the previous simulations.

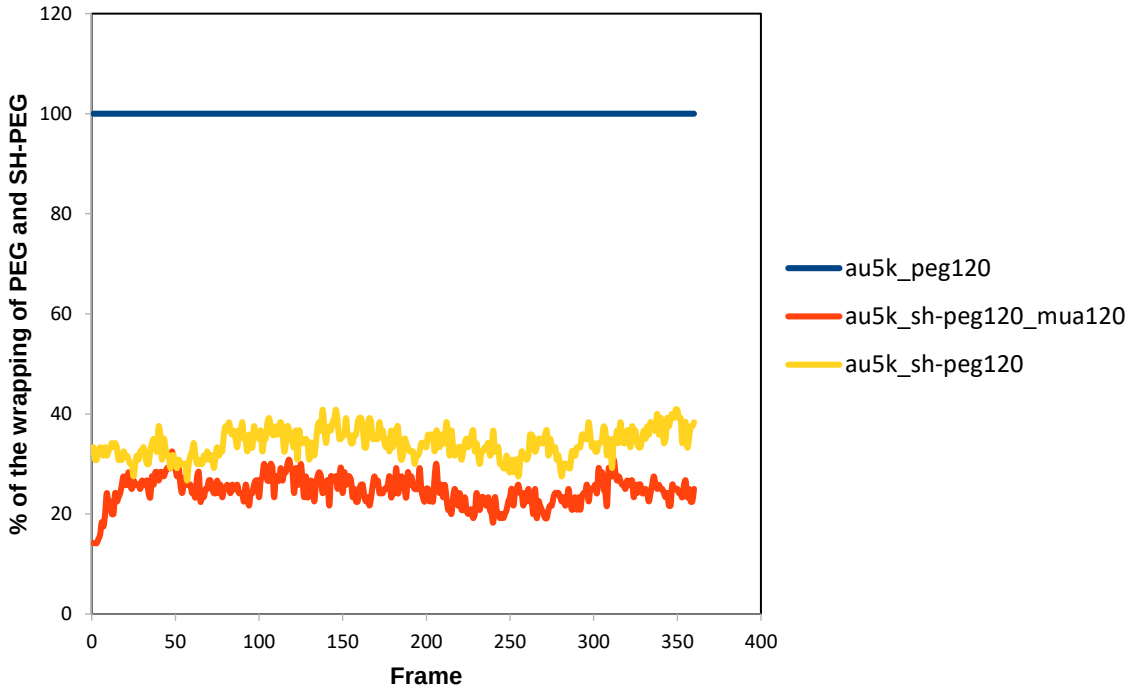

Figure 4.10 Percentage of the wrapping of PEG and SH-PEG where all systems were prepared in 30x30x30 d_0^3 water box formed by 240 000 water molecules with 15 000 gold atoms and in addition; 120 PEG without the thiol bead (In blue), 120 SH-PEG and MUA (in red), and 120 SH-PEG (In yellow).

As a proof of reproducibility, 8 jobs were prepared in the same water box of 30x30x30 d_0^3 formed by 240 000 water molecules with 15 000 gold atoms that forms the nanoparticle containing 120 MUA and 120 SH-PEG. They were run from exactly the same

starting coordinates, but each job used a different random number seed to initiate the simulations. Figure 4.11 shows the rdf for the S···S distance calculated in each simulation. A very good reproducibility was obtained.

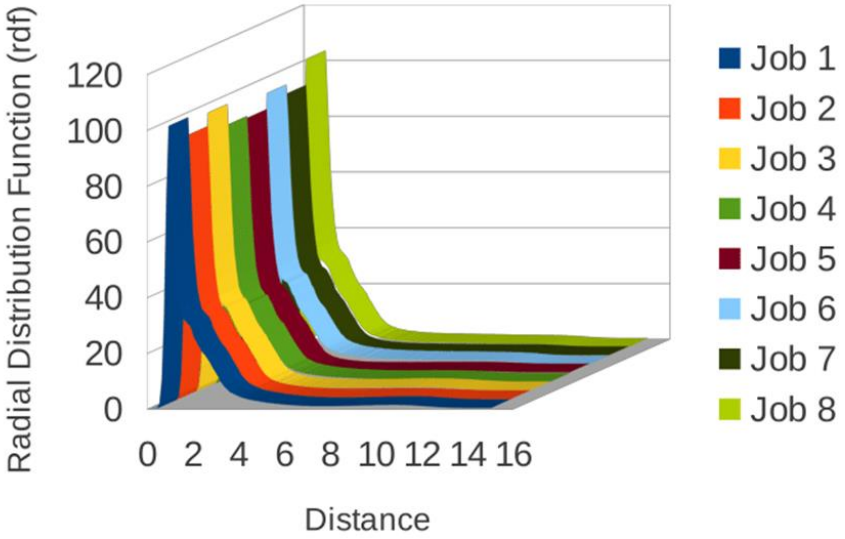

Figure 4.11 Radial Distribution Functions for the eight jobs with the only difference of random number seeds containing the AuNP with 120 MUAs and 120 SH-PEGs.

4.6 Order of Addition

To understand these systems better, our simulations were done adding the components sequentially. In the first case, we added MUAs first and SH-PEGs afterwards both at nanoparticle surface subsaturation concentrations. In the second case, we added SH-PEG molecules first, at nanoparticle surface subsaturation concentrations, and then MUA molecules afterwards. Both systems were studied in the same conditions (A box with 240 0000 water molecules, 15 000 gold atoms, 120 MUA and 120 SH-PEG molecules). In the first case (Figure 4.12.a), adding the MUA to the AuNP results in a AuNP covered by MUA patches as described above, indicating that when SH-PEG is added it occupies the remaining AuNP surface areas where MUA is not present, displaying a clear radial conformation. In the second case (Figure 4.12.b), adding SH-PEG first results in a AuNP conjugate having the SH-PEGs wrapped around the surface. However, when MUA is added, it is able to partially unwrap SH-PEG molecules and force them to change to a

more radial conformation. In addition, some small MUA micelles are remaining in solution because they cannot access to the SH-PEG protected AuNP surface.

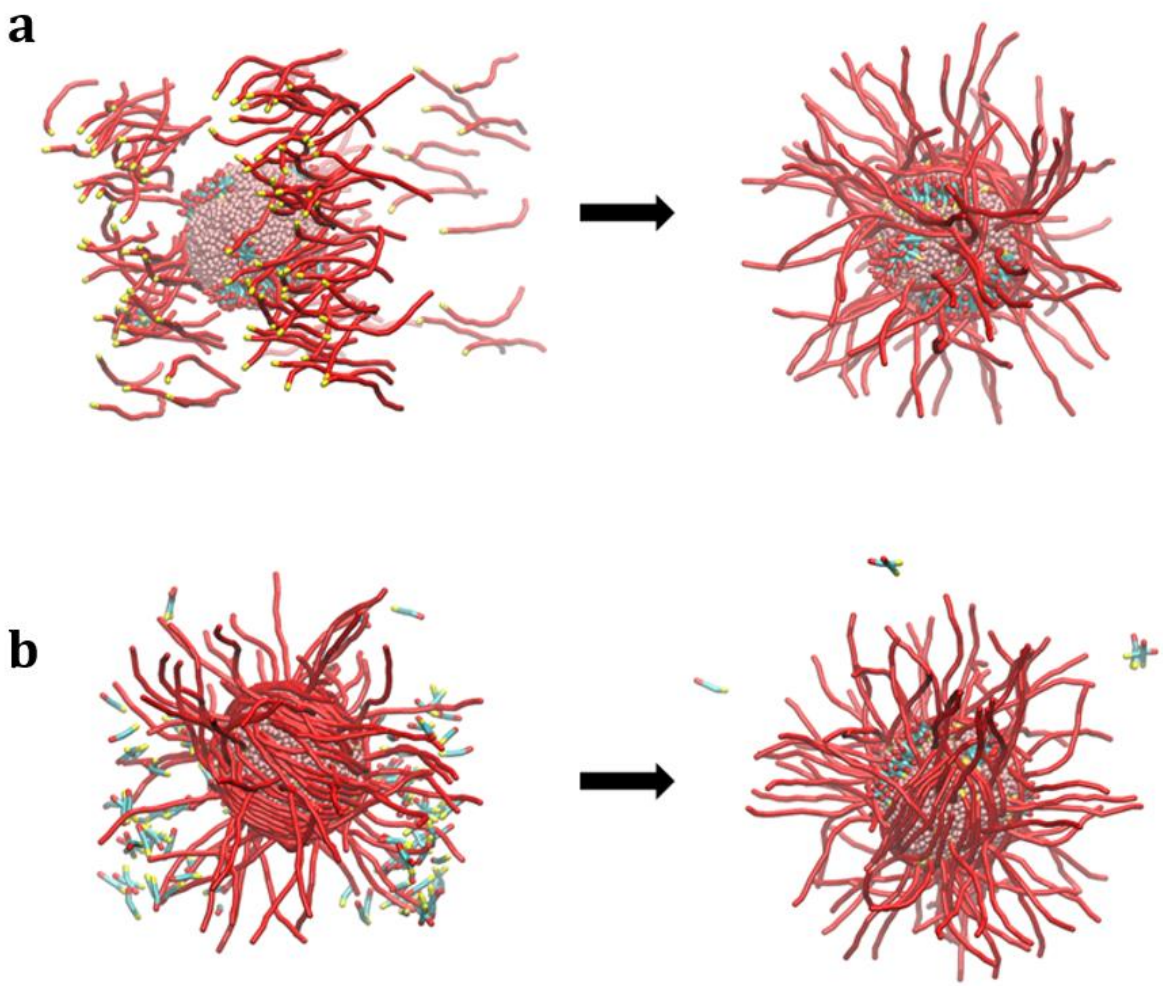

Figure 4.12 Snapshot of two models of AuNP containing MUA and SH-PEG **a.** MUA added before SH-PEG **b.** SH-PEG added before MUA (Water particles were removed for clarity). First snapshots were taken at 0.75 ns and the second snapshots were taken at 270 ns to observe the conformational change.

4.7 The Effect of the SH-PEG/MUA Ratio

In this section, we analysed how the addition of different ratios of SH-PEG/MUA affects the conformation of the mixed layers on AuNPs. As mentioned before, both

molecules compete for the AuNP surface. Even though both molecules are attaching with a thiol group, as MUA has the hydrophobic chain, their resulting interaction and packing between neighbouring molecules is favoured with respect to the SH-PEG molecules.

Using a combination of Ultraviolet–Visible Spectroscopy (UV–vis)[33] and Dynamic Light Scattering (DLS)[34] techniques, Comenge *et al.*[21] found that the changes in AuNP properties were correlated with different SH-PEG conformations. While MUA is expected to be always radial to the surface,[35] molecules as SH-PEG, at low densities, are expected to be in a folded conformation in what is known as the *mushroom* conformation.[36] At higher densities, SH-PEG molecules also take a radial conformation, known as *brush* conformation.[36] Two different conformation changes depending on the surface coverage are explained in their article:

1. At added ratios SH-PEG/MUA from 0 to 0.7, the SH-PEG has a low influence on the hydrodynamic diameter, since it is in the *mushroom* conformation. Here, the physicochemical properties are governed by MUA.
2. At added ratios from 0.7 to 1, the SH-PEG changes the conformation from *mushroom* to *brush* and new physicochemical properties are subsequently acquired.

AuNPs become stable from ratios SH-PEG/MUA higher than 0.7 and the aggregation of nanoparticles is evident for ratios of SH-PEG/MUA lower than 0.7.[21] The results from our simulations explained below show a similar effect; we observed the change of SH-PEG from tangential to radial conformation as the MUA concentration increased.

A set of simulations were designed to investigate the effect of the SH-PEG/MUA ratios, which were performed in equal cycles. The percentage of radial SH-PEG was calculated using the distances of SH-PEGs' last hydrophilic beads to the AuNP centre of mass at each frame. Figure 4.13 shows the percentage of SH-PEG in radial conformation obtained in each simulation. Similar to what was observed in experiments; at ratios more than 0.6 the conformation of SH-PEG is mainly radial where at ratios less than 0.6 the conformation of SH-PEG is less radial.

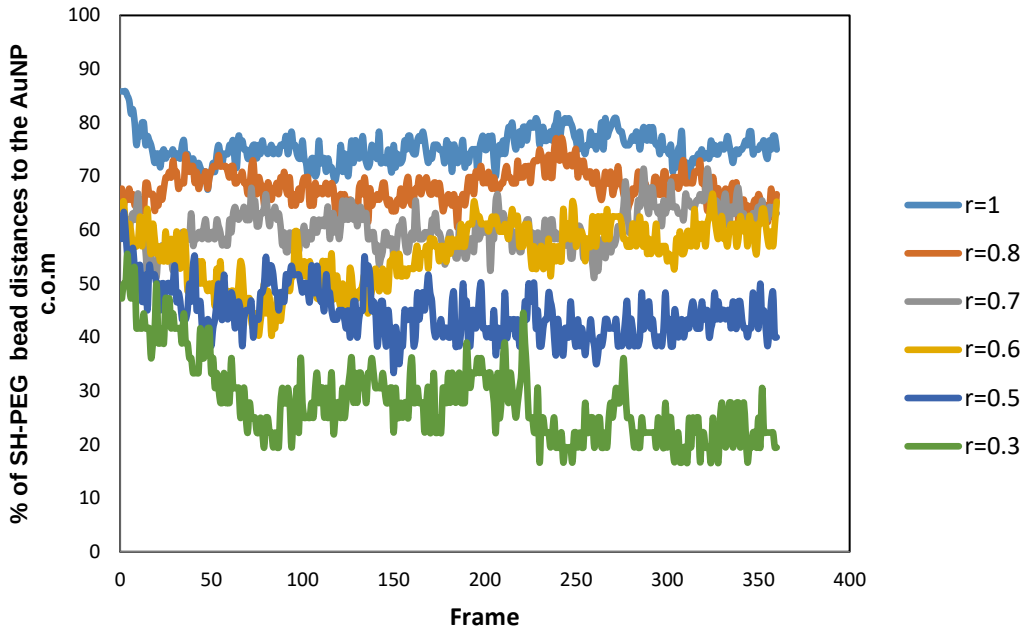

Figure 4.13 Percentage of the radial SH-PEG where all systems were prepared in 30x30x30 d_0^3 water box formed by 240 000 water molecules with 15 000 gold atoms and in addition; added SH-PEG/MUA in different ratios from 0.3 to 1.

4.8 Conclusions

The results from this work show that MUAs in solution exist in groups of 4-6 disordered micelles, while PEG and SH-PEG do not adopt any defined arrangement. When MUAs are added over a solution of AuNP, they form patches at the AuNP surface.

The presence of a thiol group is crucial for adopting a radial conformation once SH-PEG has complexed the AuNP. In the absence of the thiol group, PEG mainly wraps around the AuNP surface, while in its presence, the radial conformation can be easily observed at high coverage rates.

MUA and SH-PEG compete for occupying the AuNP surface. MUA is faster than SH-PEG in reaching and adsorbing onto the nanoparticle surface, what is very likely due to its smaller size and/or to its higher hydrophobicity. Additionally, MUA forms patches over the AuNP surface and allows the SH-PEG to occupy the empty zones.

Simulations indicate that the order of addition of the thiol containing molecules (MUA and SH-PEG) has a decisive influence in the final structure of the AuNP. When the order is first AuNP+MUA and then SH-PEG, patches for MUAs and radial conformation for SH-PEG are obtained. An opposite order of addition (AuNP+SH-PEG and then MUA) give rise to less SH-PEG in radial conformation, smaller MUA patches on the AuNP surface and some disordered micelles of MUA in the solution. Accordingly, MUA molecules are able to partially unwrap preformed SH-PEG layers.

This study indicates the natural tendency of molecules to segregate and form different domains on the nanoparticle surface. Additionally, it also shows how large molecules can present different conformations on top of the nanoparticle surface. Consequently, different nanoparticle surface states can be controlled adjusting the final molecule concentrations and order of addition.

We believe that the computational studies on these systems can be helpful in giving information on problems that cannot be easily solved experimentally, especially in a context where the fast evolution of the new applications can often be linked to a lack of understanding on the mechanisms involved on the final nanoparticle design and behaviour. Indeed, recently, computational studies have provided another point of view to help in the understanding of these systems once the initial simulation tools have been adapted and developed for the nanoscale.[37] In addition, they give valuable guidelines for the engineering of multifunctional nanoparticles and molecular surface structure of nanoparticles which is difficult to measure due to the nature of these small coatings in nanoparticle dispersions.

4.9 References

1. M. C. Daniel, D. Astruc, *Chem. Rev.* **2004**, *104*, 293.

2. C. Louis, O. Pluchery, *Gold Nanoparticles for Physics, Chemistry and Biology*, Imperial College Press, London, UK **2012**.

3. R. Sperling, P. Gil, F. Zhang, *Chem. Soc. Rev.* **2008**, *37*, 1896-1908.

4. B. Pelaz, C. Alexiou, R. A. Alvarez-Puebla, F. Alves, A. M. Andrews, S. Ashraf, L. P. Balogh, L. Ballerini, A. Bestetti, C. Brendel, S. Bosi, M. Carril, W. C. W. Chan, C. Chen, Xiaodong Chen, Xiaoyuan Chen, Z. Cheng, D. Cui, J. Du, C. Dullin, A. Escudero, N. Feliu, M. Gao, M. George, Y. Gogotsi, A. Grünweller, Z. Gu, N. J. Halas, N. Hampp, R. K. Hartmann, M. C. Hersam, P. Hunziker, J. Jian, X. Jiang, P. Jungebluth, P. Kadhiresan, K. Kataoka, A. Khademhosseini, J. Kopeček, N. A. Kotov, H. F. Krug, D. S. Lee, C. M. Lehr, K. W. Leong, X. J. Liang, M. Ling Lim, L. M. Liz-Marzán, X. Ma, P. Macchiarini, H. Meng, H. Möhwald, P. Mulvaney, A. E. Nel, S. Nie, P. Nordlander, T. Okano, J. Oliveira, T. H. Park, R. M. Penner, M. Prato, V. Puntes, V. M. Rotello, A. Samarakoon, R. E. Schaak, Y. Shen, S. Sjöqvist, A. G. Skirtach, M. G. Soliman, M. M. Stevens, H. W. Sung, B. Z. Tang, R. Tietze, B. N. Udugama, J. S. VanEpps, T. Weil, P. S. Weiss, I. Willner, Y. Wu, L. Yang, Z. Yue, Qian Zhang, Qiang Zhang, X. E. Zhang, Y. Zhao, X. Zhou, W. J. Parak, *ACS Nano* **2017**, *11*, 2313-2381.

5. E. Boisselier, D. Astruc, *Chem. Soc. Rev.* **2009**, *38*, 1759.

6. R. Sardar, A. M. Funston, P. Mulvaney, R. W. Murray, *Langmuir* **2009**, 25, 13840-13851.

7. P. Ghosh, G. Han, M. De, C. K. Kim, V. M. Rotello, *Adv. Drug Deliv. Rev.* **2008**, *60*, 1307-1315.

8. C. D. Medley, J. E. Smith, Z. Tang, Y. Wu, S. Bamrungsap, W. H. Tan, *Anal. Chem.* **2008**, *80*, 1067.

9. P. Sharma, S. Brown, G. Walter, S. Santra, B. Moudgil, *Adv. Colloid Interface Sci.* **2006**, *123-126*, 471-485.

10. P. V. Baptista, M. Koziol-Montewka, J. Paluch-Oles, G. Doria, R. Franco, *Clin. Chem.* **2006**, *52*, 1433-1434.

11. M. A. Dobrovolskaia, S. E. McNeil, *Nat. Nanotechnol.* **2007**, *2*, 469-478.

12. J. Lipka, M. Semmler-Behnke, R. A. Sperling, A. Wenk, S. Takenaka, C. Schleh, T. Kissel, W. J. Parak, W. G. Kreyling, *Biomaterials* **2010**, *31*, 6574-81.

13. E. Casals, V. F. Puntes, *Nanomedicine* **2012**, *7*, 1917-1930.

14. R. A. Sperling, W. J. Parak, *Phil. Trans. R. Soc.* **2010**, *A368*, 1333-1383.

15. T. L. Moore, L. Rodriguez-Lorenzo, V. Hirsch, S. Balog, D. Urban, C. Jud, B. Rothen-Rutishauser, M. Lattuada, A. Petri-Fink, *Chem. Soc. Rev.* **2015**, *44*, 6287.

16. K. Avgoustakis, A. Beletsi, Z. Panagi, P. Klepetsanis, A. G. Karydas, D. S. Ithakissios, *J. Control. Release* **2002**, *79*, 123-135.

17. X. Xia, M. Yang, Y. Wang, Y. Zheng, Q. Li, J. Chen, Y. Xia, Y., *ACS Nano* **2011**, *6*, 512-522.

18. V. Puntes, *Br. J. Radiol.* **2015**, *89*, 20150210.

19. E. D. Kaufman, J. Belyea, M. C. Johnson, Z. M. Nicholson, J. L. Ricks, P. K. Shah, M. Bayless, T. Pettersson, Z. Feldotö, E. Blomberg, P. Claesson, S. Franzen, *Langmuir* **2007**, *23*, 6053-6062.

20. J. Comenge, C. Sotelo, F. Romero, O. Gallego, A. Barnadas, T. G. C. Parada, F. Domínguez, V. F. Puntes, *PLoS ONE* **2012**, *7(10)*, e47562.

21. J. Comenge, V. F. Puntes, *ScienceOpen Research* **2015**, 1-10.

22. A. M. Jackson, J. W. Myerson, F. Stellacci, *Nat. Mater.* **2004**, *3*, 330-336.

23. H. Grönbeck, M. Walter, H. Häkkinen, *J. Am. Chem. Soc.* **2006**, *128*, 10268-10275.

24. R. D. Groot, P. B. Warren, *J. Chem. Phys* **1997**, *107*, 4423-4435.

25. P. Español, *Dissipative Particle Dynamics. In Handbook of Materials Modeling*, Springer, Dordrecht, Netherlands **2005**, pp 2503-2512.

26. **a.** M. Venturoli, B. Smit, M. M. Sperotto, *Biophys. J.* **2005**, *88*, 1778-1798. **b.** F. J. De Meyer, M. Venturoli, B. *Smit, Biophys. J.* **2008**, *95*, 1851-1865. **c.** F. J. M. De Meyer, J. M. Rodgers, T. F. Willems, B. Smit, *Biophys. J.* **2010**, *99*, 3629-3638. **d.** M. Kranenburg, B. Smit, *J. Phys. Chem. B* **2005**, *109*, 6553-6563. **e.** A. Benjamini, B. Smit, *Soft Matter* **2013**, *9*, 2673-2683.

27. S. Chen, C. Guo, G. H. Hu, H. Z. Liu, X. F. Liang, J. Wang, J. H. Ma, L. Zheng, *Colloid Polym. Sci.* **2007**, *285*, 1543-1552.

28. P. Atkins, T. Overton, J. Rourke, M. Weller, F. Armstrong, M. Hagerman, *Inorganic Chemistry*, 5th ed., W.H. Freeman and Company, New York, United States **2010**, p. 69.

29. C. C. You, A. Chompoosor, V. M. Rotello, *Nano Today* **2007**, *2*, 34-43.

30. S. C. Glotzer, M. J. Solomon, *Nat. Mater.* **2007**, *6*, 557-562.

31. Z. L. Zhang, S. C. Glotzer, *Nano Lett.* **2004**, *4*, 1407-1413.

32. H. Häkkinen, *Nat. Chem.* **2012**, *4*, 443-455.

33. D. R. Yarkony, *Modern Electronic Structure Theory*, vol. 3, World Scientific, Singapore **1997**, pp. 92-115.

34. B. J. Berne, R. Pecora, *Dynamic Light Scattering: With Applications to Chemistry, Biology, and Physics*, Courier Dover Publications, New York, United States **2000**.

35. Y. Wang, O. Zeiri, A. Neyman, F. Stellacci, A. I. Weinstock, *ACS Nano* **2012**, *6*, 629-640.

36. C. A. Simpson, A. C. Agrawal, A. Balinski, K. M. Harkness, D. E. Cliffel, *ACS Nano* **2011**, *5*, 3577-3584.

37. P. Charchar, A. J. Christofferson, N. Todorova, I. Yarovsky, *Small* **2016**, *12*, 2395-2418.

Chapter 5

ADDITION OF THE PROTEIN AND ALTERNATIVE GOLD NANOPARTICLE DESIGN

CHAPTER 5

ADDITION OF THE PROTEIN AND ALTERNATIVE GOLD NANOPARTICLE DESIGN

In this chapter, computational studies on gold nanoparticle (AuNP) conjugates will be expanded thoroughly. First, the addition of the protein and the reasons behind it will be explained. After that, an alternative AuNP design will be introduced. Most of the simulations explained in Chapter 4 were repeated with the addition of the protein and the new gold design in this chapter. Also, the addition of the protein in the simulations using the new gold design will be explained. The colloidal stability of AuNPs will also be discussed in the following sections.

5.1 Addition of the Protein

Nanoparticles interact with many biomolecules when immersed into a biological medium. The interaction with proteins on the nanoparticle surface is commonly referred as the nanoparticle-protein corona.[1] The nanoparticle-protein corona strongly influences the biocompatibility and biodistribution of the interacted nanoparticles.[2] This interaction determines the reactivity and functionality of nanoparticles, thus playing a very important role on the identity of the nanomaterials.[3] The single layer of proteins formed

on nanoparticle surfaces is referred as the hard corona where proteins are directly bound to the nanoparticle surface with high affinity, forming a stable coating.[4] However, proteins which are loosely attached to the nanomaterial surface, or are covering the hard protein corona *via* week interactions, are often called soft protein corona.[5,6] The composition of the protein corona is determined by many factors such as the nanoparticle size,[7] shape,[8] and surface properties like chemical composition,[9] surface charge,[10] and surface hydrophobicity.[11]

The conjugation of proteins with AuNPs results in good biocompatibility and reduces the nonspecific toxicity towards normal cells.[12] Luby *et al.*[13] stated that targeted protein corona formation is capable of stabilizing AuNP behaviour and improving delivery rate. However, the formation of protein corona may fail to stabilize nanoparticles at high concentrations in physiological media. Polyethylene glycol (PEG) can be used to avoid adsorption of proteins.[1] PEGylation reduces nonspecific protein adsorption of serum proteins thus increasing circulation time[14,15,16] and gives a "stealth character" to the nanoparticle, masking the nanoparticle from the immune cells.[17,18] In drug delivery, the term "stealth" is coming from the "low observable technology" used in military tactics, which refers to nanovehicles that are invisible to the biological system.[19] On the other hand, making nanoparticles invisible to the immune system may increase their toxicity.

Comenge *et al.*[20] used PEGylation as an alternative to achieve additional stability avoiding specific protein adsorption. This leads to a decrease of functionality which can be overcome by mixed layers. As explained in Chapter 4, 11-mercaptoundecanoic acid (MUA), and thiolated polyethylene glycol (SH-PEG) can be used for the mixed layer. MUA provides electrostatic repulsion while SH-PEG provides steric repulsion.[20] Bovine serum albumin (BSA) binds spontaneously to the surface of citrate-coated AuNPs.[21] BSA is a large and flexible protein that has multiple modes of binding and therefore provides the steric stabilization.[22] The authors stated that the proteins in media were not capable of stabilizing high concentrations of MUA-capped AuNPs.[20] They proposed PEGylation to overcome this problem. On the contrary, AuNPs capped with SH-PEG do not bind to BSA unlike what was observed with citrate-stabilized ones.[23] The protein adsorption is also dependent on the mixed layer composition and configuration. When SH-PEG adopts the radial conformation, the physicochemical properties of the conjugate changes. The

stretching of SH-PEG, being in the radial conformation, results inhibition of protein adsorption.[20] Figure 5.1 shows the *mushroom* and *brush* conformations of AuNPs. While MUA is expected to be always radial to the surface,[24] SH-PEG at high densities is referred to as *brush* and at low densities as *mushroom*.[20]

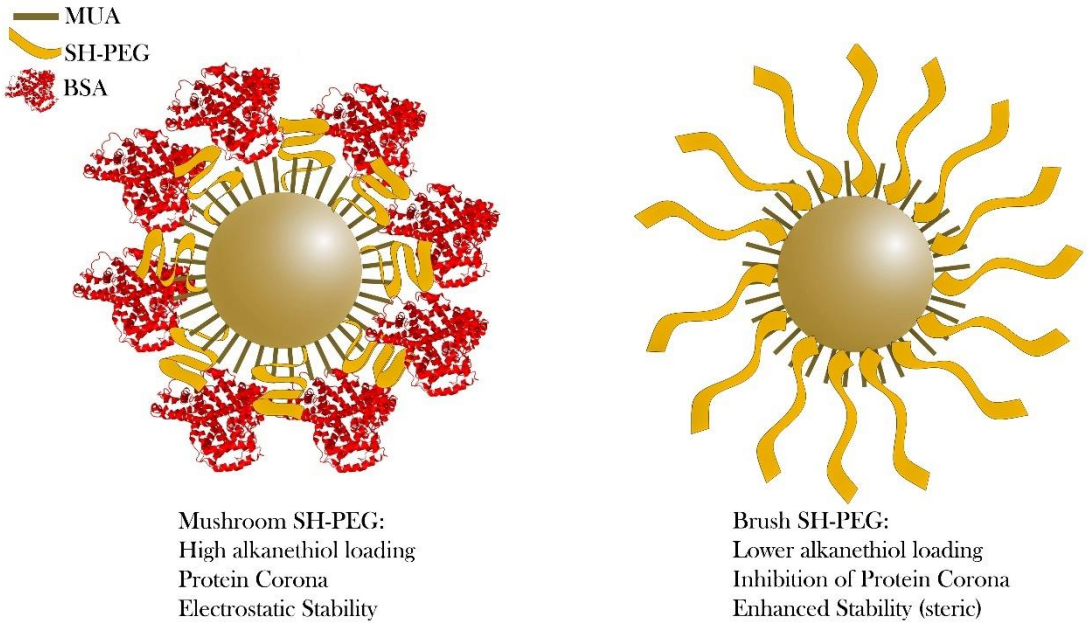

Figure 5.1 Illustration of the two different conformations of AuNPs in the presence of MUA, SH-PEG, and BSA.

The stability and composition of the corona is dependent on the nanoparticle size and surface chemistry. Huang *et al.*[25] studied the interactions of two different functionalized AuNPs with BSA and they reported that the surface structural and chemical composition of nanoparticles is important in determining the protein nanoparticle surface interaction and subsequent protein conformation.

To continue the investigation of the AuNP conjugates, the next section will explain how BSA is introduced to our simulations. Several coarse-grained studies on serum albumins will be explained to complement our studies.

5.1.1 Triangle Model of Bovine Serum Albumin

Serum albumin is a highly soluble multidomain protein, that is very stable and available at high purity and low cost.[26] It is one of the first discovered and most intensely studied proteins.[26] BSA is a serum albumin protein derived from cows which is an extensively studied group of proteins, because of its structural similarity with human serum albumin (HSA).[27] Figure 5.2 shows the crystal structures of both serum albumins. The hydrodynamic properties of proteins can be predicted from atomic level structures derived from the atomic coordinates of a Protein Data Bank (PDB) formatted file.[28]

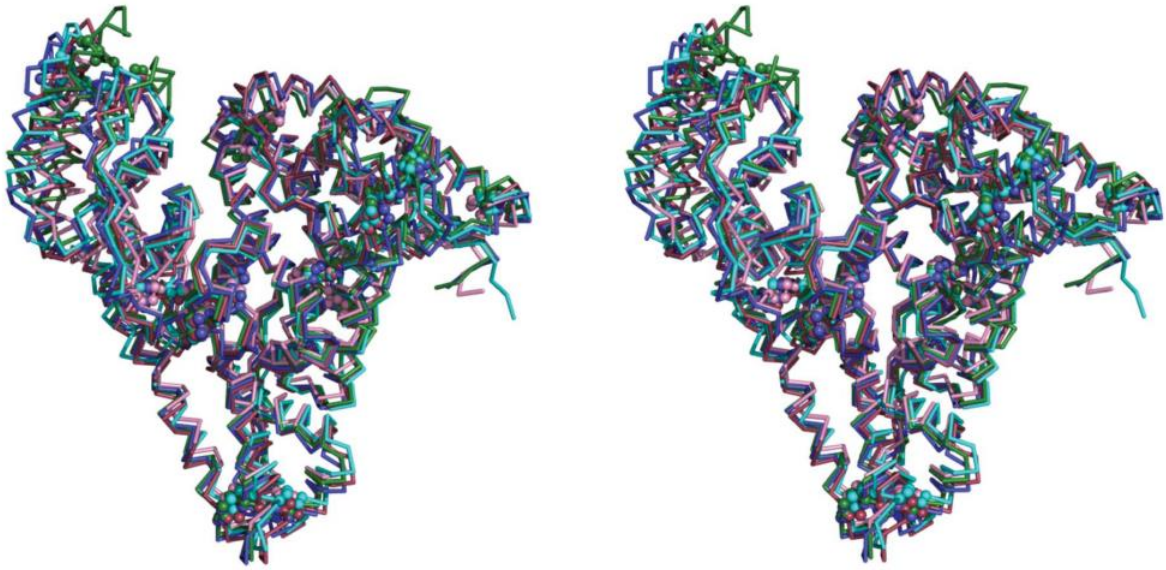

Figure 5.2 A stereoview of the aligned crystal structures of serum albumins. HSA, burgundy (PDB entry 1ao6; Sugio *et al.*, [29] 1999); BSA, cyan; equine serum albumin (ESA), blue; ESA-t, violet; leporine serum albumin (LSA), green. The disulfide bridges are shown as spheres. Adapted from reference 30.

He and Carter suggested a heart-shaped conformation crystallographic data of HSA at 1992.[31] Hydrodynamic data indicate that, under physiological conditions, BSA adopts a folded conformation, as observed in the crystalline environment.[32] Ferrer *et al.*[32] studied the hydrodynamic properties of the serum albumins with coarse grained bead-model methods which they call rough shell models. They modelled BSA as a triangular

prismatic shell with optimized dimensions of 84x84x84x31.5 Å (Figure 5.3.a). In their second model the atomic level structure of HSA obtained from crystallographic data was used to build a much more refined rough-shell model where number of beads are removed, to give the final shell model (Figure 5.3.b).

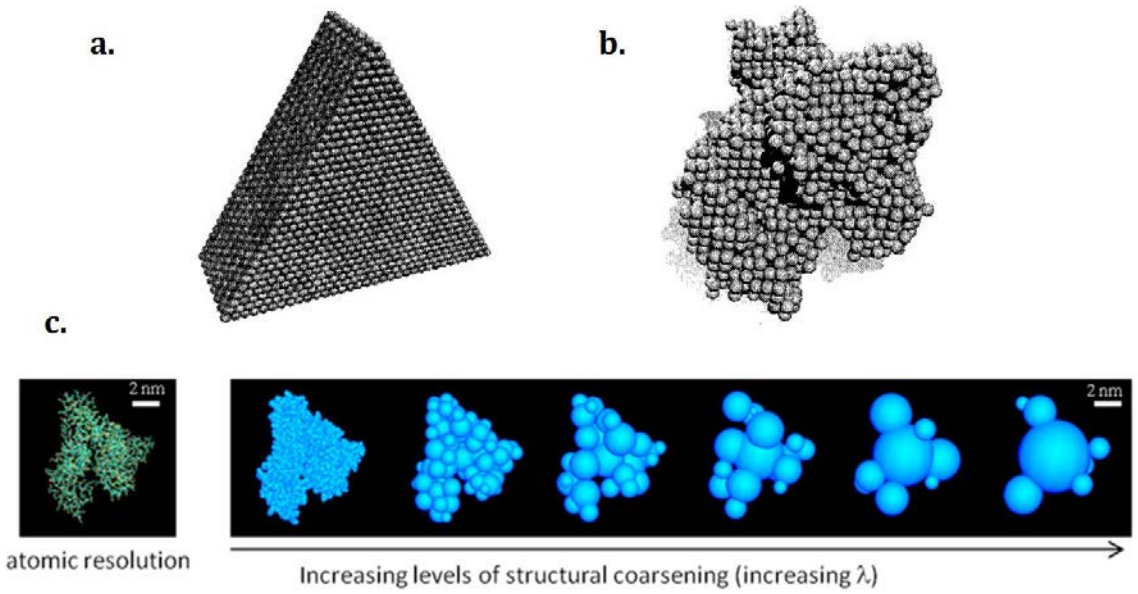

Figure 5.3 Examples of coarse-grained serum albumins: **a.** Rough shell triangular model of BSA; **b.** A Rough shell model derived from the atomic level structure of HSA (PDB entry 1bm0; Sugio *et al.*,[29] 1999); (Adapted from reference 32.) **c.** Structural coarse-graining of HSA (PDB entry 1ao6; Sugio *et al.*,29 1999) and increasing levels of structural coarsening where the parameter λ defines the level of coarsening. (Adapted from reference 33.)

Bhirde et al.[33] studied the aggregation of AuNPs with diameters in the 2-5 nm range and the role of albumin using computer simulations. They simulated HSA in a coarse-grained system can be fine-grained at any stage over the course of a simulation (Figure 5.3.c). They stated that the algorithm they used is general and it can be applied to other serum proteins, such as histone, fibrinogen, and globulins.[33] There is the limitation that these simulations are dependent on the computer resources, long dynamics simulations would be needed to properly sample the conformations, that is why they chose Monte Carlo sampling.

The triangle model of BSA suits our coarse-grained model better since our beads have fixed size.[34,35] The triangle model was built in a water box of 50x50x50 d_0^3 formed by 1 020 000 water molecules with 1 BSA with dimensions of 84x84x84x32 Å. BSA was designed to have 455 beads using only the hydrophobic bead (P) type (Figure 5.4).

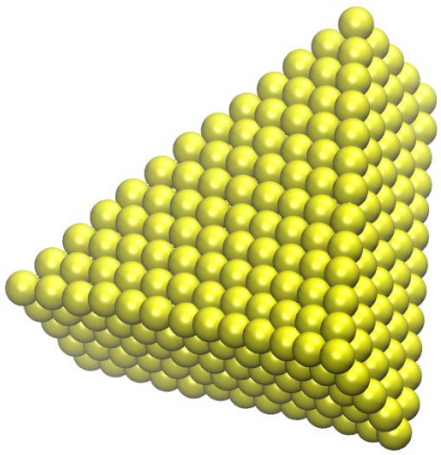

Figure 5.4 Snapshot of the triangle model of BSA using 455 beads (Water particles were removed for clarity).

Systems with two and more components were studied always using a water box of 50x50x50 d_0^3 formed by 1 020 000 water molecules with 15 000 gold atoms and 1 BSA; 15 000 gold atoms 120 MUAs and 1 BSA; 15 000 gold atoms, 120 MUAs, 120 SH-PEGs and 1 BSA.

During the analysis of the results from those simulations, severe limitations were observed forcing us in thinking of several problems while using the protein in our coarse-grained model:

1. Using such a big water box increases the simulation times dramatically;
2. The total number of beads in one simulation increased more than four times comparing to the simulations done before;

3. The coarse-grained model used in our studies needs to be changed to another algorithm which would let us to speed up the simulations (parallelizing the code or transforming it into CUDA source);
4. Another option would be to consider changing the coarse-grained model to a parallel Molecular Dynamics code like Nanoscale Molecular Dynamics (NAMD),[36] or GROningen MAchine for Chemical Simulations (GROMACS).[37]

5.2 Alternative Gold Nanoparticle Design

The stability of AuNPs should be considered in most applications; for example, in drug delivery, cell and animal imaging, and diagnostic assays. Thiol compounds can efficiently improve the stability and dispersity of colloidal AuNPs in aqueous solution due to the strong Au-S binding.[38,39] The colloidal stability of AuNPs for biological applications has been demonstrated by a variety of thiol-based ligands such as MUA,[22] mercaptopropionic acid,[40] SH-PEG,[41,42,43] thiol-terminated DNA,[44] cysteine-containing peptides,[45] and BSA.[46] Herein, we are going to focus on the stability of AuNPs in the presence of MUA.

MUA is an alkanethiol commonly used in the study of AuNPs due to the high affinity of the thiol for the gold and the hydrophobic chain conferring electrostatic stability to the nanoparticles.[47] On the other side, the packing density of the ligands also plays an important role in the stability of nanoparticles.[48] In high MUA ratios, due to the compactness of the layer, MUAs could digest the nanoparticle.[20,48] AuNPs saturated with a thiol ligand on the surface, the maximum ratio of the thiols will be directly proportionally to the volume-to-surface area ratio.[49]

A set of simulations were designed to investigate the behaviour of MUA under high concentrations. All the simulations were performed in the same water box of 30x30x30 d_0^3 formed by 240 000 water molecules with 15 000 gold atoms that forms the nanoparticle. In addition, increasing number of MUAs from 100 to 2000 were added to the simulations. The deformation of the nanoparticle was observed with the increasing number of MUAs added to the simulations (Figure 5.5). It is observed that when the

number of MUAs reach 1500, the nanoparticle was more in a disc form than spherical. The distortion was even more when the number of MUAs reached 2000.

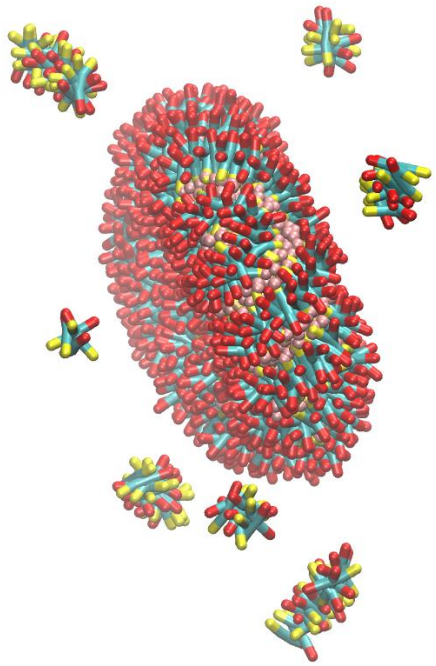

Figure 5.5 Snapshot of a model AuNP with 1500 MUAs (Water particles were removed for clarity). The snapshot was taken at 270 ns.

Figure 5.6 represents the distance from the 666 nearest gold beads to the AuNP centre of mass depending on the frame and on the number of MUAs. The number of 666 was deduced by considering a close-packed spherical arrangement (26% of unoccupied space)[50] of gold beads. There is a slight change of the nanoparticle shape when increasing the number of MUAs from 100 to 1400. When the number of MUAs reaches 2000 the behaviour is not constant, indicating a strong deformation of the AuNP which loses its spherical form. According to Figure 5.6, the saturation of our AuNP surface is reached when the number of MUAs is more than about 500 (homogeneous sphere with radius very close to the isolated AuNP).

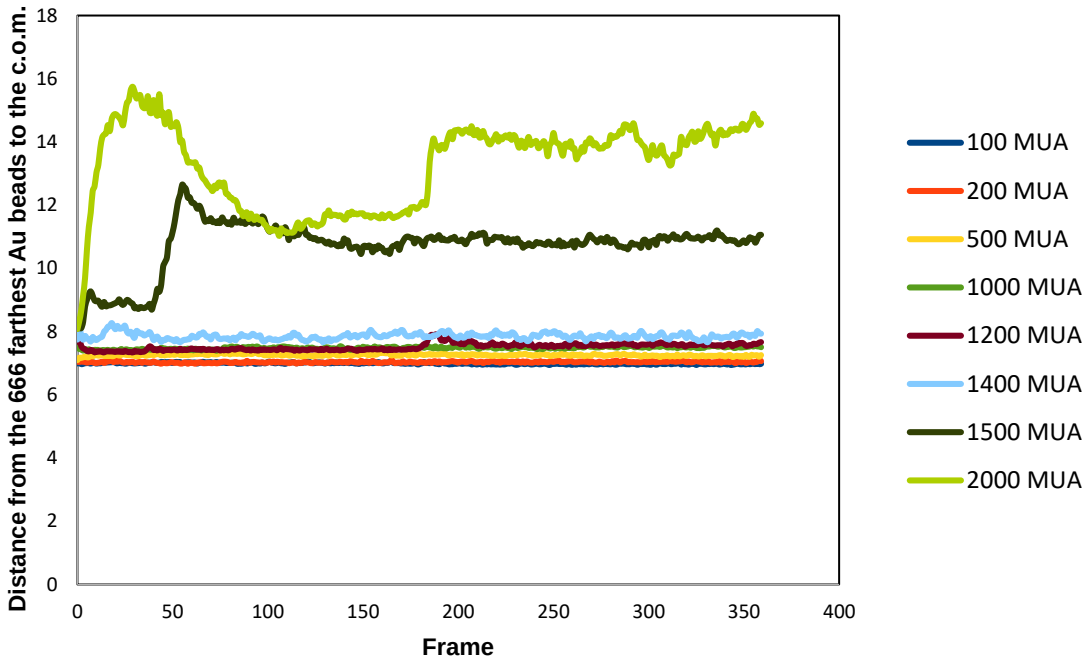

Figure 5.6 The distance from the surface of the nanoparticle to the AuNP centre of the mass for simulations with 100 MUAs to 2000 MUAs. The distances are shown in reduced units.

5.2.1 Dome Model of the Gold Nanoparticle

An alternative AuNP design was proposed to overcome the deformation caused by the oversaturation of the ligands. This model is inspired by the works of the architect Buckminster Fuller who was known by his geodesic dome designs. He was an inspiration to many; as it is shown by the naming of Buckminsterfullerene (C60), because of its similar shape to his dome creations.[51]

The dome model was built with the help of a program for creating dome structures.[52] Simulations were run using the water box of 30x30x30 d_0^3 formed by 240 000 water molecules with a dome gold formed by 252 beads with a diameter of 4.5 nm (Figure 5.7). While it is possible to build the dome model of the AuNP, our maximum is 1000 gold beads with a diameter of 10 nm.

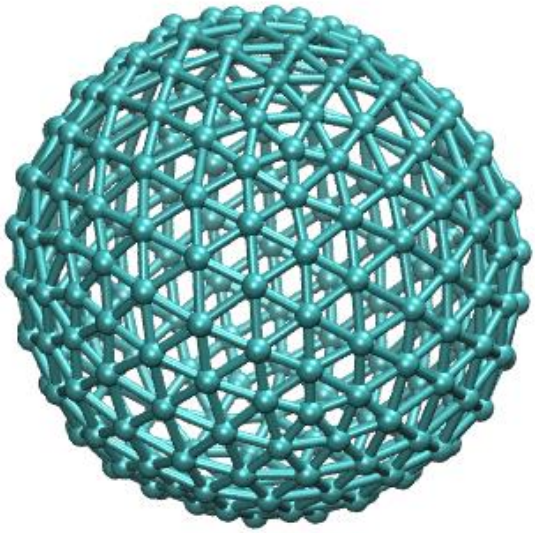

Figure 5.7 Snapshot of the dome model of the AuNP using 252 gold beads (Water particles were removed for clarity).

The simulations mentioned in Chapter 4 in the section 4.5, where we investigate the interactions between gold and other components were repeated to test the new AuNP design. All the simulations were performed in a water box of 30x30x30 d_0^3 formed by 240 000 water molecules with the new gold model. First, we checked the model and behaviour of each individual component in the simulations where we performed with only MUA and only SH-PEG. Later, the competition between both thiolated compounds is studied within the new system. Finally, the effect of the order of addition is studied. BSA was studied with the new gold model in a larger water box of 50x50x50 d_0^3 formed by 1 020 000 water molecules with the new gold model and MUA and SH-PEG. Several problems and limitations occurred during these computations. The most important problem was the overlapping/inter-crossing of particles. The penetration of the SH-PEGs into the AuNP was observed in several simulations, an example can be seen in Figure 5.8. It is known that in dissipative particle methods this problem might occur. Dissipative Particle Dynamics (DPD) simulations have the advantage of a length scale larger than the atomistic scale,[53] however the interactions between particles are soft. Thus, in some cases it might cause bond crossing and interpenetration between particles.[54]

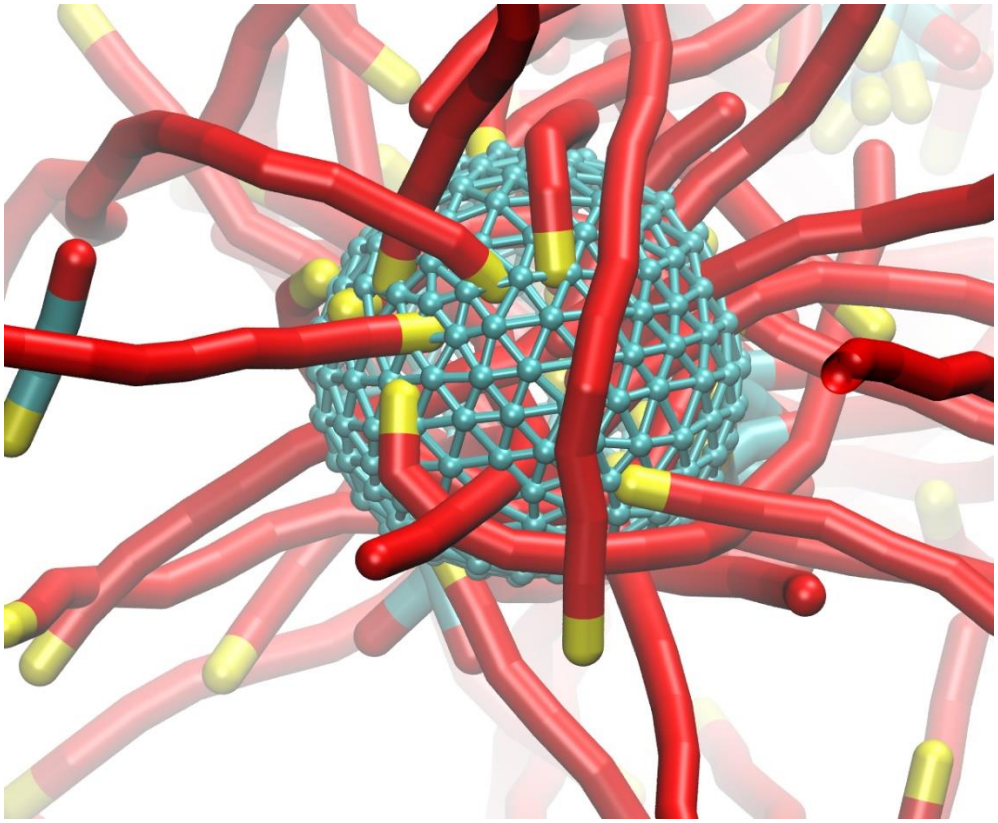

Figure 5.8 Snapshot of a dome model AuNP containing MUA and SH-PEG (Water particles were removed for clarity).

DPD is successfully applied in investigating a variety of soft matter problems because of its correct hydrodynamic behaviour of fluids. However, the soft interparticle interaction might result in overlapping among the DPD particles in some cases. To avoid and solve the particle interpenetration problem several attempts had been developed. Briels and co-workers[55,56] considered the entangled bonds as elastic bands and then determined the entanglement positions by calculating the energy minimization. Pan and Manke[57] introduced the segmental repulsive forces between the points of nearest contact of the chains to reduce the frequency of bond crossing. Nikunen et al.[58] and Liu et al.[59] considered another method to avoid bond crossing simply by adopting a segmental repulsion model and a mixed hard-soft potential to each DPD particle by modifying the form of the conservative force based on the original DPD method.

A mix model combining both of the AuNP models used in our studies could be the solution to the problems mentioned above. The mix model is designed in a water box of 50x50x50 d_0^3 formed by 1 020 000 water molecules and a AuNP combining the dome model using 812 gold beads and the first gold model using 3000 gold beads (Figure 5.9). This time the penetration of gold beads from inside to outside of the gold dome was observed. Probably, creating a new gold type for the inner gold beads with a strong repulsion parameter for the interaction with the dome gold beads might help avoiding the penetration through the outside layer of the dome gold.

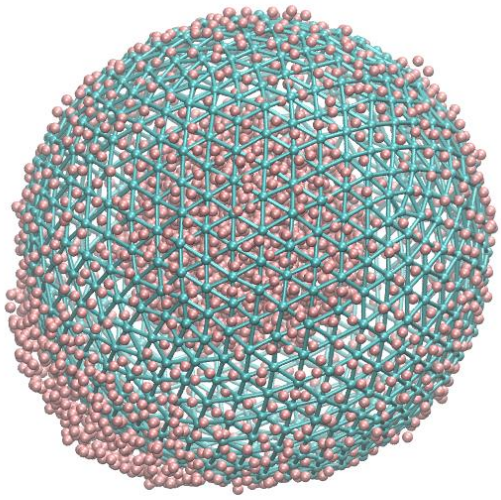

Figure 5.9 Snapshot of the mixed model of the AuNP combining the dome model using 812 gold beads and the first gold model using 3000 gold beads (Water particles were removed for clarity).

5.3 Conclusions

BSA was successfully designed and added to the AuNP conjugates in this study. Several limitations were observed in simulating such large systems. The parallelization of the coarse-grained model on a multi-core CPU might solve/reduce these problems.

Another approach would be to consider changing the coarse-grained model to a parallel code such as NAMD.

The colloidal stability of AuNPs was discussed in this chapter. The first AuNP model is not stable when over saturated with MUAs. An alternative design was done to overcome the deformation caused by the over saturation of the ligands. The problems continued in this design too. Future studies are needed to explore the limitations caused by these problems.

5.4 References

1. S. R. Saptarshi, A. Duschl, A. L. Lopata, *Journal of Nanobiotechnology* **2013**, *11*, 26.

2. E. Casals, T. Pfaller, A. Duschl, G. J. Oostingh, V. Puntes, *ACS Nano* 2010, 4, 3623-3632.

3. M. P. Monopoli, C. Aberg, A. Salvati, K. A. Dawson, *Nat. Nanotechnol.* **2012**, *7*, 779-786.

4. S. Winzen, S. Schoettler, G. Baier, C. Rosenauer, V. Mailaender, K. Landfester, K. Mohr, *Nanoscale* **2015**, *7*, 2992-3001.

5. S. Milani, F. Baldelli Bombelli, A. S. Pitek, K. A. Dawson, J. Rädler, *ACS Nano* **2012**, *6*, 2532-2541.

6. W. Liu, J. Rose, S. Plantevin, M. Auffan, J.-Y. Bottero, C. Vidaud, *Nanoscale* **2013**, *5*, 1658-1668.

7. M. Lundqvist, J. Stigler, G. Elia, I. Lynch, T. Cedervall, K. A. Dawson, *Proc Natl Acad Sci* **2008**, *105*, 14265-14270.

8. S. Chakraborty, P. Joshi, V. Shanker, Z. A. Ansari, S. P. Singh, P. Chakrabarti, *Langmuir* **2011**, *27*, 7722-7731.

9. F. Meder, T. Daberkow, L. Treccani, M. Wilhelm, M. Schowalter, A. Rosenauer, L. Madler, K. Rezwan, *Acta Biomater.* **2012**, *8*, 1221-1229.

10. K. Chen, Y. Xu, S. Rana, O. R. Miranda, P. L. Dubin, V. M. Rotello, L. Sun, X. Guo, *Biomacromolecules* **2011**, *12*, 2552-2561.

11. T. Cedervall, I. Lynch, S. Lindman, T. Berggård, E. Thulin, H. Nilsson, K. A. Dawson, S. Linse, *Proc. Natl. Acad. Sci. U. S. A.* **2007**, *104*, 2050-2055.

12. R. Shukla, V. Bansal, M. Chaudhary, A. Basu, R. R. Bhonde, M. Sastry, *Langmuir* **2005**, *21*, 10644-10654.

13. A. O. Luby, E. K. Breitner, K. K. Comfort, *Appl Nanosci* **2016**, *6*, 827.

14. Arnida, A. Malugin, H. Ghandehari, *J. Appl. Toxicol.* **2010**, *30*, 212-217.

15. T. A. Larson, P. P. Joshi, K. Sokolov, *ACS Nano* **2012**, *6*, 9182-9190.

16. C. D. Walkey, J. B. Olsen, H. Guo, A. Emili, W. C. W. Chan, *J. Am. Chem. Soc.* **2012**, *134*, 2139-2147.

17. R. Gref, M. Lück, P. Quellec, M. Marchand, E. Dellacherie, S. Harnisch, T. Blunk, R. H. Müller, *Colloids Surf., B* **2000**, *18*, 301-313.

18. E. Boisselier, D. Astruc, *Chem. Soc. Rev.* **2009**, *38*, 1759.

19. S. Salmaso, P. Caliceti, *J Drug Deliv* **2013**, *2013*, 1-19.

20. J. Comenge, V. F. Puntes, *ScienceOpen Research* **2015**, 1-10.

21. S. H. Brewer, W. R. Glomm, M. C. Johnson, M. K. Knag, S. Franzen, *Langmuir* **2005**, *21*, 9303-9307.

22. E. D. Kaufman, J. Belyea, M. C. Johnson, Z. M. Nicholson, J. L. Ricks, P. K. Shah, M. Bayless, T. Pettersson, Z. Feldotö, E. Blomberg, P. Claesson, S. Franzen, *Langmuir* **2007**, 23, 6053-6062.

23. S. Dominguez-Medina, S. McDonough, P. Swanglap, C. F. Landes, S. Link, *Langmuir* **2012**, *28*, 9131-9139.

24. Y. Wang Y, O. Zeiri, A. Neyman, F. Stellacci, A. I. Weinstock, *ACS Nano* **2012**, *6*, 629-640.

25. R. Huang, R. R. Carney, K. Ikuma, F. Stellacci, B. L. T. Lau, *ACS Nano* **2014**, *8*, 5402-5412.

26. T. Jr. Peters, *All About Albumin*, Academic Press, New York, United States **1996**.

27. S. Dubeau, P. Bourassa, T. J. Thomas, H. A. Tajmir-Riahi, *Biomacromolecules* **2010**, *11*, 1507-1515.

28. J. García de la Torre, M. L. Huertas, B. Carrasco, *Biophys. J.* **2000**, *78*, 719-730.

29. S. Sugio, A. Kashima, S. Mochizuki, M. Noda, K. Kobayashi, *Protein Eng.* **1999**, *12*, 439-446.

30. A. Bujacz, *Acta Crystallogr. Sect. D* **2012**, *68*, 1278-1289.

31. X. M. He, D. C. Carter, *Nature* **1992**, *358*, 209-215.

32. M. L. Ferrer, R. Duchowicz, B. Carrasco, J. G. de la Torre, A. U. Acuña, *Biophys. J.* **2001**, *80*, 2422-2430.

33. A. A. Bhirde, S. A. Hassan, E. Harr, X. Chen, *J. Phys. Chem. C* **2014**, *118*, 16199-16208.

34. F. J. M. De Meyer, J. M. Rodgers, T. F. Willems, B. Smit, *Biophys. J.* **2010**, *99*, 3629-3638.

35. H. I. Ingólfsson, C. A. Lopez, J. J. Uusitalo, D. H. de Jong, S. M. Gopal, X. Periole, S. J. Marrink, *WIREs Comput Mol Sci* **2014**, *4*, 225-248.

36. http://www.ks.uiuc.edu/Research/namd/

37. http://www.gromacs.org/

38. J. Gao, X. Huang, H. Liu, F. Zan, J. Ren, *Langmuir* **2012**, *28*, 4464-4471.

39. M. Brust, M. Walker, D. Bethell, D. J. Schiffrin, R. Whyman, *J. Chem. Soc., Chem. Commun.* **1994**, *7*, 801-802.

40. T. Yonezawa, T. Kunitake, *Colloids Surf. A Physicochemical. Eng. Aspects* **1999**, *149*, 193-199.

41. F. Schulz, T. Vossmeyer, N. G. Bastus, H. Weller, *Langmuir* **2013**, *29*, 9897-9908.

42. A. G. Kanaras, F. S. Kamounah, K. Schaumburg, C. J. Kiely, M. Brust, *Chem. Commun.* **2002**, 2294-2295.

43. W. P. Wuelfing, S. M. Gross, D. T. Miles, R. W. Murray, *J. Am. Chem. Soc.* **1998**, *120*, 12696-12697.

44. Z. Li, R. C. Jin, C. A. Mirkin, R. L. Letsinger, *Nucleic Acids Res.* **2002**, *30*, 1558-1562.

45. R. Levy, N. T. K. Thanh, R. C. Doty, I. Hussain, R. J. Nichols, D. J. Schiffrin, M. Brust, D. G. J. Fernig, *Am. Chem. Soc.* **2004**, *126*, 10076-10084.

46. A. G. Tkachenko, H. Xie, Y. L. Liu, D. Coleman, J. Ryan, W. R. Glomm, M. K. Shipton, S. Franzen, D. L. Feldheim, *Bioconjugate Chem.* **2004**, *15*, 482-490.

47. J. C. Love, L. A. Estroff, J. K. Kriebel, R. G. Nuzzo, G. M. Whitesides, *Chem. Rev.* **2005**, *105*, 1103-1169.

48. B. C. Mei, E. Oh, K. Susumu, D. Farrell, T. J. Mountziaris, H. Mattoussi, *Langmuir* **2009**, *25*, 10604-10611.

49. H. Hinterwirth, S. Kappel, T. Waitz, T. Prohaska, W. Lindner, M. Lämmerhofer, *ACS Nano* **2013**, *7*, 1129-1136.

50. P. Atkins, T. Overton, J. Rourke, M. Weller, F. Armstrong, M. Hagerman, *Inorganic Chemistry*, 5th ed., W.H. Freeman and Company, New York, United States **2010**, p. 69.

51. Sussex Fullerene Group http://www.chm.bris.ac.uk/motm/buckyball/c60a.htm

52. https://code.google.com/p/pydome

53. R. D. Groot, P. B. Warren, *J. Chem. Phys* **1997**, *107*, 4423.

54. H. Liu, Y. H. Xue, H. J. Qian, Z. Y. Lu, C. C. Sun, *J. Chem. Phys.* **2008**, *129*, 024902.

55. J. T. Padding, W. J. Briels, *J. Chem. Phys.* **2001**, *115*, 2846.

56. P. Kindt, W. J. Briels, *J. Chem. Phys.* **2005**, *123*, 224903.

57. G. Pan, C. W. Manke, *Int. J. Mod. Phys. B* **2003**, *17*,231.

58. P. Nikunen, I. Vattulainen, M. Karttunen, *Phys. Rev. E* **2007**, **75**, 036713.

59. H. Liu, Y. H. Xue, H. J. Qian, Z. Y. Lu, C. C. Sun, *J. Chem. Phys.* **2008**, *129*, 024902.

Chapter 6

CONCLUSIONS

Chapter 6

CONCLUSIONS

This dissertation has demonstrated how computational chemistry can be applied to solve problems in the nanoscale. Better understanding of gold nanoparticle (AuNP) conjugates by computational studies was achieved thanks to the cooperation with several experimental groups. Current discussions and controversial reactions were reviewed striving to have an objective point of view. Herein, a general overview of concluding remarks is presented as follows:

- Dissipative Particle Dynamics (DPD) is a simple yet powerful tool for studying AuNP conjugates;
- An in house mesoscopic method using DPD was adopted to get it to work with our needs;
- DPD has been proved to be efficient in the simulation and explanation of experimental observations in the formation of AuNP conjugates;
- The simulations used here demonstrated that, despite its limitations, the bead model for AuNP provided an insight into the behaviour of AuNP conjugates.

Besides these conclusions, this dissertation opens up new possibilities for future work in exploring AuNPs with the use of other coarse-grained methods or exploring the possibilities of parallelization of the current coarse-grained model.